Copernicus Climate Change

The Integration of Climate Data into the SAVi model

C3S_428h_IISD-EU: Sustainable Asset Valuation (SAVi): Demonstrating the business case for climate-resilient and sustainable infrastructure

Issued by: IISD-EU / Oshani Perera

Date: September 2020

Ref:

C3S_428h_IISD-EU_D428h.1.1 _202006_Integration of climate data in the SAVi model_v2

Official reference number service contract:

2019/C3S_428h_IISD-EU/SC1

Contributors

International Institute for Sustainable Development
Bechauf, Ronja
Casier, Liesbeth
Lago, Sergio
Perera, Oshani
Perrette, Mahé
Uzsoki, David
Wuennenberg, Laurin

KnowlEdge Srl
Bassi, Andrea M.
Pallaske, Georg

Table of Contents

Abbreviations and Acronyms

API	application programming interface
BAU	business as usual
C3S	Copernicus Climate Change Service
CBA	cost–benefit analysis
CDD	cooling degree day
CDS	Climate Data Store
CLD	causal loop diagram
CMIP5	Coupled Model Intercomparison Project 5
CN	curve number
CO_2e	carbon dioxide equivalent
COD	Chemical Oxygen Demand
CSO	combined sewer overflow
EGP	efficiency of gas-powered generation
EPA	U.S. Environmental Protection Agency
EWP	extractable wind power
Ia	initial abstraction
IR	irrigation requirement
IRR	internal rate of return
KE	KnowlEdge
HDD	heating degree day
IBPG	interlocking block pavement with gravel
IISD	International Institute for Sustainable Development
ISO	International Organization for Standardization
IVCW	integrated vertical-flow constructed wetlands
LAI	leaf area index
N	nitrogen
NH^+_4	ammonium
NO^-_3	nitrate
O&M	Operations and maintenance
OWC	oscillating water column
P	phosphorus
PCP	porous concrete pavement
$PM_{2.5}$	particulate matter
PM	Pierson–Moskowitz
PO_4^{3-}	phosphate
PV	photovoltaic
RCP	Representative Concentration Pathway
RMS	root-mean-square
SAVi	Sustainable Asset Valuation
SD	system dynamics
SS	suspended soils
TN	total nitrogen
TP	total phosphorus
WCE	Water conveyance efficiency
WPD	wind power density

1 Introduction

This report outlines the integration of Copernicus Climate Data authoritative climate data from the Climate Data Store into the Sustainable Asset Valuation (SAVi) tool. It describes how several climate indicators obtained from the Copernicus Climate Data Store (CDS) were integrated into SAVi and how the analysis performed by SAVi has improved as a result. In light of this integration, IISD is able to generate sophisticated SAVi-derived analyses on the costs of climate-related risks and climate-related externalities.

This report also marks the end of the first phase of the contract between the International Institute for Sustainable Development (IISD) and KnowlEdge (KE) with the Copernicus Climate Change Service (C3S), one of the six thematic information services provided by the European Union's Copernicus Earth Observation Programme. The contract pertained to connecting authoritative data on climate in Europe and the rest of the world to the SAVi tool.

This document presents:

- A summary of the literature review conducted on the impact of weather on several subsectors of infrastructure—energy, water, nature-based infrastructure, buildings, materials management, roads, and transport.
- Equations found in the literature that link climate variables to the performance of infrastructure services across all of these subsectors. For example, these services include power generation, irrigation, wastewater treatment, and mobility solutions. In the case of nature-based infrastructure, these services include ecosystem services and their derived infrastructure and climate adaptation benefits.
- How the above information was used to select relevant indicators from the Copernicus database.
- An indication of how outputs of the CDS datasets are integrated into the SAVi system dynamics models and how simulation results can be affected by the use of this new and improved set of indicators.

This report is organized as follows:

Literature Review

- Subsection 1: Overview of climate impact on the asset (e.g., wind speed affects power generation; precipitation affects roads, buildings, and wastewater; temperature affects natural infrastructure).
- Subsection 2: Presentation of papers/reports that provide case studies that summarize the range of impacts estimated or observed (e.g., across countries).
- Subsection 3: Description of the methodology found in the literature for the calculation of climate impacts on the infrastructure asset. Text box: presentation of selected case studies to illustrate the results emerging from the use of a given equation/approach.
- Subsection 4: A selection of CDS datasets required by the equations

Integration of the Literature Review with the CDS Dataset

For each asset, we summarize information on what datasets are being used from the Copernicus database and what additional processing was applied before integration into SAVi. We first reviewed the equations to determine their usefulness for SAVi models. We then assessed what data requirements for each of the equations are available in the Copernicus database. We created indicators for climate variables that are relevant for the equations selected. Finally, in certain cases, we created indicators in the CDS Toolbox for first-order impacts on infrastructure. Second and third-order impacts will be estimated with SAVi, making use of additional equations included in the system dynamics (SD) model.

Integration of Climate Indicators Into the SAVi Energy Model

Next, we introduce how the CDS indicators are used in the SAVi sustainbale development model for each asset. This includes the identification of specific indicators of performance for each asset that are impacted by climate indicators (e.g., efficiency and cost).

Behavioural Impacts Resulting From the Integration of Climate Variables

We proceed to discuss how these indicators affect asset performance in the sustainbale development model, providing early insights as to how the results of the SAVi analysis may change when equipping the model with more and better refined climate indicators (e.g., the cost of infrastructure being higher due to increased maintenance and the economic viability of the infrastructure asset, expressed as the internal rate of return [IRR], being lower than expected).

Simulation Results

Finally, we finally present the equations used and quantitative results emerging from the inclusion of climate indicators in SAVi for the asset under various climate scenarios. This is the end product of the enhanced SAVi model, which is used to inform policy and investment decisions for infrastructure.

Table 1 provides an overview of climate drivers, impacts, and relevant SAVi output indicators.

The CDS datasets are accessed via the CDS application programming interface (API), and additional processing and packaging for use in SAVi is done offline. Technical information about the offline code is found in Annex I. We also selected a subset of the most-used indicators and created an app in the CDS Toolbox with interactive visualization for demonstration purposes.

Table 1. Overview of variables and impacts implemented in the SAVi model (by module)

SAVi module	Implemented impact	Main climate drivers	Affected output indicators
Roads	Stormwater runoff from roads	• Precipitation	• Stormwater management cost
	Effect of precipitation on road lifetime	• Precipitation	• Depreciation of roads • Cost of road construction and maintenance • Road-related energy use • Energy-related emissions • Social cost of carbon
	Weather effects on accident rates	• Precipitation • Temperature	• Number of accidents • Economic cost of accidents
Energy	Impact on load factor	• Coal: Temperature • Gas: Temperature • Nuclear: Temperature • Biomass: Temperature • Hydro: Precipitation • Wind: Wind speed • Solar: Temperature	• Electricity generation • Revenues from electricity generation • Fuel expenditure • Energy-related emissions (for fossil generators) • Social cost of carbon • Cost of air pollution
	Impact on thermal efficiency	• All thermal generators: Temperature	• Fuel use • Fuel expenditure • Fuel-related emissions • Social cost of carbon
	Impact on grid efficiency	• Temperature	• Revenues from electricity sales
Buildings	Stormwater harvesting yield	• Precipitation	• Water use in buildings • Water cost
	Effect of temperature on load factor of rooftop solar photovoltaic (PV)	• Temperature	• Solar PV generation • Electricity cost • Emissions from electricity use • Social cost of carbon
	Heating degree days	• Temperature	• Heating energy expenditure • Heating energy use • Energy use-related emissions

SAVi module	Implemented impact	Main climate drivers	Affected output indicators
			• Social cost of carbon
	Cooling degree days	• Temperature	• Cooling energy expenditure • Cooling energy use • Energy use-related emissions • Social cost of carbon
Wastewater	Urban stormwater runoff	• Precipitation	• Wastewater energy use • Energy-related cost • Nutrient removal • Environmental cost of nutrients • Social cost of carbon
	Urban flood indicator	• Precipitation	• Wastewater energy use • Energy-related cost • Nutrient removal • Environmental cost of nutrients • Social cost of carbon
	Effect of temperature on wetland phosphorus (P) removal efficiency	• Temperature	• P removal in wetlands • Water quality • P-related mitigation costs • Eutrophication • Tourism revenues • Fishery revenues
Irrigation	Seasonal precipitation	• Precipitation	• Irrigation water requirements • Crop water supply • Average crop yields
	Average precipitation	• Precipitation	• Irrigation water requirements • Crop water supply • Average crop yields
	Seasonal temperature	• Temperature	• Irrigation water requirements • Crop water supply • Average crop yields
	Average temperature	• Temperature	• Irrigation water requirements

SAVi module	Implemented impact	Main climate drivers	Affected output indicators
			• Crop water supply • Average crop yields
	Net irrigation requirements per hectare	• Precipitation	• Water cost for irrigation • Average crop yields
	Total irrigation requirements per hectare	• Precipitation	• Total annual irrigation requirements • Water cost for irrigation
	Indicated surface water supply	• Precipitation • Temperature	• Annual water supply from surface water sources • Quantity of water available for irrigation from surface water • Water stress • Water balance
	Indicated groundwater supply	• Precipitation • Temperature	• Annual water supply from surface water sources • Quantity of water available for irrigation from surface water • Water stress • Water balance
Natural infrastructure	Labour productivity impact indicator	• Temperature	• Months with potential labour productivity impacts
	Air temperature considering vegetation cover	• Temperature	• Effect of 25%, 50%, and 75% vegetation cover • Labour productivity impact indicator

2 Power Generation Infrastructure

2.1 Literature Review

2.1.1 Wind Technology

2.1.1.1 Wind Speed

Wind turbines convert wind kinetic energy into electricity or electric energy. They can be grouped into vertical axis and horizontal axis, but this review covers only turbines with horizontal axis. The components of a wind turbine are the rotor, the generator, and the surrounding structure.

- **Climate impact**

Wind power generation is affected by wind speed. Changes in mean wind speed have an impact on wind power generation (Harrison & Wallace, 2005). If there is no or too little wind, turbines cannot produce electricity. On the contrary, when the wind speed is too strong, efficiency is lost because turbines have a cut-out limit where they stop generating electricity.

- **Summary of results**

In Scotland, the estimated range of variation of change in wind speed (m/s) [-20; -10; +10; +20] has an impact on turbine output from the base case of [-26,06%; - 11,52%; +8,37%; +13,66%]. For Davy et al. (2018), from Representative Concentration Pathway (RCP) 4.5 and RCP 8.5 for Coupled Model Intercomparison Project 5 (CMIP5), the prevision of the impact of change in wind speed to extractable power is under 10% for both scenarios.

- **Results**

The relationship between wind speed and power generation output has been documented by Manwell et al. (2002, 2010). Many other studies present similar information for other types of wind turbines (considering technology, size, and location of installation). The Harrison and Wallace (2005) study focuses on offshore turbines located in Western Scotland. Table 2 shows power generation in relation to changes in wind speed.

Table 2. Wind turbine performance altered by wind speed

Wind turbine performance with base case and uniformly altered wind speed

Measure	Base case	Annual mean wind speed change (%)			
		−20	−10	+10	+20
Mean turbine output (kW)	1493	1104	1321	1618	1697
Production (GWh/year)	13.08	9.67	11.57	14.17	14.85

Source: Harrison & Wallace, 2005

Davy et al. (2018) focus on extractable power energy in the region of the Black Sea for a 120 m hub-height, 7.6 MW capacity, Enercon E-126 turbine. They show that, under RCP 4.5 and RCP 8.5 scenarios, on average, "the projected changes to the [extractable wind power] EWP in all cases are small (< 10% of the historical EWP [1979–2004])," and "there is a 15%–20% difference in the EWP and wind power density (WPD) over the different regions of the Black Sea" (Davy et al., 2018).

- **Methodology**

Method 1 (Harrison & Wallace, 2005)

1. Wind Energy

"Power in wind varies with the cube of the wind speed U (m/s) such as" (Harrison & Wallace, 2005):

$$P = \frac{1}{2}\rho U^3 \qquad P = \frac{1}{2}\rho U^3$$

"Where P is the power per unit area (W/m2) and "rho" is the air density. Turbine Output is defined by production curves, which specify output over the wind speed range between the cut-in and cut-out speeds. When combined with the wind speed information, production and, with appropriate data, the economic performance can be estimated" (Harrison & Wallace, 2005).

2. Wind speed distribution

"A range of models has been used to describe the wind resource, including the well-known Weibull distribution. A special case of this, the Rayleigh distribution, is commonly used and is defined solely by the mean wind speed U (mean)" (Harrison & Wallace, 2005):

$$p(U) = \frac{\pi}{2}\left(\frac{U}{\bar{U}^2}\right)\exp\left[-\frac{\pi}{4}\left(\frac{U}{\bar{U}}\right)^2\right]$$

"Here p (U) is the probability of occurrence of wind speed U and, when modelled incrementally, it gives the probability and, for a given period, the duration of time (in hours) for which each wind speed increment is experienced. The use of the appropriate wind turbine output at each

increment and summation across all increments provides an estimate of energy production in the period" (Harrison & Wallace, 2005).

Particular application: *West coast of Scotland* (Harrison & Wallace, 2005)

"The wind speed was defined in 0.25 m/s increments (up to 30 m/s) with the probability of occurrence and duration calculated from wind speed distribution function" (Harrison & Wallace, 2005).
"In order to maintain simplicity, the mean annual wind speed (at 19.5 m) was estimated at 10 m/s (base case). The turbine chosen for the analysis is the 3 MW Vestas V90" (Young & Holland, 1996).
"The corrected mean wind speed at hub height was found to be just over 11 m/s using the power law profile" (Harrison & Wallace, 2005):

$$U_{65} = U_{19.5}\frac{\ln(h_{65}/z_0)}{\ln(h_{19.5}/z_0)}$$

"Where h65 and h19.5 are the hub and reference heights while z0 is the roughness length of the water surface, which is generally very low. The turbine power curve follows the traditional shape with cut-in at 4 m/s, cut-out at 25 m/s and rated output at 15 m/s" (Harrison&Wallace, 2005).

Considerations for integration into the CDS Toolbox

- Units**:** Wind speed = m/s, air density = kg m^{-3}
- ERA5 (Fifth major global re-analysis produced by the European Centre for Medium-Range Weather Forecasts) monthly averaged and hourly data on single levels from 1979 to present for wind speed and air density
- CORDEX regional climate model data on single levels for Europe (Wind speed)
- CMIP5 monthly data on single levels (Wind speed)

Method 2 (Davy et al., 2018)

Intensity and variability of near surface winds and roughness impact wind energy production.

"While it is common to use simple power-law approximations to extrapolate wind speeds to turbine hub-heights, in this work we developed a roughness-length dependency in our calculation of wind speeds based on established boundary-layer profiles for winds" (Davy et al., 2018, p. 1653).

1. Wind Speed

$$W_z = \frac{u_*}{k} ln \frac{z}{z_0}$$

"Where W_z is the wind speed at height z; k is the von Karman constant, taken to be 0.4; z_0 is the roughness length; and u_* is the friction velocity" (Davy et al., 2018).

2. Friction velocity

"U_* is calculated from the surface wind stress (τ) and the air density (ρ)" (Davy et al., 2018):

$$u_* = \sqrt{\tau/\rho} \qquad (2)$$

where $\tau = \sqrt{\tau_U^2 + \tau_V^2}$, and we take $\rho = p_s/RT_s$, with $R = 287.06$ J kg^{-1} K^{-1}.

"With T_s being surface air temperature, P_s being surface pressure, and T_u and T_v being surface wind stress" (Davy et al., 2018).

For (1) and (2) "we have to calculate the friction velocity from the available data using (2), and then use the 10 m wind speeds to calculate the roughness length using Wind speed eq. We enforced a lower limit on the roughness length, based on values found over calm water, such that z ≥ 0.0002m. The derived friction velocity and roughness length were then substituted back into wind speed eq. to obtain the wind speed at a height of 120 m above the surface–the turbine height" (Davy et al, 2018).

"Note that (1) includes an implicit assumption that the atmosphere is neutrally stratified, and, in principle, a term accounting for the stability of the atmosphere should be included. However, this was not possible here given the limited availability of data" (Davy et al., 2018).

As a result, "when we use this formulation to estimate wind speeds at 120 m, we will tend to overestimate wind speeds in convective conditions and underestimate wind speeds instably stratified conditions" (Davy et al., 2018)

3. Wind Power Density (WPD):

"The power (P) per unit area (A), is defined from the air density (ρ) and the wind speed (W)" (Davy et al., 2018):

$$WPD = \frac{P}{A} = \frac{1}{2}\overline{\rho W^3}$$

"Where W is wind speed at a height of 120 m and over-bar indicates an averaging over time. WPD is sensitive to small timescale variations in wind speed because of this cubed dependence. Here constrained to use daily-mean wind speed data so WPD will be under-estimated. We used 3 hourly resolutions and compared by doing W^3 (3hr)/W^3 (daily) for each day. … Biggest difference seen in Mediterranean region with less than 20% difference over water although still geographical variations" (Davy et al., 2018).

4. Extractable Wind Power (EWP)

"Power-curve data from a typical 120 m hub-height wind turbine was used. The data is from the high capacity, 7.6 MW Enercon E-126 turbine" (Davy et al., 2018).

"A spline interpolation was used to calculate the wind power produced at each time-step, which was then averaged over the period of interest to obtain the typical EWP for a given location," (Davy et al., 2018). Results of the study indicate an S-shaped function, with 20% of capacity being used with 7.5 m/s wind speed, 50% with 10 m/s wind speed, 75% with 12 m/s wind speed and 100% capacity utilization with 15 m/s wind speed.

Considerations for integration into the CDS Toolbox

- Input: ERA5, hourly data, "100m_u_component_of_wind and 100m_v_component_of_wind"
- Wind power density ½ rho U**3
- Extractable wind power (look-up)

We select wind speed at 100 m from ERA5, on an hourly basis, as it represents more accurately the wind experienced by large turbines, unaffected by the boundary layer. For future projections, we use CMIP5, 10 m wind speed at daily resolution, which we scale to match ERA5 100 m during the period of overlap (2006 to 2019, which resulted in a scaling coefficient of 1.65).

- Two scenarios were used: RCP 4.5 and RCP 8.5 for CMIP5
- Units: Wind speed = m/s, Surface pressure = Pa, Surface air temperature = K, Roughness length = m, air density = kg m^{-3}
- Daily data are used in the article:

- CORDEX regional climate model data on single levels for Europe (wind speed)
- CMIP5 daily and monthly data on single levels (wind speed)
- ERA5 hourly and monthly averaged data on single levels from 1979 to present (wind speed, surface air temperature, air density)
- ERA5-Land hourly and monthly averaged data from 1981 to present (surface pressure)

Method 3 (Manwell et al., 2010)

"Mass flow of air d*m*/d*t* through a rotor disc of area A can be determined with an equation involving air density and air velocity" (Manwell et al., 2010):

$$\frac{dm}{dt} = \rho A U$$

The "kinetic energy per unit time of the flow" is then calculated (Manwell et al., 2010):

$$P = \frac{1}{2}\frac{dm}{dt}U^2 = \frac{1}{2}\rho A U^3$$

Which we can transform to get the wind power per area *P/A* (Manwell et al., 2010):

$$\frac{P}{A} = \frac{1}{2}\rho U^3$$

Note: conditions assumed here are "sea-level, 15˚C" and "density of air of 1.225 kg/m^3"(Manwell et al., 2010). "Power from wind is proportional to area swept by the rotor and wind power density is proportional to the cube of the wind velocity" (Manwell et al., 2010).

Considerations for integration into the CDS Toolbox

- ERA5 hourly and monthly averaged data on single levels from 1979 to present

Method 4 (Farkas, 2011)

P=1/2 × the density of air × the area swept out by the turbines × (wind speed) ^{3}

"The most important variable is wind speed. The area swept out by the turbine is a constant, and the density of air is generally taken as 1.225 kg/m^3, its value at sea level at 15°C" (Manwell et al. 2015).

Considerations for integration into the CDS Toolbox

- ERA5 hourly and monthly averaged data on single levels from 1979 to present

2.1.2 Wave Technology

The kinetic (motional) energy of water can be used to generate electricity. In addition, some of the kinetic energy of water is caused by wind, and so there is a connection between wind speed and kinetic energy in water. The three main technologies used to harness electricity from water kinetic energy are the oscillating water column (OWC), the surface-following attenuator (line absorber), and the buoyancy unit/point absorber.

2.1.2.1 Wind Speed

- **Climate impact**

"As ocean waves are predominantly the result of wind action, changes in wind patterns will ultimately alter wave regimes. Waves are created by the transfer of energy from wind flowing over water bodies. The energy transfer defines the size of waves, and this is dependent on the strength and duration of the wind and the available fetch" (Harrison & Wallace, 2005).

- **Summary of results**

The estimated range of impact of change in wind speed (m/s) [-20%; -10%; +10%; +20%] on wave energy production (GWh/year) from the base case is [-42,16%; -21,08%; +20,1%; +38,73%].

- **Results**

Harrison and Wallace (2005) estimate the impact of wind speed on wave power generation (surface-following attenuator, see Table 3). More details on the methodology are presented next.

Table 1. Wave energy and changes in wind speed

Wave energy and device performance with base case and uniformly altered wind speed

Measure	Base case	Annual mean wind speed change (%)			
		−20	−10	+10	+20
Mean wave height, H_S (m)	2.70	1.73	2.19	3.27	3.88
Mean wave period, T_e (s)	6.25	5.00	5.63	6.88	7.50
Mean available wave power (kW/m)	83.7	27.5	49.5	134.4	205.6
Mean device power output (kW)	232.8	134.4	183.8	279.4	322.5
Production (GWh/year)	2.04	1.18	1.61	2.45	2.83
Load factor (%)	31.0	17.9	24.5	37.3	43.0

Source: Harrison & Wallace, 2005

- **Methodology**

1. Wave energy (Evans & Antonio, 1986)

"The power in the waves varies with the square of the wave height and linearly with the wave period and can be defined as" (Evans & Antonio, 1986):

$$P = 0.49 H_S T_e$$

"Where P is power (kW/m of wave front), H_s is the significant wave height (m), and T_e is the wave energy period (s). H_s and T_e are representative of the wide spectrum of waves of different heights, periods, and directions that make up real seas. Together, they allow the specification of a range of 'sea states' that have given a probability of occurrence based on the joint coincidence of H_s and T_e" (Evans & Antonio, 1986).

"H_s is defined as four times the root-mean-square (RMS) elevation of the sea surface (H_{rms}) and where m_0 is the zero moment (or variance) of the wave spectrum" (Evans & Antonio, 1986).

$$H_S = 4H_{rms} = 4\sqrt{m_0}$$

"T_e is defined as the energy period, which is one of several representative wave period measures in use, although it is favoured for wave energy approaches as it weights waves according to spectral energy content where m-1 is the reciprocal of the first spectral moment (the mean frequency)" (Evans & Antonio, 1986):

$$T_e = m_{-1}/m_0$$

2. Wind-Wave Model (Pierson Jr & Moskowitz, 1964)

The "relationship between wind and wave conditions can be defined using the classic Pierson–Moskowitz (PM) spectrum. … This describes fully developed (steady-state) wind-created seas that may occur when the wind has been blowing over a long period (6–18 h) and fetch (200–600 km). The spectrum is empirically derived and uses the wind speed, U_0 (at a height of 19.5 m above mean sea level) as the single parameter that defines the energy spectrum of wave energies" (Pierson Jr & Moskowitz, 1964):

$$S(\omega) = 0.0081 g^2 \omega^{-5}\, 0.25 \exp\left[-0.74\left(\frac{g}{U_0\omega}\right)^4\right]$$

"Where S (u) is the spectral energy as a function of frequency, u (rads). Practical use is through determination of H_s and T_e through analysis of the spectral moments using point (i) (W energy)" (Pierson Jr & Moskowitz, 1964), we get:

$$H_S = 0.0212 U_0$$

$$T_e = 0.625 U_0$$

These parameters "specify significant wave height and wave period (wave energy) for any given wind speed" (Pierson Jr & Moskowitz, 1964).

Particular application:

Harrison and Wallace (2005) conduct a wave energy appraisal using a wave–energy converter developed by Edinburgh-based Ocean Power Delivery Ltd[1] (surface-following attenuator). The "Pelamis is a 120 m long floating device that resembles a sea snake with four articulated sections that flex (and produce up to 750 kW) as waves run down the length of the device. It is designed to maximize production in normal sea conditions while surviving heavy seas (HS>8 m) through power limitation" (Harrison & Wallace, 2005).

Considerations for integration into the CDS Toolbox

- ERA5 daily and monthly averaged data on single levels from 1979 to present

2.1.3 Solar Technology

Solar panels convert sunlight into electricity. This is performed by converting photons (particles of sunlight) into electrons. Solar panels have to be used in conjunction with inverters, to convert direct into alternating current.

The performance of PV systems is determined by technology, materials, how the panels are mounted, and by weather conditions (e.g., solar radiation, shading, temperature, wind and air pollution).

2.1.3.1 Solar radiation, temperature, wind

- **Climate impact**

Solar panels' efficiency is affected by solar radiation. In a way, it is linked to clear-sky radiation and cloud cover. If a PV panel is exposed to too high temperatures (hence, higher radiation), it

[1] http://www.oceanpd.com/

loses efficiency; sometimes when it is cloudier, efficiency increases (Flowers et al., 2016; Jerez et al., 2015).

"PV systems present a negative linear relationship between the energy output and the temperature change, while the increase of solar radiation is proportional to the PV energy output" (Panagea et al., 2014).

- **Summary of results**

From our literature review, for air temperature, an increase of 1˚C would decrease solar PV efficiency by 2% for the most pessimistic study and by 0.5% per 10˚C increase for the optimistic one. Concerning irradiance, an increase of 1 unit (W/m^2) will increase solar output by 5%. Finally for wind, an increase of speed by 1 m/s will lead to an increase of efficiency of 0.5%.

- **Results**

Adeh et al. (2019) found that "solar PV efficiency diminishes as a function of air temperature at a rate of approximately 0.5% per 10 °C. Light winds lead to increased energy efficiency relative to quiescent conditions with a 0.5% increase in efficiency from 0.5 m/s to 1.5 m/s."

In Greece, Panagea et al. (2014) found regional differences, but, on average, the individual increase of "1 unit in irradiance results in a significant increase in PV energy output up to 5%, while the increase of one unit of temperature causes a decrease up to 2% in solar PV efficiency."

- **Methodology**

Method 1 (Photovoltaic Softwares, 2020)

Electricity generated in the output of a PV system can be estimated using the following global formula (Photovoltaic Softwares, 2020):

$$E = A * r * H * PR$$

E: Energy (kWh)
A: Total solar panel area (m^2)
R: Solar panel yield or efficiency (%) given by the ratio = electrical power (in kWp) of one solar panel divided by the area of one panel.
H: Annual average solar radiation on tilted panels (shadings not included). You have to find the global annual radiation incident on your PV panels with your specific inclination (slope, tilt) and orientation (azimut) with unit = kWh/m2.
PR: Performance ratio, coefficient for losses (range between 0.5 and 0.9, default value = 0.75). It is a very important value to evaluate the quality of a PV installation because it gives the performance of the installation independently of the orientation, inclination of the panel. It includes all losses.

"Example: The solar panel yield of a PV module of 250 Wp with an area of 1.6 m^2 is 15.6%. This nominal ratio is given for standard test conditions (STC): radiation=1000 W/m^2, cell

temperature=25 Celsius degree, Wind speed=1 m/s, AM=1.5. The unit of the nominal power of the photovoltaic panel in these conditions is called "Watt-peak" (Wp or kWp=1000 Wp or MWp=1,000,000 Wp)" (Photovoltaic Softwares, 2020).

Considerations for integration into the CDS Toolbox

- ERA5 monthly: "mean_surface_downward_short_wave_radiation_flux" (W/m^2)
- CMIP5 monthly: "surface_solar_radiation_downwards" (W/m^2)

Method 2 (Gomes et al., 2014)

The "efficiency of a PV system is almost independent of the solar irradiance, while on solar thermal systems, the efficiency is strongly dependent. The efficiency of a thermal collector is often zero at low light intensities" (Gomes et al., 2014).

"Values were chosen in order to represent standard market panels. Thus, the PV panel has an efficiency of 15% and the solar thermal collector has a maximum efficiency of 80% and a total U value of 4 with $\Delta T = [T_{med} - T_{amb}] = 50^oC$ which was considered to be frequent" (Gomes et al., 2014).

As indicated above, "there are more factors to consider, such as the fact that the temperature of the solar cells will increase together with the solar radiation, which will lead to a decrease in solar cell efficiency. … This means that the efficiency of the PV collector is not a straight line as shown but decreases with solar radiations following a coefficient of around 0.45%/K for mono crystalline solar cells. In the same manner, the PV power curve will continue to increase with solar radiation, but the real curve is less steep than that shown above. However, the efficiency of solar cells is also increased for higher radiation, which compensates for this effect" (Gomes et al., 2014).

Considerations for integration into the CDS Toolbox

- Solar radiation (J/m^2): ERA5 monthly averaged and hourly data on single levels from 1979 to present
- Ambient and median temperature (K): ERA5-Land monthly averaged and hourly data on single levels from 1981 to present

Method 3 (Panagea et al., 2014)

1. "Estimation of PV Energy Output under Variable Conditions of Temperature and Irradiance" (Panagea et al., 2014).

"In order to calculate the potential percentage change in PV output, the fractional change $\Delta P_{PV}/P_{PV}$ is calculated from the ratio between (2) and (3) taken from Crook et al. (2011)" *(refer to it for all equations)* (Panagea et al., 2014). **"[**Regional climate model] RCM temperature and

irradiance outputs were corrected for their biases in mean and standard deviation for each calendar month, following the methodology presented in an article by Haerter et al. (2011)" (Panagea et al., 2014).

Consider the following (Panagea et al., 2014):

$$\begin{aligned}&\frac{\Delta P_{PV}}{\eta_{ref}}\\&= -\Delta T G_{tot}\beta c_2 + \Delta G_{tot}\left(1 - \beta c_1 + \beta T_{ref} - 2\beta c_3 - T\beta c_2\right)\\&\quad - \Delta G_{tot}^2\beta c_3 - \Delta G_{tot}\Delta T\beta c_2 + \Delta G_{tot}\gamma \log_{10}\left(G_{tot} + \Delta G_{tot}\right)\\&\quad + G_{tot}\gamma \log_{10}\left(\frac{G_{tot} + \Delta G_{tot}}{G_{tot}}\right),\end{aligned} \tag{2}$$

$$\frac{P_{PV}}{\eta_{ref}} = G_{tot}\left(1 - \beta\left(c_1 + c_2 T + c_3 G_{tot} - T_{ref}\right) + \gamma \log_{10} G_{tot}\right), \tag{3}$$

$$\begin{aligned}&\frac{\Delta P_{PV}}{\eta_{ref}}\\&= -\Delta T G_{tot}\beta c_2 + \Delta G_{tot}\left(1 - \beta c_1 + \beta T_{ref} - 2\beta c_3 - T\beta c_2\right)\\&\quad - \Delta G_{tot}^2\beta c_3 - \Delta G_{tot}\Delta T\beta c_2 + \Delta G_{tot}\gamma \log_{10}\left(G_{tot} + \Delta G_{tot}\right)\\&\quad + G_{tot}\gamma \log_{10}\left(\frac{G_{tot} + \Delta G_{tot}}{G_{tot}}\right),\end{aligned} \tag{2}$$

$$\frac{P_{PV}}{\eta_{ref}} = G_{tot}\left(1 - \beta\left(c_1 + c_2 T + c_3 G_{tot} - T_{ref}\right) + \gamma \log_{10} G_{tot}\right), \tag{3}$$

Where (Panagea et al., 2014):

ΔP_{PV} is the change in PV power output

η_{ref} is the reference PV efficiency

ΔT is the change in temperature between the baseline and the scenario period

ΔG is the change in irradiance between the baseline and the scenario period

T is the daytime temperature for the baseline period, estimated by (4) as it can be found in Crook et al. (2011)

G_{tot} is the irradiance over the daylight for the actual cloud cover for the baseline period, calculated by (5) taken from Crook et al. (2011)

T_{ref} is the reference temperature in which the performance of PV cell is estimated by the manufacturer

β is the temperature coefficient set by cell material and structure

γ is the irradiance coefficient set by cell material and structure

$c1$, $c2$, and $c3$ are coefficients that depend on details of the module and mounting that affect heat transfer from the cell (Panagea et al., 2014).

2. Daytime temperature

$$T = \overline{T} + \frac{\overline{\mathrm{DTR}}}{4}, \qquad (4)$$

"DTR is the diurnal range of the temperature (difference between minimum and maximum temperature) and T is the monthly average temperature" (Panagea et al., 2014).

3. Irradiance

$$G_{\mathrm{tot}} = \overline{G}\frac{t_{24\mathrm{h}}}{t_{\mathrm{daylength}}}, \qquad (5)$$

"G is the monthly average irradiance, $t_{\mathrm{daylength}}$ is the time of the daylight, calculated as monthly average, for all latitudes of the study site every 0.25°[C]" (Panagea et al., 2014).

Considerations for integration into the CDS Toolbox

- Temperature (K): Temperature statistics for Europe derived from climate projections

Irradiance:

1. Dimensionless: Surface albedo 10-daily gridded data from 1981 to present
2. W/m^2: Climate data for the European energy sector from 1979 to 2016 derived from ERA-Interim

Method 4 (Hassanpour et al., 2019)

The results of this study confirm that "the PV panel efficiency is influenced by the solar radiation, air temperature, wind speed and relative humidity. The solar PV potential fundamentally depends on the incoming solar radiation, which is strongly dependent on geographic location, but it is also well-known that the system's efficiency depends on the temperature of the solar cells, and the temperature of the solar cells is a function of the local microclimate" (Hassanpour et al., 2019).

1. Energy Balance

"Steady state is assumed, and the atmosphere is modeled under a neutral stratification as a first order approximation. The consequence is that the energy storage term is neglected and that the ground temperature is equal to the air temperature. The resultant energy balance of the panel is expressed as" (Hassanpour et al., 2019):

$$(1-\alpha-\varepsilon)R_{\downarrow}^{sun}+L_{\downarrow}^{sky}+L_{\uparrow}^{g}-2L^{p}-2q_{conv}=0,$$

Where **ε** is the efficiency of the solar panel, **α** = 0.2 is the PV panel surface albedo**,** R^{sun} is the measured incoming shortwave radiation from the sun.

Particular application: Oregon, USA (Hassanpour et al., 2019)

The microclimate-informed PV efficiency model is validated using field data (Hassanpour et al., 2017) from a 1.5 MW solar array located at Oregon State University in Corvallis, Oregon (Hassanpour et al., 2018). Climatic variables (temperature, relative humidity, wind speed, and incoming short-wave radiation) were collected at a height of two metres (as the solar panel height) and one-minute intervals over two years. The impact of air temperature, wind speed, and vapour pressure are available in boxplot format. We cannot assess a precise result due to standard deviation and confidence intervals but, nonetheless, tendencies are clear. Air temperature has a linear decreasing impact on panel efficiency. Wind speed is more spurious but seems to have a decreasing return to scale tendency. Finally, regarding vapour pressure, we cannot stipulate any clear tendency.

The following equation is was used (Hassanpour et al., 2019):

$$\varepsilon=\varepsilon_{ref}\left[1-A\left(T_{p}-T_{ref}\right)\right],$$

Where "ε_{ref} = 0.135, is the reference efficiency of the panel at a reference temperature", "T_{ref} = 298 K, and A=0.0051/°K is the change in panel efficiency associated with a change in panel temperature." "This linear relationship is assumed valid when the absolute value of $[T_p - T_{ref}] \leq 20$ °K" (Hassanpour et al., 2019).

"Nighttime periods and times of low sun angles (≤15°) were excluded from the analysis. In the global scale analysis, the input environmental data were provided for each 0.5°×0.5° pixel" (Hassanpour et al., 2019).

Considerations for integration into the CDS Toolbox

- Albedo (Dimensionless): ERA5-Land monthly averaged data from 1981 to present
- Irradiance (W/m^2): Climate data for the European energy sector from 1979 to 2016 derived from ERA-Interim
- Radiation (W/m^2): ERA5 monthly averaged data on single levels from 1979 to present

- Air temperature (K): ERA5 monthly averaged data on single levels from 1979 to present

2.1.3.2 Dust and Ash

- **Climate impact**

Dust and ash deposition on the PV cells reduces efficiency of solar panels because they impede panels from totally absorbing solar radiation, and hence, the energy produced decreases.

- **Summary of results**

The impact of dust accumulation on solar PV efficiency is -1.5% per 0.4mg/cm^2. We also find that efficiency decreases by 7% for any dust accumulation. For power output, the decrease is in the range [2.5%; 30%; 84%] for dust accumulation in mg/cm^2 of [0.06; 0.4; 25].

- **Results**

In a study done by Kaldellis & Fragos (2011), "a considerable deterioration of the PV panels' performance is obtained, that is, an almost 30% energy reduction per hour or a 1.5% efficiency decrease (in absolute terms) for ash accumulation on the panels' surface reaching up to 0.4 mg/cm^2." Even a relatively small ash deposition (i.e., 0.06 mg/cm^2) may cause an almost 2.5% reduction in the generated power output (Kaldellis & Fragos, 2011).

Furthermore, the effects of dust accumulation on PVs' surfaces have been experimentally investigated by El-Shobokshy and Hussein (1993) to aimed to relate the dust deposition density with the short circuit current and power output variation. According to the results obtained, "atmospheric dust particles with a mean diameter of 80 mm may reduce the PV panel's short circuit current and the power output by about 82% and 84%, respectively, when the dust deposition density is almost 250 g/m^2."

Kaldellis and Fragos (2011) describe Kappos et al.'s 1996 study to determine "the relationship of"natural dust deposition on PV surfaces with the corresponding voltage output under various PV panels' tilt angles [which] showed that the particle deposition is directly proportional to the inclination of the PV panel." Particularly, for the vertically placed PV modules, the mean decrease of the PV voltage output after three months of observation was 5% in contrast to the respective 20% for the PV modules placed horizontally.

Finally, Meral and Dincer (2011) estimated that, for a "100 MW solar panel," the impact of dust is typically a reduction factor of 0.93. "A manufacturer may rate a particular PV module output at 100 W of power under standard test conditions and call the product a '100 W PV module.'"

Example: The "output power of a PV module reduces as the module temperature increases. When operating on a roof, a PV module will heat up substantially, reaching inner temperatures of 50–75°C. For crystalline modules, a typical temperature reduction factor is 89% or 0.89. So the 100 W module will typically operate at about 95W× 0.89 = 85W under full sunlight conditions" (Meral & Dincer, 2011). Concerning dust, a typical annual dust reduction factor to use is 93% or

0.93. A “100 W module” may operate on average at about 85 W × 0.93 = 79 W” (Meral & Dincer, 2011).

2.1.4 Hydropower Technology

Hydropower is using water that is constantly moving through a vast global cycle, which is an endless and constant recharging system that can be used to produce electricity. Hydropower represents the process and technology required to turn water flow into electricity. Turbines are used to convert the kinetic energy of water into electricity and the process is aided by natural water flow.

2.1.4.1 Stream Flow

- **Climatic impact**

Stream flow is a component of the water cycle, as it depends mainly on precipitation, runoff, and sun. The stronger the stream flow is, the more power a hydropower plant is able to produce.

- **Summary of results**

For RCP 4.5 and RCP 8.5 scenarios, annual energy production would decrease in the range of 6.1% to 58.6%. We also learn that a 1% change in river discharge would result in a 1% change in power generation.

- **Results**

In southeast Brazil, in the Rio Grande River basin region, De Oliveira et al. (2017) found out that, in general, based on their baseline period (1961–2005) and scenarios (RCP 4.5 and 8.5, 200–2099), stream flow will decrease and lead to “reductions in hydropower potential, decreasing the annual energy production from between 6.1% and 58.6% throughout the 21st century” (De Oliveria et al., 2017).

From an article by Wilbanks et al.(2008), we learn that the “sensitivity of hydroelectric generation to changes in precipitation and river discharge is high: a 1 percent change in precipitation or river discharge typically results in 1 percent change in generation (ORNL, 2007)” (Wilbanks, 2008).

- **Methodology**

Method 1 (De Oliveira et al., 2017)

The SWAT model taken from Ullrich and Volk (2009) "was used to simulate the hydrological behaviour of the headwaters under the Representative Concentration Pathways 4.5 and 8.5 scenarios" (De Oliveira et al., 2017).

Hydropower potential (De Oliveira et al., 2017):

$$N_P = Q \times H \times \rho_w \times g \times \eta \qquad (6)$$

where N_P is the hydropower potential (W); Q is the stream-flow ($m^3 s^{-1}$); H is the hydraulic head (m); ρ_w is the water density ($kg\,m^{-3}$); g is the gravitational acceleration ($m\,s^{-2}$); and n is the total plant efficiency.

Considerations for integration into the CDS Toolbox

- Water quantity indicators for Europe
- CDS API ONLY: River discharge and related historical data from the Global Flood Awareness System

Method 2 (Eliasson & Ludvigsson, 2000)

Produced Power (Eliasson & Ludvigsson, 2000):

$$F_{re}(t) = \gamma\, Q(t)\, H_{br}$$

F_{re}	Produced power
$Q(t)$	Flow through the station.
H_{br}	Gross head
γ	Unit weight of water
t	time

Method 3 (Engineering ToolBox, n.d.)

The practically available power is estimated as follows (Engineering ToolBox, n.d.):

$P_a = \mu \rho q g h$ (2)

where

P_a = power available (W)

μ = efficiency (in general in the range 0.75 to 0.95)

ρ = density (kg/m^3) (~ 1000 kg/m^3 for water)

q = water flow (m^3/s)

g = acceleration of gravity (9.81 m/s^2)

h = falling height, head (m)

Considerations for integration into the CDS Toolbox

- Water quantity indicators for Europe

2.1.4.2 Precipitation/Runoff

- **Climate impact**

Precipitation influences hydropower generation through water availability. If there are droughts, water quantity may be insufficient to generate electricity or for a hydropower plant to operate at full capacity.

Runoff is the result of the incapacity of the soil to absorb or contain high levels of water. When water is not absorbed, it is conveyed into rivers, becoming usable for hydropower stations.

- **Summary of results**

We found that a 1% change in precipitation implies a 1% change in power generation.

- **Results**

In the Zambezi River Basin, Yamba et al. (2011) discovered that future power potential will fluctuate over time (2010–2070). It is forecasted that, between 2010 and 2030, there will be a decrease, followed by a partial recovery between 2030 and 2050, and finally a more marked decline until 2070.

In the United States, the U.S. Department of Energy and Department of Homeland Security indicates that the "sensitivity of hydroelectric power generation to changes in precipitation and river discharge is high; in the range of 1.0+ which means that a sensitivity level of 1.0 means that

one percent change in precipitation results in one percent change in power generation" (Choi et al., 2011).

- **Methodology**

Method 1 (Yamba, et al., 2011)

1. Precipitation (Yamba, et al., 2011):

$$P = Q + E \pm S \pm G$$

P	precipitation or rainfall
Q	surface and subsurface run-off
E	evapo-transpiration losses
S	change in soil moisture
G	change in groundwater, (Pitman, 2001)

2. Efficiency (Yamba, et al., 2011)

$$P_{Gross} = \frac{\rho_{WATER} * g * H_{GROSS} * Q}{10^6}$$

P_{Gross}	gross power (MW)
ρ_{WATER}	density of water (kg/m^3)
G	acceleration due to gravity (m^2/s)
H_{GROSS}	gross head (m)
Q	annual run-off into the reservoir (m^3/s)

Considerations for integration into the CDS Toolbox

- ERA5-Land monthly averaged and hourly data from 1981 to present
- Soil moisture gridded data from 1978 to present

2.1.5 Gas Power

Natural gas, after extraction, is mixed with air for combustion and, through the use of turbines, it generates electricity.

Gas turbines in power stations are composed of three parts: the compressor, which draws air into the engine; the combustion system, where the natural gas is mixed and combusted with air; and the turbine, where the hot combustion gas comes and rotates the blades.

In the next sections, International Organization for Standardization (ISO) standard reference conditions are cited, which are conditions on levels for ambient air temperature (15˚C),

atmospheric pressure (101.32 kPa), and relative air humidity (60%) to determine the efficiency of thermal power generation.

2.1.5.1 Air Temperatures

- **Climate impact**

"Gas turbine power output increases when it is cold and decreases when it is hot. This is due to the following:

- A gas turbine is a fixed volume machine. You can only squeeze a fixed volume of air through the compressor and turbine.
- The density of air increases when it is cold. Colder air means more mass of air in the same amount of volume.
- The amount of power generated in the turbine increases with a higher mass of air flowing through the turbine.

Ambient temperature also has an effect on the compressor. Colder air improves compressor efficiency. This means that the compressor consumes less power, leading to more power supplied to the generator" (Green, 2020).

- **Summary of results**

From our literature, it emerges that, for air temperature range [+1˚C; +5.56˚C (10˚F); +10˚C (10K); +35˚C], the impact on gas power plant output (decrease) is [0.12%–0.45% and 0.5%–0.9% on average; 3%–4%; 5%–10%; 24%], respectively.

For absolute values, two of our references state a decrease in MW with values of [1.47; 2.4] for an increase in temperatures in the order of [+1˚C; +5.56˚C (10˚F)], respectively.

- **Results**

In the United States (East Coast for most of the plants), Maulbetsch and Di Filippo (2006) estimated output regarding ambient temperature for wet- and dry-cooled plants. A marked decline in efficiency can be observed, especially for dry-cooled power plants, with plant output being 500,000 kW with 35°F and declining to 450,000 kW with 105°F for both wet- and dry-cooled plants.

In Dubai, De Sa and Al Zubaidy (2011) compared efficiency relative to ISO conditions and found that "for every Kelvin (K) rise in ambient temperature above ISO conditions, the gas turbine loses 0.1% in terms of thermal efficiency and 1.47 MW of its gross (useful) power output" (De Sa & Al Zubaidy, 2011).

In Greece, Kakaras et al. (2006) found that, “depending on the gas turbine type, power output is reduced by a percentage between 5% and more than 10% of the ISO-rated power output: 15°C for every 10K increase in ambient air temperature” (Kakaras et al., 2006). .

In Saudi Arabia, Basha et al. (2011) showed that, in absolute terms, plant net output from a 70 MWe gas turbine frame using natural gas increases from 53.3 to 55.7 MWe for a decrease in temperature by 10°F.

In Vietnam, for a particular application, Asian Development Bank (2012) found that

> there is an approximate 0.57% decrease in power output for each degree increase in air temperature. … It may appear peculiar that power output decreases over the entire range of temperature while net efficiency increases up to 29˚C. With a gas turbine, power output and energy efficiency decrease as air temperature increases. On the other hand, with a steam turbine, air temperature increase leads to a rise in exhaust gas temperature, which in turn improves the power output and efficiency of the steam turbine. The CCGT O Mon IV power plant has a configuration of 2-2-1: two gas turbines each with a power output of 260–290 MW, two heat recovery steam generators with a capacity of 714 tonnes/h, and one steam turbine with a power output of 264–289 MW. A decrease in the output of the gas turbines would have caused greater impact to the system than the increase in the output of the steam turbine. Since gas turbines represents 2/3 of the overall power output from O Mon IV, overall output decreases with temperature increase.

Petchers (2003) arrived at the conclusion that, for every “1˚C increment in the ambient temperature, the amount of the reduction in power output is nearly 0.9%, with the increase of the ambient temperature, the density of the air decreases. Consequently, the air mass flow rate into the turbine decreases so the gas turbine power output reduces.”

Shukla and Singh (2014) affirmed that the “gas turbine output is a strong function of the ambient air temperature, with its power output dropping by 0.5%–0.9% for every 1˚C increase in ambient temperature.”

Finally, Ghamami et al. (2016) estimated that for each “that for one degree Celsius rise in temperature ambient air, intake and exhaust gas temperature of the turbine decline by an average of 0.4 degrees Celsius, respectively for a 0.17°C increase.”

On the other hand, it is worth mentioning that impacts vary, and other factors have to be considered. For instance, Henry and Pratson (2016) criticize studies that “predict that droughts and hotter water and air temperatures caused by climate warming will reduce the efficiency (η) of thermoelectric plants,” specifically citing the range 0.12%−0.45% for each 1°C of warming. The article notes that efficiency and power output are not significantly correlated, and magnitude is lower than assumed. The authors indicate that efficiency and power output depend also on plant attributes such as age, nameplate capacity, fuel type, average heat rate, and location (Henry & Pratson, 2016).

In a specific case study elaborated by Singh and Kumar (2012), in estimating the impact of air temperature change impact on a specific plant, they find that an "11% decrease in the mass flow rate of air is caused by the increased in ambient air temperature from 5 to 40˚C." Following the same changes, "net power output from the gas turbine decreases by 24% and plant efficiency by 9%. Power output from a steam turbine is found to decrease by 9%. Also, the mass flow rate of steam is decreased by 10%" (Singh & Kumar, 2012).

According to a report by Acclimatise (2009), "there is a linear relationship between air temperature and turbine efficiency: a 10 degree Fahrenheit (5.56˚C) increase in ambient temperature would produce as much as a 3–4% reduction in power output" (also valid for coal power plants).

- **Methodology**

Method 1 (Maulbetsch & Di Filippo, 2006)

Relative EGP = 1 - (MAX (0, "Td" - "2.7") * "0.21")/100

Relative EGP = relative efficiency of gas-powered generation
2.7 = the lowest temperature in the Maulbetsch study
Td = daily temperature
0.21 = the percent reduction in efficiency per °C

Considerations for integration into the CDS Toolbox

- 2 m Temperature: ERA5 monthly data
- 2 m Temperature: CMIP5 monthly data

Method 2¨(Asian Development Bank, 2012)

Particular application to a project and established power plant named O Mon IV, located in Vietnam.

"The net plant efficiency under the PECC3 simulations peaked at 29°C and then exhibited a gradual linear decrease in efficiency with further increases in temperature…. This relationship can be approximated as linear for temperatures greater than 29°C, with a 0.01% decrease in efficiency with each 1°C increase in temperature. Power output of O Mon IV showed a strong and decreasing linear trend (R2 = 0.999) according to the equation" (Asian Development Bank, 2012):

$$P(T) = -24{,}54T + 4465{,}6$$

"Where P(T) is energy output measured in GWh/year. Based on this trend, there is an approximate 0.57% decrease in power output for each degree increase in air temperature" (Asian Development Bank, 2012).

Considerations for integration into the CDS Toolbox

- Temperature (K): ERA5-Land hourly data from 1981 to present

2.1.5.2 Ambient Pressure

- **Climate impact**

With increases in elevation, the density of the air reduces, thus ambient pressure reduces and has a negative impact on gas power output.

- **Results**

Petchers (2003) estimated that, "as a result of mass flow rate, fuel rate and the power output of the gas turbine reduce nearly by 3.5% for each 1,000 feet (305m) of elevation above the sea level."

2.1.5.3 Humidity

- **Climate impact**

Humidity is related to air temperature. In general, lower temperatures imply more humidity and a more efficient gas power plant.

- **Summary of results**

We observe that there is a +0.65% in thermal efficiency for every +15% relative humidity. At an ambient condition of 60˚C, having relative humidity of 100% leads to -1% in efficiency and +25% in specific work output.

- **Results**

Jabboury and Darwish (1990) found that "a decrease of 1% in efficiency and an increase of 25% in specific work output were observed when operating at an ambient condition of 60°C and 100% relative humidity, over that of 60°C and 0% relative humidity. This shows the reason for injecting steam in the compressed air before the combustion chambers in some experiments to increase the power output."

In another article, Shukla and Singh (2014) state that thermal efficiency increases with an increase in "relative humidity from 0 to 100 percent for a particular CIT. There is 0.65 percent increase in thermal efficiency for every 15 percent increase of relative humidity."

Considerations for integration into the CDS Toolbox

- ERA5 single level hourly data from 1981 to present

2.1.5.4 Water temperature

- **Climate impact**

Increasing water temperature has a negative impact on the cooling system, mainly in a combined-cycle gas turbine power plant.

- **Results**

In a report based in Vietnam, the Asian Development Bank (2012) estimated that, based on their analysis, “annual power output in 2040 could be reduced by 25.3 GWh due to changes in river water temperature alone, representing a 0.6% reduction in power output. Net efficiency could also decrease by 0.3%, down to 55.2%.”

- **Methodology**

”The relative efficiency [of production is] a function of river water temperature. For river water temperatures greater than 25˚C, there is an approximately parabolic relationship between water temperature and efficiency, expressed by the following equation” (Asian Development Bank, 2012):

$$\varepsilon = -0.006\ T_{river}^2 + 0.2988\ T_{river} + 51.96$$

where T_{river} is the river water temperature in degrees Celsius.

Considerations for integration into the CDS Toolbox

- Water quantity indicators for Europe

2.1.6 Coal Power

More than half of the electricity produced in the world is from coal. In order to extract energy from coal, power plants burn it in furnaces to extract carbon and oxygen that, combined, will produce carbon dioxide and heat. Then the heat is used to boil water to produce high-pressure and high-temperature steam, which is then piped into turbines that rotate and generate electricity.

Coal power plants are subject to climate risks that would affect their production efficiency in about the same order as other power plants. Some of the impacts are similar to gas power plants.

Many of the results shown below apply also to gas and nuclear power plants.

2.1.6.1 Precipitation

- **Climate impact**

Precipitation has an impact on coal power plants through soil moisture. While soil moisture also depends on region and soil characteristics, precipitation plays a big role as it infiltrates soil. When coal becomes more humid, power plants need a higher amount of energy to burn it.

- **Summary of results**

Precipitation increases moisture (and coal humidity): for each +1% in moisture there is a -4% plant load factor. In one of the studies reviewed, 1,048 heavy precipitation events were recorded for one year, and their impact on the power distribution network, on average, was of 0.99 outage-hour/year.

- **Results**

In India, Bhatt and Rajkumar (2015) compared inherent soil moisture to surface moisture regarding soil characteristics. Bhatt analyzed the cost of production and efficiency of power generation and estimated that an increase of 1% of total moisture will reduce the plant load factor by 4%.

In Malaysia, Handayani et al. (2019) studied the impact of many climate variables on coal power plants (as well as nuclear and gas power plants). In 2014, Bali and Java experienced 354 floods and in 2015 it experienced 19 floods. As a result, they experienced an average “16 outage hours and 1.7 outage hours, respectively, for each affected customer.”

Extreme rain events also impacted the distribution of electricity. “Between 2014 and 2015, heavy precipitation caused 1048 events of power outages in the Java-Bali distribution network. These events resulted in 8.3 gigawatt-hour ENS (energy not supplied) that is equal to an estimated loss of more than 0.5 million USD over the two years. Each underwent an annual average of 0.99-outage-hour due to heavy-precipitation-related failures in distribution networks” (Handayani et al., 2019).

- **Methodology**

Decrease in boiler efficiency due to moisture increase (Bhatt & Rajkumar, 2015):

$$Y = -0.02X^2+0.358X+81.87$$

Unit heat rate:

$$Y = 0.631X^2-11.56X+2628$$

Considerations for integration into the CDS Toolbox

- Soil moisture gridded data from 1978 to present

2.1.6.2 Air and Water Temperature

- **Climate impact**

Coal combustion in the boiler requires air. If air temperature increases, density decreases and more air will be needed for the combustion. “Water is used to extract, wash, and sometimes transport coal; cool the steam used to make electricity in the power plant; and control pollution from the plant.” When water temperature increases, cooling of the steam system becomes less efficient and the power plant loses efficiency. (How it works: Water for Coal, 2010)

- **Summary of results**

As water temperature increases by 1˚C, the impact on coal power plant efficiency is -0.02% (once-through cooling system) and -0.017% (open-loop system).

Air temperature change from a base case (42˚C) of range (˚C) [42; 42.7; 45; 47; 50] has an impact on air pre-heater efficiency change of [89.94; 86.22; 79.99; 77.6; 76.04], respectively, and also on overall change in efficiency of [77.29; 73.38; 65.54; 62.43; 55.38], respectively. Another study without a base case estimated that, for each +5˚C, there would be a decrease in efficiency of 0.34%.

- **Results**

In the United States, Colman (2013) used regressions drawing on U.S. Geological Services and the National Oceanic and Atmospheric Administration (NOAA) air and water temperature data and Environment Protection Agency records of power plant fuel consumption and power output to conclude that “a 1°C increase in water temperature is correlated with a 0.02 percentage point decrease in plant efficiency when using a once-through cooling system. For an open-loop coal power plant, mean water temperature increase of 1˚C effect is of -0.017 reduction in efficiency.”

In India, Bhattacharya and Sengputa (2016) estimate the effect of change in ambient air temperature “to assess the performance of regenerative air pre heater with reference to a field study of 135 MWe subcritical steam power plant.”

T_{ae} (°C) change [42; 42.7; 45; 47; 50] translated into η_{APH} (%) [89.94; 86.22; 79.99; 77.6; 76.04] and lately into overall change in efficiency $\eta_{overall}$ (%) [77.29; 73.38; 65.54; 62.43; 55.38].

In a report for European Commission, Rademaekers et al. (2011) found that fossil-fuelled power plants will be impacted by an extreme rise (5˚C–10 ˚C) in sea water temperature (for power plants

close to shores). Additional investments will be needed for cooling towers at around EUR 100 per kW.

2.1.7 Nuclear Power

The energy generated by a nuclear power plant is extracted from atomic energy resulting from a fission process from radioactive isotopes. Water is required to cool nuclear reactors, preventing it from overheating and melting down.

2.1.7.1 Water Temperature

- **Climate impact**

Water temperature has an important effect on the cooling systems required by nuclear power plants. If the water is too hot, the cooling system won't be efficient and it could result in a decrease in power output, shutdown, or even physical damage to the plant.

- **Summary of results**

When compiling all our references and establishing averages and ranges, it emerges that an increase of water temperature (in ˚C) of [+1; +5; +10; +15-30] has a negative impact on efficiency of [0.12%–0.16%; 0.76%–1%; 1.52%; 2.27%], respectively. The power output decrease is in the range of [0.39%-0.45%; 2.17%; 4.37%; 6.55%], respectively. Also, we found that the summer capacity of a power plant decreases by 6.3–19% in Europe and 4.4%–16% in the United States for an average increase in water temperature of 1.4–2.4˚C.

- **Results**

Ibrahim et al. (2014) estimated that, when the "cooling water inlet temperature increases by 1°C, 5°C, 10° C, and 15–30°C, the thermal efficiency decreases by 0.16, 0.76, 1.52, and up to 2.27%, respectively."

The authors also estimated "the variation of net power output with cooling water inlet temperature and found that an increase [of water inlet temperature] of 1°C, 5°C, 10°C, and 10–35°C corresponds to decrease in W_{net} by 0.39293%, 2.166%, 4.3683%, and 6.547%, respectively" (Ibrahim et al. 2014).

In another article, Van Vilet et al. (2012) estimate the water temperature impact related to nuclear power plants close to river flows. "The performance of the modelling framework was tested for the historical period 1971–2000. Observed daily series of river flow and water temperature for 1,267 river discharge stations and 240 water temperature monitoring stations were used to evaluate the quality of the simulations for Europe and North America. They calculated changes in daily water temperature for the 2040s and 2080s.

"The overall projected increase in mean summer (21 June–20 September) water temperatures is 0.7–0.9 (1.4–2.4 ˚C) for the US and 0.8–1.0 (1.4–2.3) ˚C for EU. This implies a summer average decrease in capacity of power plants of 6.3–19% in Europe and 4.4–16% in the United States depending on cooling system type and climate scenario for 2031–2060. In addition, probabilities of extreme (>90%) reductions in thermoelectric power production will on average increase by a factor of three" (Van Vilet et al., 2012).

Additional information was provided by Durmayaz and Sogut (2006) who stipulated that "the impact of 1˚C increase in temperature of the coolant extracted from environment is predicted to yield a decrease of ~0.45 and ~0.12% in the power output and the thermal efficiency of the pressurized-water reactor nuclear-power plant considered, respectively."

A report for the European Commission, Rademaekers et al. (2011) indicate that "an increase of 5K of water temperature would decrease nuclear powerplant efficiency by 1%."

Finally, in a study on the Mediterranean region, Attia (2015) arrived at the conclusion "that an increase of one degree Celsius in temperature of the coolant extracted from environment is forecasted to decrease by 0.444% and 0.152% in the power output and the thermal efficiency of the nuclear-power plant considered."

- **Methodology**

Several equations could be derived from the examples listed above. Durmayaz and Sogut (2006) provide one example, presented in Figure 1.

Figure 2. Impact of cooling seawater temperature on thermal efficiency and power output

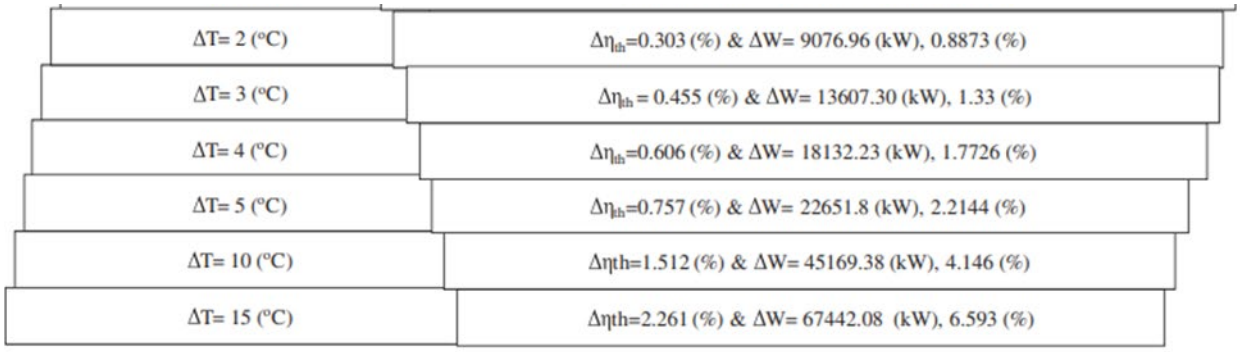

Fig. 8. The impact of cooling seawater temperature, T_{cwi} on the thermal efficiency and output power of the NPP.

Source: Durmayaz & Sogut, 2006.

Considerations for integration into the CDS Toolbox

- Water quantity indicators for Europe

2.1.7.2 Air temperature

- **Climate impact**

Ambient temperature is linked to water temperature and hence the cooling system efficiency. A warmer climate may result in lower thermal efficiency and a reduced load—including shutdowns—in thermal power plants.

- **Summary of results**

An increase of 1˚C results in the reduction in efficiency of a nuclear power plant of 0.2425% on average (0.27 (x1 article), 0.1 (x2), and 0.5 (x 1)). Another article gives two different scenarios for an increase of temperature of 1˚C: when ambient temperature is 0˚C or 20˚C, the impact is a 0.7% and a 2.3% decrease in output, respectively.

- **Results**

In France, Rousseau (2013) estimated that "the average loss in electrical output is 0.32% per increase of one degree in air temperature, with a wide difference between reactors. This average is 0.27% for the 16 median reactor."

In a report for the European Commission, Rademaekers et al. (2011) state that, "for air temperature (cooling towers), an increase in 1(K) air temperature will result in a reduction of 0.1% in efficiency.."

In a more general study across Europe, Linnerud et al. (2011) showed that "a rise in temperature of 1˚C reduces the supply of nuclear power by about 0.5% through its effect on thermal efficiency. During droughts and heat waves, the production loss may exceed 2.0% ˚C because power plant cooling systems are constrained by physical laws, regulations and access to cooling water. … When the monthly ambient temperature increases with 1˚C, nuclear power plant production is on average reduced with 0.7 percent for temperatures around 0˚C and 2.3 percent for temperatures around 20˚C" (Linnerud et al., 2011).

A study led by Lise and van der Laan (2015) provides estimated costs and efficiency changes due to various climate variables. Table 4 presents the results from their article.

Table 3. Climate change effect on power generation and the investment need for different technologies

Climate change effect	Technology	Lost power generation €/MWh/climate change effect	Investment Need €/kW	Threshold value	Remark
Change in air temperature	Nuclear	0.07	50	5	0.1% less per 1 °C increase
	Biomass	0	150	5	Negligible impact
	Natural gas	0.07	75	5	0.1% efficiency decrease per 1 °C
	Coal	0	100	5	Negligible impact
	Oil	0.07	85	5	0.1% efficiency decrease per 1 °C
	Grids	0.14	40	5	0.2% extra transmission losses per 1 °C
Change in water temperature	Nuclear	0.14	50	5	0.2% per 1 °C increase
	Biomass	0.14	150	5	Small plants have larger cost per unit
	Natural gas	0.14	75	5	Low investment costs
	Coal	0.14	100	5	
	Oil	0.14	85	5	Higher than natural gas

Source: Lise & Van Der Laan, 2015.

Considerations for integration into the CDS Toolbox

- ERA5-Land monthly averaged data from 1981 to present
- ERA5 (present) and CMIP5 (future) 2m air temperature

2.1.8 Geothermal Power

Geothermal power is generated by making use of the temperature difference existing between surface and water in underground wells. Dry steam or hot water is extracted and used to generate electricity with turbines.

2.1.8.1 Air Temperature

- **Climate impact**

Higher temperatures have a negative impact on the efficiency of the geothermal power plants cooling down the system.

- **Summary of results**

Power output will decrease by about 1% for each 0.56˚C (1˚F) increase in air temperature.

- **Results**

An article published by the U.S. Department of Energy indicates that climate change could affect geothermal energy production in “the same way that higher temperatures reduce the efficiency of fossil fuel boiler electric turbines” (Wilbanks et al., 2008). On the other hand, “there is no recent research on other potential impacts in this sector due to climate change. For a typical air-cooled binary cycle geothermal plant with a 330°F resource, power output will decrease about 1% for each 1°F rise in air temperature” (Wilbanks, 2008).

Considerations for integration into the CDS Toolbox

- ERA5-Land monthly averaged data from 1981 to present

2.1.9 Power Grid Efficiency

The power grid is the network of power lines, alternators, cables, etc. that provides electricity from power plants to consumers. Weather can have an impact on these infrastructures, resulting in power shutdown or loss of efficiency. When efficiency drops, power plants will have to produce more electricity in order to meet consumer demand.

Climate hazards such as earthquakes, storms, and lightning can create physical damage will results in a need to replace or repair the infrastructure. Climate drivers such as wind, precipitation, and mainly temperature can directly affect components, such as the cables, resulting in loss of efficiency.

2.1.9.1 Temperature

- **Climate risk**

As mentioned above, extreme changes in temperature affect the physical properties of the infrastructures, such as cables, resulting in higher losses.

- **Summary of results**

For transformers, for each 1˚C increase in temperature, there is a 1% reduction in efficiency.
For the overall network, for each 1˚C increase there is also a decrease of 1% on output capacity. Furthermore, for each supplementary 3˚C increase, for an initial network with 8% initial losses, there is a 1% loss in output.

One study assessed that the impacts of carbon “emission scenarios RCP 2.6, 4.5 and 8.5” on the transmission capacity are decreases by 1.9%–3.9%, 2.2%–4.3%, and 3.6%–5.8%, respectively.

- **Results**

In a report for the European Commission, Rademaekers et al. (2011) disclose that the “maximum temperature at which the electrical network is bounded is, in general, 80˚C at the conductor surface.” Naturally, when the temperature rises, network capacity declines as the resistance of metals increases and the system reaches its “maximum operating temperature” sooner. “The capacity of transformers, for example, can decrease by up to 1% for each 1°C (Martikainen et al., 2007). Similarly, the resistance of copper lines increases by approximately 0.4% for each 1°C. Altogether, network capacity falls by around 1 percent for each for each 1°C of temperature increase. In addition, network losses can increase by 1% if temperature increases by 3°C, in a

network with initial losses of 8% (International Energy Agency, 2008)" (Rademaekers, et al., 2011). Cables sag with higher temperatures, though "the extent of sagging depends on the conductor material; the span width and other environmental conditions like wind-speed. For conventional aluminum cables it is approximately 4.5 cm per 1°C rise at the conductor surface with a threshold of 50˚C" (Rademaekers et al., 2011).

Bartos et al. (2016) present a case study in the United States on the ambient temperature's effect on electric transmission capacity. They found out that, "by mid-century (2040–2060), rising air temperatures may reduce summertime transmission capacity by 1.9%–5.8% on average, relative to the 1990–2010 reference period (with the range of impacts being dependent on GCM model and RCP scenario selection)."

They also investigated three scenarios and stipulated that, "by mid-century, average transmission capacity reductions range from 1.9%–3.9% under the lowest carbon concentration scenario (RCP 2.6), to 2.2%–4.3% under the medium carbon concentration scenario (RCP 4.5), to 3.6%–5.8% under the highest carbon concentration scenario (RCP 8.5)" (Bartos et al., 2016).

"On a website section, from Drax, a company specialized in the electricity sector, we can read that when ambient temperatures rise, the ceiling gets lower and their efficiency drops – about 1% for every one degree Celsius gain in temperature. At scale, this can have a significant effect: overall, grids can lose about 1% in efficiency for every three degrees hotter it gets" (Drax, 2017).

2.2 Integration of the Literature Review with the CDS dataset

As indicated in the Introduction, a subset of the indicators and equations presented above have been integrated into the CDS Toolbox. We have (i) reviewed the equations to determine their usefulness for SAVi; (ii) assessed what data requirements for each of the equations is available in the Copernicus database, to be accessed via the CDS API; and (iii) created indicators for climate variables that are relevant for the equations selected, which involves additional processing offline.

The code to download and create the indicators is detailed in Annex I.
The demonstration app in the CDS Toolbox is available at these links:

- Source code: https://cds.climate.copernicus.eu/toolbox-editor/27053/iisd-demo
- App: https://cds.climate.copernicus.eu/apps/27053/iisd-demo

Scientific considerations

We used a systematic approach in all asset classes. We focused on climate variables that are available in two datasets: ERA5 for past re-analysis data (year 1979 to 2019) and CMIP5 for future projections (2006 to 2100, but also including historical simulation from 1979 to 2005). The datasets differ in various ways, including model formulation, time-step, and available variables. For some variables, harmonization was necessary, such as conversion of units of measure, as indicated below. ERA5 is a more detailed dataset, and integrates climate observations, whereas

CMIP5 is a coarser dataset specifically intended to test the effect of human activities on the climate, useful for long-term projections but less precise for past and present days. To make CMIP5 data more useful, they were corrected it so that monthly mean over the historical period (1979–2019) matches ERA5. This is a typical operation commonly called bias-correction. The CMIP5 dataset provides climate variables for various models and future climate scenarios. In this work, we use four climate models (IPSL CM5A MR, BNU ESM, CSIRO MK3 6.0, and MPI ESM MR) and two climate scenarios (RCP 8.5 for a fossil fuel-intensive, high-emission scenario and RCP 4.5 for mitigation scenario with carbon dioxide emissions peaking in 2040). We thus have nine versions of each climate indicator (1 ERA5 and 8 CMIP5). Using different climate models and scenarios is useful to assess the robustness of the results. To perform a full uncertainty analysis, SAVi simulations should be performed for each of the versions, and statistics like mean or range should be calculated on SAVi results rather than the other way around (we do not recommend using the mean across models before reading into SAVi). Alternatively, if only one climate scenario should be used, we recommend using RCP 8.5, with IPSL CM5A MR as default climate model. We recommend always comparing to an ERA5 simulation, which shall be considered a reference dataset for the past period.

App design considerations

The data is retrieved via the CDS API for all practical purposes, but a demonstration app was also developed for the following indicators: “temperature_2m,” “precipitation,” “runoff,” “evaporation,” “10m_wind_speed.”

2.2.1 Wind Technology

Datasets:

- ERA5 single-level monthly data
  - 10 m wind speed
  - 100 m wind speed (from u and v component)
- CMIP5 monthly data on single level:
  - 10 m wind speed

Indicators created:

- **10 m wind speed:**
  - **Units: m/s**
  - Frequency: monthly
  - Versions: ERA5 and CMIP5
- **100 m wind speed:**
  - **Units: m/s**
  - Frequency: monthly

- Versions: ERA5 and CMIP5
- CMIP5 10 m wind speed was scaled by 1.65 as first-order harmonization with ERA5 100 m (see additional information below).

Additional information:
In addition to 10 m wind speed, we use wind speed at 100 m from ERA5, as it represents more accurately the wind experienced by large turbines and unaffected by the boundary layer. For future projections, we use CMIP5, 10 m wind speed, which we scale to match ERA5 100 m during the period of overlap (1979 to 2019, which resulted in a scaling coefficient of 1.65 for an example location).

Before use, wind data must be corrected to match the appropriate height based on methods listed in the review (Davy et al., 2018).

2.2.2 Wave Technology

See 10 m wind speed and 100 m wind speed above.

2.2.3 Solar technology

Datasets:

- ERA5 monthly data on single level:
  - "mean_surface_downward_short_wave_radiation_flux"
    - Note: another variable, "surface_solar_radiation_downwards" was also available but expressed in J/m^2 (cumulative), which is why we opted for the above variable, as we prefer mean flux W/m^2
  - "2-m air temperature"
  - "10 m wind speed"
- CMIP5 monthly data on single level:
  - "surface_solar_radiation_downwards"
  - "2-m air temperature"
  - "10 m wind speed"

Indicator created:

- **Solar radiation**:
  - Units: W/m^2
  - Frequency: monthly
  - ERA5 and CMIP5 versions
  - Note this variable already integrates cloud cover, so we do not provide the cloud cover variable here.
- **Air temperature**:

- Units: degrees Celsius
- Frequency: monthly
- Versions: ERA5 and CMIP5
- Note: converted from Kelvin to degrees Celsius

- **10 m wind speed:**
  - **Units: m/s**
  - Frequency: monthly
  - Versions: ERA5 and CMIP5
  - **Not yet implemented**

Additional information

Dust and ashes data were not considered specifically, though they should be accounted for in the "solar radiation" indicator, as CMIP5 models typically include a component for dust and volcano eruption (the latter only in the historical period).

2.2.4 Hydropower

Datasets:

- ERA5 monthly data on single level: "Mean total precipitation rate"
- CMIP5 monthly data on single level: "Mean precipitation flux"

Indicators created:

- **Precipitation**:
  - Units: mm per month
  - Frequency: monthly

Additional information

Precipitation changes shall be used here as a proxy for river discharge changes in hydropower equations. We decided to use precipitation data instead of specific products for river discharge estimation because this is the only variable that is available: 1) globally and 2) for past and future.

In particular, we decided against the following datasets:

- "River discharge and related historical data from the Global Flood Awareness System": available globally but only until present.
- "Water quantity indicators for Europe": available for future but only in Europe.

More detailed information about the precipitation variable in ERA5/CMIP5 can be found in the road asset ("road runoff").

2.2.5 Gas Power

Datasets:

- ERA5 monthly data on single level:
  - "2 m air temperature"
  - "2 m dewpoint temperature"
- CMIP5 monthly data on single level:
  - "2 m air temperature"
  - "near_surface_relative_humidity"

Indicators created:

- **Air temperature**:
  - Units: degrees Celsius
  - Frequency: monthly
  - Versions: ERA5 and CMIP5
  - Note: converted from Kelvin to degrees Celsius

- **Relative humidity**
  - Units: %
  - Frequency: monthly
  - Versions: ERA5 and CMIP5
  - Method: available out-of-the-box for CMIP5, not for ERA5. For ERA5, we calculated relative humidity from 2-m temperature T and 2-m dewpoint temperature TD (both in degrees Celsius) with the thermodynamic formula
    - 100*(exp((17.625*TD)/(243.04+TD))/exp((17.625*T)/(243.04+T)))

2.2.6 Coal Power

Datasets:

- Same as for gas power generation

Indicator created:

- **Air temperature**
  - Same as for gas power generation
- **Relative humidity**
  - Same as for gas power generation

2.2.7 Nuclear Power

Datasets:

- ERA5 monthly data on single level:
  - "2 m air temperature"
  - "Mean total precipitation rate"
- CMIP5 monthly data on single level:
  - "2 m air temperature"
  - "Mean precipitation flux"

Indicators created:

- **Air temperature**:
  - Units: degrees Celsius
  - Frequency: monthly
  - Versions: ERA5 and CMIP5
  - Note: converted from Kelvin to degrees Celsius
- **Precipitation**:
  - Units: mm per month
  - Frequency: monthly

Additional information

Some equations investigated in this section take river temperature as input. However, river temperature was not available as global datasets, as far as we could tell. In particular, we decided not to use the following dataset:

- "Water quality indicators for European rivers": only available for Europe

As a result, we suggest that river temperature can be derived from air temperature and precipitation. Additional research must be done to find a useful model formulation.

One indicator in the literature review was based on sea water temperature (for plants using sea water as a cooling source). As none of the use cases are located at the sea, nor do they relate to such a plant, we did not include sea surface temperature as a climate indicator here.

2.2.8 Geothermal Power

Datasets:

- ERA5 monthly data on single level: "2 m air temperature"
- CMIP5 monthly data on single level: "2 m air temperature"

Indicators created:

- **Air temperature**:
  - Units: degrees Celsius
  - Frequency: monthly
  - Versions: ERA5 and CMIP5

- Note: converted from Kelvin to degrees Celsius

2.3 Integration of Climate Indicators Into the SAVi Energy Model

Figure 2 presents the causal loop diagram (CLD) for the SAVi Energy model. Climate-related variables and parameters developed for and extracted from the CDS Toolbox are illustrated in pink. Energy-related climate indicators developed in the CDS Toolbox include impacts on the efficiency of thermal and renewable power generation assets as well as temperature-related impacts on grid efficiency.

Figure 4. CLD for the energy sector (CDS variables included in pink)

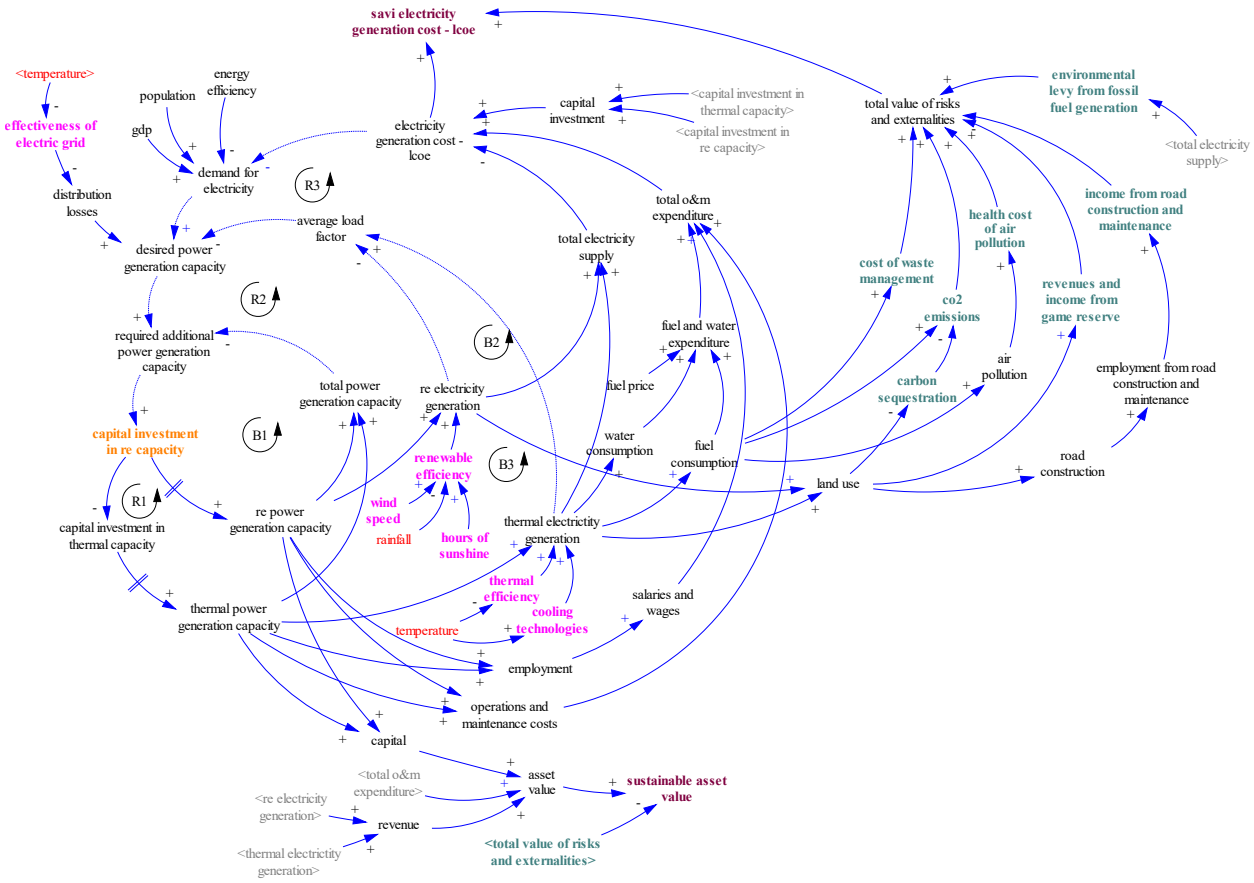

The impact of climate variables on power generation efficiency varies between thermal and renewable power plants. Thermal efficiency is reflected in the load factor of generation assets and determines the electricity yield given the amount of inputs (fossil fuels) used, technological specifications of the plant, and location. The thermal efficiency indicator is calculated based on the outside temperature and affects electricity generation output based on the extent to which an asset is affected by outside temperatures. In the case of coal, gas, and nuclear, reductions in generation efficiency were observed as outside temperatures increased. In addition to fossil fuel

generation, the efficiency of biomass technologies using heat-based technologies is also affected by temperature.

Renewable power generation potential depends on the availability of "inputs" required for renewable power generation. Climate impacts on renewable generation are technology specific. Inputs for calculating this indicator include, for example, solar radiation, cloud cover, and wind speed.

Grid efficiency indicates the amount of electricity that is lost throughout the transmission process, commonly referred to as "transmission losses." With increases in mean air temperature, the efficiency of the electricity grid declines. The grid effectiveness indicator developed for and extracted from the CDS provides information about current and future grid effectiveness, given changes in temperature. The projections forecast grid-related transmission losses, which, when added to the electricity demand, gives the amount of power generation required. This can contribute to supporting the development of energy strategies and power generation projects.

2.4 Behavioural Impacts Resulting From the Integration of Climate Variables

Power generation efficiency indicators developed for and obtained from the CDS Toolbox cause seasonal fluctuations in electricity generation and transmission efficiency. Using these CDS indicators allows us to assess the economic and environmental consequences emerging from changes in generation efficiency.

A reduction in thermal generation efficiency leads to higher fuel use and, hence, higher generation cost. In case of a reduction in plant output, either total generation will decrease and generation will be lower or the asset owners will be forced to implement site-specific measures to maintain generation at the same level or expand capacity.

The efficiency of renewable generation uses climate data to forecast generation efficiency and indicates seasonal changes in the power output of renewable generation assets. As a consequence, this indicator supports the site-specific feasibility assessment of different renewable generation technologies (e.g., revenue generation changes with seasons affecting the potential cash flow and debt repayment). Specifically, since renewable energy sources (excluding biomass) do not rely on fuel inputs and have primarily fixed costs, the profitability of the asset is more predominantly affected by the fluctuations in generation. In other words, if generation declines, electricity sales decline as well, causing the return on investment to be lower than a no-climate-impact scenario.

2.5 Simulation Results

The results presented in this section consider seven different technologies with an annual generation of 4.89 million MWh in the context of Johannesburg, South Africa. Information concerning technology types and their baseline load factors are provided in Table 5. This analysis

assumes that all technologies are established in 2020 and produce electricity between 2022 and 2100[2].

Table 5. Installed capacity and load factor

	Coal	Gas	Nuclear	Biomass	Hydro	Solar	Wind
Capacity	630.0	1,116.9	620.5	797.8	1,329.6	2,252.7	1,583.8
Load factor	88.6%	50.0%	90.0%	70.0%	56.4%	24.8%	35.3%

Three CDS-based impacts were integrated into the SAVi Energy model: (1) climate impacts on load factor, (2) the effect of temperature on thermal efficiency, and (3) the effect of temperature on transmission line efficiency.

2.5.1 Climate Impacts on Load Factor

Weather conditions and changes therein affect the degree to which capacity can be utilized to produce electricity. Furthermore, different technologies are impacted by different climate variables and to different extents. While thermal generators depend on cold water for cooling purposes, the load factor of renewables depends on the availability of the respective inputs to the energy production process (e.g., water, wind speed, solar radiation) and impacts related to technological constraints (e.g., impacts of temperature on the efficiency of solar panels).

The equations used for the integration of climate impacts on the load factor of the different technologies are listed in Table 6.

Table 6. Climate impacts on load factor by generation technology

Technology	Equation	Source
Coal Gas Nuclear Biomass	IF THEN ELSE (seasonal temperature > THRESHOLD TEMPERATURE FOR THE OPERATION OF POWER PLANTS, ((2/52) + (2/52) * (temperature relative to threshold - 1) ^ ELASTICITY OF LOAD FACTOR FOR EXCEEDING THE THRESHOLD LIMIT) ,1)	U.S. Department of Energy, 2013
Hydro	Mean annual precipitation$_{t+n}$ / Mean annual precipitation$_{t0}$	Wilbanks et al., 2008
Solar	1 - IF THEN ELSE (Mean annual temperature > Temperature threshold for optimal functioning, (Mean annual temperature - Temperature threshold for optimal functioning) * 0.01, 0)	Panagea et al., 2014

[2] Capacity lifetime varies by technology, which indicates that reinvestments would be required to maintain the installed capacity level over 80 years. The presented simulation serves for illustration purposes and does not reconsider reinvestment in capacity.

Wind	Effect of relative wind speed on load factor(Monthly wind speed$_{tn}$ / Mean monthly wind speed$_{t1-5}$)	Harrison & Wallace, 2005

Table 7 presents the average load factor and climate impacts for the context of Johannesburg for each decade between 2020 and 2100 by technology.[3]

Table 7. Load factor and climate impacts by technology

Load factor by technology	2020–2030	2030–2040	2040–2050	2050–2060	2060–2070	2070–2080	2080–2090	2090–2100
Coal								
Initial load factor	88.64%	88.64%	88.64%	88.64%	88.64%	88.64%	88.64%	88.64%
Climate impacts on load factor	0.00%	0.00%	0.00%	-0.68%	-2.05%	-9.56%	-12.97%	-27.99%
Real load factor	88.64%	88.64%	88.64%	87.96%	86.59%	79.08%	75.67%	60.65%
Gas								
Initial load factor	50.00%	50.00%	50.00%	50.00%	50.00%	50.00%	50.00%	50.00%
Climate impacts on load factor	0.00%	0.00%	0.00%	-0.39%	-1.16%	-5.39%	-7.32%	-15.79%
Real load factor	50.00%	50.00%	50.00%	49.61%	48.84%	44.61%	42.68%	34.21%
Nuclear								
Initial load factor	90.00%	90.00%	90.00%	90.00%	90.00%	90.00%	90.00%	90.00%
Climate impacts on load factor	0.00%	0.00%	0.00%	-0.69%	-2.08%	-9.71%	-13.17%	-28.42%
Real load factor	90.00%	90.00%	90.00%	89.31%	87.92%	80.29%	76.83%	61.58%
Hydropower								
Initial load factor	56.35%	56.35%	56.35%	56.35%	56.35%	56.35%	56.35%	56.35%
Historical weather impacts on load factor	14.35%	14.35%	14.35%	14.35%	14.35%	14.35%	14.35%	14.35%
Climate impacts on load factor	-1.21%	-0.56%	-4.23%	-2.97%	-2.69%	-4.03%	-5.36%	-8.00%
Real load factor	40.79%	41.44%	37.77%	39.03%	39.31%	37.97%	36.64%	34.00%
Solar								
Initial load factor	24.79%	24.79%	24.79%	24.79%	24.79%	24.79%	24.79%	24.79%
Climate impacts on load factor	-0.80%	-0.91%	-1.13%	-1.23%	-1.29%	-1.58%	-1.73%	-1.95%
Real load factor	23.99%	23.88%	23.66%	23.56%	23.50%	23.21%	23.06%	22.84%
Wind								
Initial load factor	35.26%	35.26%	35.26%	35.26%	35.26%	35.26%	35.26%	35.26%
Climate impacts on load factor	2.41%	3.22%	3.40%	3.14%	3.89%	4.34%	4.00%	4.53%
Real load factor	37.67%	38.48%	38.66%	38.40%	39.15%	39.60%	39.26%	39.79%

[3] The temperature thresholds for thermal generation and solar power were artificially reduced to show impacts in the context of Johannesburg. The threshold for thermal power plants was reduced from 35°C to 27°C and the threshold for solar power from 25°C to 15°C.

The results indicate significant reductions in the load factor for thermal producers. For illustration purposes, the temperature threshold for potential shutdowns was set to 25°C. With a projected maximum annual temperature in Johannesburg of 30°C (Climate scenario: IPSL RCP 8.5), impacts on thermal generation are forecasted to start occurring between 2050 and 2060, and increase in severity until 2100.

For renewable capacity, the results indicate a decline in load factor for hydropower and solar generation, while wind shows an increase in the load factor for wind power. In the case of hydropower, the decline in load factor is caused by the forecasted decline in precipitation for Johannesburg. Lower precipitation reduces water availability for hydropower generation and consequently reduces the potential for hydropower-based electricity generation. For solar-powered generation, impacts are throughout the simulation, with an absolute decline of 1.15% by 2100 compared to 2020. This is because the seasonal temperature exceeds the temperature threshold for optimal functioning until the last decade (2090–2100). Wind-powered generation benefits from higher wind speeds in the future, which increase the load factor on average by 4.5% by 2100.

2.5.1.1 Economic Implications of Load Factor Impacts

Table 8 presents the integrated cost–benefit analysis (CBA) assessment of the economic consequences of climate-related impacts on the load factor. The reduction in load factor has implications for the amount of electricity that can be produced with each technology, which translates into direct impacts on revenues and profits.

Between 2020 and 2100, a net reduction of between 5.15% and 8.54% in cumulative revenues is observed for all technologies as a consequence of lower capacity utilization. The only exception is onshore wind, for which results indicate an increase of 9.88% in cumulative revenues.

Table 8. Integrated cost benefit analysis impact on load factor in billion ZAR – Thermal generators

Technology	Coal			Gas			Nuclear			Biomass		
Scenario	Climate impacts	No climate impacts	*Impacts vs. no impacts*	Climate impacts	No climate impacts	*Impacts vs. no impacts*	Climate impacts	No climate impacts	*Impacts vs. no impacts*	Climate impacts	No climate impacts	*Impacts vs. no impacts*
Investment and cost												
Capital cost	17.5	17.5	*0.0%*	11.3	11.3	*0.0%*	36.6	36.6	*0.0%*	24.6	24.6	*0.0%*
Operations and maintenance (O&M) cost	42.5	42.5	*0.0%*	25.5	25.5	*0.0%*	99.2	99.2	*0.0%*	64.1	64.1	*0.0%*
Fuel cost	94.4	102.3	*-7.7%*	201.4	218.4	*-7.7%*	0.0	0.0	*0.0%*	7.6	7.6	*0.0%*
Transitional risk												
Carbon tax	51.7	56.0	*-7.7%*	13.0	14.1	*-7.7%*	0.0	0.0	*0.0%*	0.0	0.0	*0.0%*
(1) Total costs	**206.1**	**218.4**	***-5.6%***	**251.3**	**269.3**	***-6.7%***	**135.8**	**135.8**	***0.0%***	**96.2**	**96.2**	***0.0%***
Externalities												
Social cost of carbon	196.85	213.36	*-7.7%*	49.96	54.12	*-7.7%*	0.27	0.27	*0.0%*	0.31	0.31	*0.0%*
Wastewater treatment cost	6.73	7.29	*-7.7%*	14.20	15.40	*-7.7%*	37.38	40.52	*-7.7%*	22.43	24.31	*-7.7%*
Cost of ash disposal	48.66	52.74	*-7.7%*	0.00	0.00	*0.0%*	0.00	0.00	*0.0%*	0.00	0.00	*0.0%*
Health cost of air pollution	3.29	3.29	*0.0%*	1.58	1.58	*0.0%*	0.03	0.03	*0.0%*	5.24	5.24	*0.0%*
(2) Total externalities	**255.5**	**276.7**	***-7.7%***	**65.7**	**71.1**	***-7.5%***	**37.7**	**40.8**	***-7.7%***	**28.0**	**29.9**	***-6.3%***
(1) + (2) Total cost and externalities	**513.3**	**551.1**	***-6.9%***	**330.1**	**354.6**	***-6.9%***	**173.5**	**176.6**	***-1.8%***	**124.2**	**126.1**	***-1.5%***
(3) Revenues from electricity generation	283.5	307.3	*-7.7%*	283.5	307.3	*-7.7%*	283.5	307.3	*-7.7%*	283.5	307.3	*-7.7%*
(1) - (3) Cost minus revenues	**-77.34**	**-88.88**	***-13.0%***	**-32.12**	**-37.92**	***-15.3%***	**-147.63**	**-171.44**	***-13.9%***	**-187.23**	**-211.04**	***-11.3%***
(1) + (2) - (3) Net societal cost of power generation	**229.9**	**243.8**	***-5.7%***	**46.6**	**47.3**	***-1.4%***	**-110.0**	**-130.6**	***-15.8%***	**-159.3**	**-181.2**	***-12.1%***

Table 9. Integrated cost benefit analysis impact on load factor in billion ZAR – Renewable generators

Technology	Hydropower			Solar			Wind (onshore)		
Scenario	Climate impacts	No climate impacts	*Impacts vs. no impacts*	Climate impacts	No climate impacts	*Impacts vs. no impacts*	Climate impacts	No climate impacts	*Impacts vs. no impacts*
Investment and cost									
Capital cost	21.0	21.0	*0.0%*	35.2	35.2	*0.0%*	26.7	26.7	*0.0%*
O&M cost	30.4	30.4	*0.0%*	27.0	27.0	*0.0%*	54.8	54.8	*0.0%*
Fuel cost	0.0	0.0	*0.0%*	0.0	0.0	*0.0%*	0.0	0.0	*0.0%*
Transitional risk									
Carbon tax	0.0	0.0	*0.0%*	0.0	0.0	*0.0%*	0.0	0.0	*0.0%*
(1) Total costs	**51.3**	**51.3**	***0.0%***	**62.2**	**62.2**	***0.0%***	**81.5**	**81.5**	***0.0%***
Externalities									
Social cost of carbon	0.21	0.21	*0.0%*	0.52	0.52	*0.0%*	0.51	0.51	*0.0%*
Wastewater treatment cost	0.00	0.00	*0.0%*	0.00	0.00	*0.0%*	0.00	0.00	*0.0%*
Cost of ash disposal	0.00	0.00	*0.0%*	0.00	0.00	*0.0%*	0.00	0.00	*0.0%*
Health cost of air pollution	0.00	0.00	*0.0%*	0.00	0.00	*0.0%*	0.00	0.00	*0.0%*
(2) Total externalities	**0.2**	**0.2**	***0.0%***	**0.5**	**0.5**	***0.0%***	**0.5**	**0.5**	***0.0%***
(1) + (2) Total cost and externalities	**51.6**	**51.6**	***0.0%***	**62.8**	**62.8**	***0.0%***	**82.0**	**82.0**	***0.0%***
(3) Revenues from electricity generation	279.9	307.3	*-8.9%*	290.6	307.3	*-5.4%*	338.9	307.3	*10.3%*
(1) - (3) Cost minus revenues	**-228.59**	**-255.92**	***-10.7%***	**-228.35**	**-245.03**	***-6.8%***	**-257.39**	**-225.76**	***14.0%***
(1) + (2) - (3) Net societal cost of power generation	**-228.4**	**-255.7**	***-10.7%***	**-227.8**	**-244.5**	***-6.8%***	**-256.9**	**-225.3**	***14.0%***

2.5.2 Climate Impacts on Thermal Efficiency

Studies suggest that, as temperatures rise, the conversion efficiency of thermal power plants will decline. For this assessment, we assume that generators can maintain the same level of output; however, they need to use additional fuel to maintain the desired generation.

Temperature impacts on power generation efficiency only apply to thermal generators and are related to the optimal operation conditions determined by the respective technology. The equations used for each thermal technology are presented in Table 10.

Table 10. Climate impacts on thermal efficiency by generation technology

Technology	Equation	Source
Coal	Impact = 1-IF THEN ELSE (Tair>Threshold for optimal functioning, (Tair-Threshold for optimal functioning)*0.038, 0)	Bhattacharya & Sengupta, 2016
Gas	Impact = 1 - ((T - 2.76) * 0.21)/100	Maulbetsch & Di Filippo, 2006
Nuclear	Impact = 1-IF THEN ELSE (Tair>Threshold for optimal functioning, (Tair-Threshold for optimal functioning)*0.005, 0)	U.S. Department of Energy, 2013

Based on the above, climate change-related impacts on thermal efficiency cause producers to use more fuel, and, hence, incur higher costs, compared to the no-climate-impact scenario. The projected fuel use for coal and gas power generation is indicated in Figure 3 for illustration purposes.

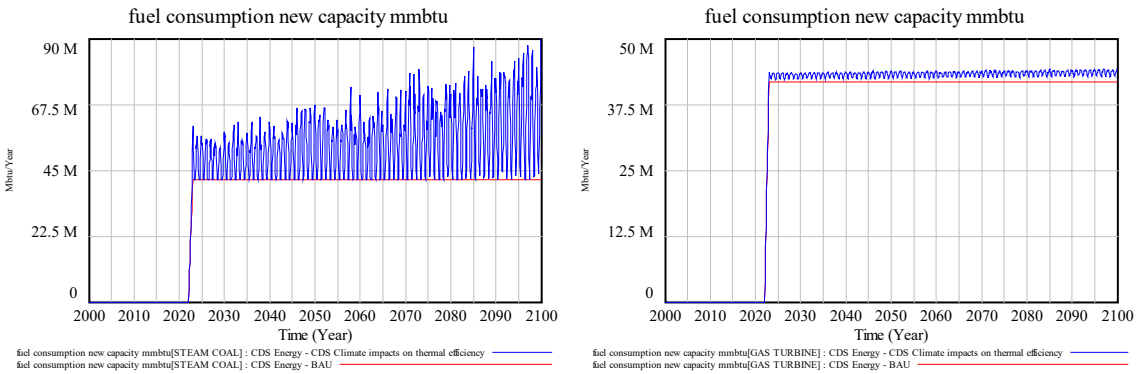

Figure 3. Fuel use for coal- and gas-powered generation with and without climate impacts

The reduction in efficiency causes thermal producers to incur higher average fuel costs with each decade. The impacts on the fuel expenditure for coal- and gas-powered power plants are presented in Table 11.

Table 11. Fuel use CDS climate-impact scenario relative to the no-climate-impact scenario

Technology	2022–2030	2030–2040	2040–2050	2050–2060	2060–2070	2070–2080	2080–2090	2090–2100
Coal	15.5%	18.1%	23.8%	26.4%	28.1%	37.5%	42.0%	50.7%
Gas	3.1%	3.2%	3.4%	3.6%	3.7%	4.0%	4.2%	4.4%

2.5.2.1 Economic Implications of Thermal Efficiency Impacts

The integrated CBA for the impacts on thermal efficiency is presented in Table 12. Climate impacts on thermal efficiency are reflected in higher fuel costs for fossil fuel-based producers. Consequently, all externalities related to fuel use, such as the social cost of carbon or the cost of fly ash disposal, increase proportionally with the use of fuel. As the tables show, there are no impacts on renewable power generation. Compared to the no-climate-impact scenario, there are no changes in capital cost or power generation-related externalities.

Table 12. Integrated CBA for climate impacts on thermal efficiency in billion ZAR – Thermal generators

Technology	Coal			Gas			Nuclear			Biomass		
Scenario	Climate impacts	No climate impacts	*Impacts vs. no impacts*	Climate impacts	No climate impacts	*Impacts vs. no impacts*	Climate impacts	No climate impacts	*Impacts vs. no impacts*	Climate impacts	No climate impacts	*Impacts vs. no impacts*
Investment and cost												
Capital cost	17.5	17.5	*0.0%*	11.3	11.3	*0.0%*	36.6	36.6	*0.0%*	24.6	24.6	*0.0%*
O&M cost	42.5	42.5	*0.0%*	25.5	25.5	*0.0%*	99.2	99.2	*0.0%*	64.1	64.1	*0.0%*
Fuel cost	133.9	102.3	*30.9%*	226.5	218.4	*3.7%*	0.0	0.0	*0.0%*	7.6	7.6	*0.0%*
Transitional risk												
Carbon tax	73.3	56.0	*30.9%*	14.6	14.1	*3.7%*	0.0	0.0	*0.0%*	0.0	0.0	*0.0%*
(1) Total costs	**267.3**	**218.4**	***22.4%***	**278.0**	**269.3**	***3.2%***	**135.8**	**135.8**	***0.0%***	**96.2**	**96.2**	***0.0%***
Externalities												
Social cost of carbon	279.13	213.36	*30.8%*	56.12	54.12	*3.7%*	0.27	0.27	*0.0%*	0.31	0.31	*0.0%*
Wastewater treatment cost	9.54	7.29	*30.9%*	15.97	15.40	*3.7%*	41.67	40.52	*2.8%*	24.31	24.31	*0.0%*
Cost of ash disposal	69.02	52.74	*30.9%*	0.00	0.00	*0.0%*	0.00	0.00	*0.0%*	0.00	0.00	*0.0%*
Health cost of air pollution	4.31	3.29	*30.9%*	1.64	1.58	*3.7%*	0.03	0.03	*2.8%*	5.24	5.24	*0.0%*
(2) Total externalities	**362.0**	**276.7**	***30.8%***	**73.7**	**71.1**	***3.7%***	**42.0**	**40.8**	***2.8%***	**29.9**	**29.9**	***0.0%***
(1) + (2) Total cost and externalities	**702.6**	**551.1**	***27.5%***	**366.4**	**354.6**	***3.3%***	**177.8**	**176.6**	***0.6%***	**126.1**	**126.1**	***0.0%***
(3) Revenues from electricity generation	307.3	307.3	*0.0%*	307.3	307.3	*0.0%*	307.3	307.3	*0.0%*	307.3	307.3	*0.0%*
(1) - (3) Cost minus revenues	**-40.01**	**-88.88**	***-55.0%***	**-29.24**	**-37.92**	***-22.9%***	**-171.44**	**-171.44**	***0.0%***	**-211.04**	**-211.04**	***0.0%***
(1) + (2) - (3) Net societal cost of power generation	**395.3**	**243.8**	***62.1%***	**59.1**	**47.3**	***25.0%***	**-129.5**	**-130.6**	***-0.9%***	**-181.2**	**-181.2**	***0.0%***

Table 13. Integrated CBA for climate impacts on thermal efficiency in billion ZAR – Renewable generators

Technology	Hydropower			Solar			Wind (onshore)		
Scenario	Climate impacts	No climate impacts	*Impacts vs no impacts*	Climate impacts	No climate impacts	*Impacts vs no impacts*	Climate impacts	No climate impacts	*Impacts vs no impacts*
Investment and cost									
Capital cost	21.0	21.0	0.0%	35.2	35.2	0.0%	26.7	26.7	0.0%
O&M cost	30.4	30.4	0.0%	27.0	27.0	0.0%	54.8	54.8	0.0%
Fuel cost	0.0	0.0	0.0%	0.0	0.0	0.0%	0.0	0.0	0.0%
Transitional risk									
Carbon tax	0.0	0.0	0.0%	0.0	0.0	0.0%	0.0	0.0	0.0%
(1) Total costs	**51.3**	**51.3**	**0.0%**	**62.2**	**62.2**	**0.0%**	**81.5**	**81.5**	**0.0%**
Externalities									
Social cost of carbon	0.00	0.00	0.0%	0.52	0.52	0.0%	0.51	0.51	0.0%
Wastewater treatment cost	0.00	0.00	0.0%	0.00	0.00	0.0%	0.00	0.00	0.0%
Cost of ash disposal	0.00	0.00	0.0%	0.00	0.00	0.0%	0.00	0.00	0.0%
Health cost of air pollution	0.00	0.00	0.0%	0.00	0.00	0.0%	0.00	0.00	0.0%
(2) Total externalities	**0.0**	**0.0**	**0.0%**	**0.5**	**0.5**	**0.0%**	**0.5**	**0.5**	**0.0%**
(1) + (2) Total cost and externalities	**51.3**	**51.3**	**0.0%**	**62.8**	**62.8**	**0.0%**	**82.0**	**82.0**	**0.0%**
(3) Revenues from electricity generation	307.3	307.3	0.0%	307.3	307.3	0.0%	307.3	307.3	0.0%
(1) - (3) Cost minus revenues	**-255.92**	**-255.92**	**0.0%**	**-245.03**	**-245.03**	**0.0%**	**-225.76**	**-225.76**	**0.0%**
(1) + (2) - (3) Net societal cost of power generation	**-255.9**	**-255.9**	**0.0%**	**-244.5**	**-244.5**	**0.0%**	**-225.3**	**-225.3**	**0.0%**

2.5.3 Climate Impacts on Transmission Lines

The conductivity of transmission lines is affected by the surrounding air temperature and decreases as summer air temperatures increase (U.S. Department of Energy, 2013). As a consequence of reduced transmission efficiency, not all the electricity produced can be sold on the market. The impacts of transmission lines in the SAVi model are assumed to affect the revenues of power producers.

According to the International Energy Agency (2008), a network with initial losses of 8% will see a 1% reduction in transmission efficiency for each 1°C increase in temperature relative to a reference temperature. This is equivalent to a 12.5% increase in grid losses per degree Celsius in additional air temperature. The formulation used for the climate impacts assumes a grid loss factor of 15% and, hence, an increase in losses of 0.63% per 1°C (12.5% out of 15%). The following equation is used to determine the impacts of temperature changes in grid efficiency:

*Temperature impacts on grid efficiency = 1 - IF THEN ELSE (Tair>Treference, (Tair-Treference) * 0.0063, 0)*

The impacts are hence dependent on whether air temperature exceeds the reference temperature for the initial losses.

The reduction in revenues is affected by the seasonality of temperature, as illustrated in Figure 4. Since the generation of all assets is assumed equal in this assessment, revenues generated by coal power plants serve to illustrate.

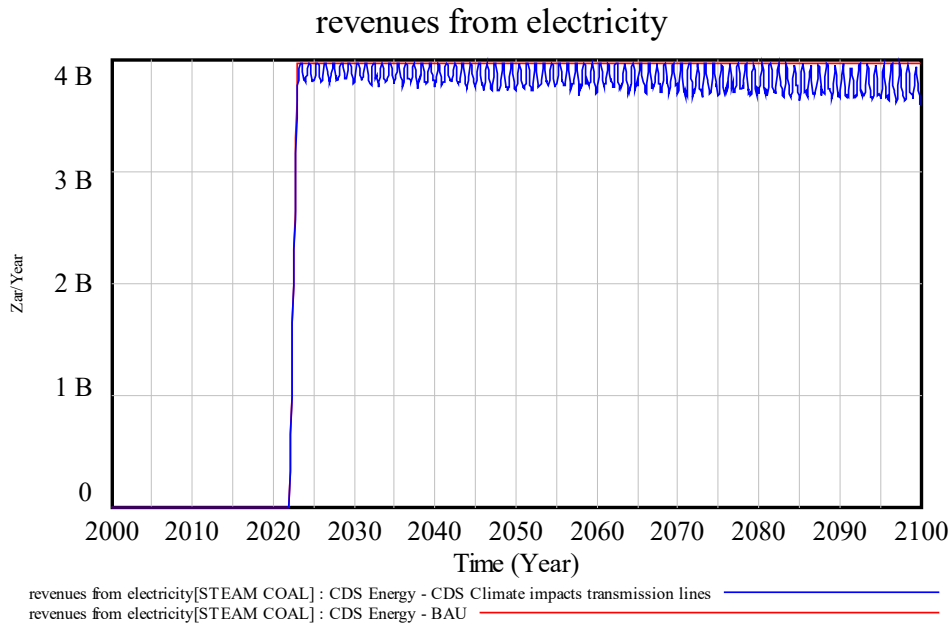

Figure 4. Impacts of grid efficiency on revenues from power generation

For all producers, revenue generation in the no-climate-impact scenario averages ZAR 3.94 billion per year between 2022 and 2100. In the scenario including CDS climate impacts, average annual

revenues are projected at ZAR 3.81 billion, which is 3.4% lower compared to the no-climate-impact scenario. Cumulatively, the losses incurred from reduced grid efficiency total ZAR 10.42 billion between 2022 and 2100, which is equivalent to annual foregone revenues of ZAR 134 million per year on average.

2.5.3.1 Economic Implications of Grid Efficiency Impacts

The forecasted impacts of changes in grid efficiency on revenues from power generation between the no-climate-impact and climate-impact scenarios is presented in Table 14. Aside from revenue generation, the changes in forecasted grid efficiency do not affect the operational costs of the power plants. Consequently, this effect changes the revenues from generators, which in turn affects profitability and the total societal cost of power generation.

Table 14. Integrated CBA for climate impacts on transmission lines – Thermal generators

Technology	Coal			Gas			Nuclear			Biomass		
Scenario	Climate impacts	No climate impacts	*Impacts vs. no impacts*	Climate impacts	No climate impacts	*Impacts vs. no impacts*	Climate impacts	No climate impacts	*Impacts vs. no impacts*	Climate impacts	No climate impacts	*Impacts vs. no impacts*
Investment and cost												
Capital cost	17.5	17.5	*0.0%*	11.3	11.3	*0.0%*	36.6	36.6	*0.0%*	24.6	24.6	*0.0%*
O&M cost	42.5	42.5	*0.0%*	25.5	25.5	*0.0%*	99.2	99.2	*0.0%*	64.1	64.1	*0.0%*
Fuel cost	102.3	102.3	*0.0%*	218.4	218.4	*0.0%*	0.0	0.0	*0.0%*	0.0	0.0	*0.0%*
Transitional risk												
Carbon tax	56.0	56.0	*0.0%*	14.1	14.1	*0.0%*	0.0	0.0	*0.0%*	0.0	0.0	*0.0%*
(1) Total costs	**218.4**	**218.4**	***0.0%***	**269.3**	**269.3**	***0.0%***	**135.8**	**135.8**	***0.0%***	**88.6**	**88.6**	***0.0%***
Externalities												
Social cost of carbon	213.36	213.36	*0.0%*	54.12	54.12	*0.0%*	0.27	0.27	*0.0%*	0.31	0.31	*0.0%*
Wastewater treatment cost	7.29	7.29	*0.0%*	15.40	15.40	*0.0%*	40.52	40.52	*0.0%*	24.31	24.31	*0.0%*
Cost of ash disposal	52.74	52.74	*0.0%*	0.00	0.00	*0.0%*	0.00	0.00	*0.0%*	0.00	0.00	*0.0%*
Health cost of air pollution	3.29	3.29	*0.0%*	1.58	1.58	*0.0%*	0.03	0.03	*0.0%*	5.24	5.24	*0.0%*
(2) Total externalities	**276.7**	**276.7**	***0.0%***	**71.1**	**71.1**	***0.0%***	**40.8**	**40.8**	***0.0%***	**29.9**	**29.9**	***0.0%***
(1) + (2) Total cost and externalities	**551.1**	**551.1**	***0.0%***	**354.6**	**354.6**	***0.0%***	**176.6**	**176.6**	***0.0%***	**118.5**	**118.5**	***0.0%***
(3) Revenues from electricity generation	296.8	307.3	*-3.4%*	296.8	307.3	*-3.4%*	296.8	307.3	*-3.4%*	296.8	307.3	*-3.4%*
(1) - (3) Cost minus revenues	**-78.46**	**-88.88**	***-11.7%***	**-27.50**	**-37.92**	***-27.5%***	**-161.02**	**-171.44**	***-6.1%***	**-208.20**	**-218.63**	***-4.8%***
(1) + (2) - (3) Net societal cost of power generation	**254.3**	**243.8**	***4.3%***	**57.7**	**47.3**	***22.0%***	**-120.2**	**-130.6**	***-8.0%***	**-178.3**	**-188.8**	***-5.5%***

Table 15. Integrated CBA for climate impacts on transmission lines – Renewable generators

Technology	Hydropower			Solar			Wind (onshore)		
Scenario	Climate impacts	No climate impacts	*Impacts vs. no impacts*	Climate impacts	No climate impacts	*Impacts vs. no impacts*	Climate impacts	No climate impacts	*Impacts vs. no impacts*
Investment and cost									
Capital cost	21.0	21.0	*0.0%*	35.2	35.2	*0.0%*	26.7	26.7	*0.0%*
O&M cost	30.4	30.4	*0.0%*	27.0	27.0	*0.0%*	54.8	54.8	*0.0%*
Fuel cost	0.0	0.0	*0.0%*	0.0	0.0	*0.0%*	0.0	0.0	*0.0%*
Transitional risk									
Carbon tax	0.0	0.0	*0.0%*	0.0	0.0	*0.0%*	0.0	0.0	*0.0%*
(1) Total costs	**51.3**	**51.3**	***0.0%***	**62.2**	**62.2**	***0.0%***	**81.5**	**81.5**	***0.0%***
Externalities									
Social cost of carbon	0.00	0.00	*0.0%*	0.52	0.52	*0.0%*	0.51	0.51	*0.0%*
Wastewater treatment cost	0.00	0.00	*0.0%*	0.00	0.00	*0.0%*	0.00	0.00	*0.0%*
Cost of ash disposal	0.00	0.00	*0.0%*	0.00	0.00	*0.0%*	0.00	0.00	*0.0%*
Health cost of air pollution	0.00	0.00	*0.0%*	0.00	0.00	*0.0%*	0.00	0.00	*0.0%*
(2) Total externalities	**0.0**	**0.0**	***0.0%***	**0.5**	**0.5**	***0.0%***	**0.5**	**0.5**	***0.0%***
(1) + (2) Total cost and externalities	**51.3**	**51.3**	***0.0%***	**62.8**	**62.8**	***0.0%***	**82.0**	**82.0**	***0.0%***
(3) Revenues from electricity generation	296.8	307.3	*-3.4%*	296.8	307.3	*-3.4%*	296.8	307.3	*-3.4%*
(1) - (3) Cost minus revenues	**-245.49**	**-255.92**	***-4.1%***	**-234.60**	**-245.03**	***-4.3%***	**-215.34**	**-225.76**	***-4.6%***
(1) + (2) - (3) Net societal cost of power generation	**-245.5**	**-255.9**	***-4.1%***	**-234.1**	**-244.5**	***-4.3%***	**-214.8**	**-225.3**	***-4.6%***

3 Irrigation Infrastructure

3.1 Literature Review

3.1.1 Demand for Irrigation

Crop efficiency, or land productivity, depends on soil quality, climate, and human inputs. Climate considers precipitation, evapotranspiration, moisture, and more. Water availability is critical for agriculture production. Due to varying degrees of resilience to water scarcity and different growing cycles, its relevance changes depending on the type of crop considered.

There is an optimal amount of water required for each crop. To realize the maximum yield potential, the water that is not made available by precipitation has to be provided by irrigation infrastructure. Weather can also impact the irrigation system regarding different water pumping technologies, such as photovoltaic, diesel motors, or grid efficiency.

3.1.1.1 Water and Irrigation Requirement

- **Climate impact**

Precipitation influences the amount of water a crop has at his disposal (this is called rainfed agriculture in the absence of irrigation infrastructure). In the case of water shortages, a crop either grows less or doesn't grow at all.

- **Summary of results**

Yield decrease relative to changes in air temperatures depends on type of field, location, and several ecological indicators. We found that, for each 1˚C increase in temperature, the impact on [wheat; rice; maize; soybean; barley] would be a decrease in yield of [-6.0 ± 2.9% per °C increase in temperature and -50 to 100% under RCP 2.6-8.5; -3.2 ± 3.7%; −7.4 to -4 ± 4.5%; -3.1%; -50 to 100% under RCP 2.6-8.5], respectively.

In a specific study for maize, the crop water use efficiency was 1.53 kg/m^3, and the irrigation or field water use efficiency was 1.74 kg/m^3. Crop water use efficiency was defined as "the yield of the crop per unit of water lost through evapotranspiration of the crop" (Djaman et al., 2018). In contrast, "field water use efficiency is the ratio of yield of the crop to total amount of water used in the field" (Djaman et al., 2018). So, the difference between the two indicators is that the field water use efficiency considers water losses, while the crop water use efficiency only considers the water directly used by the plant.

For winter wheat/barley and fodder maize, under RCP 2.6 and RCP 8.5, the irrigation water requirement will increase by 38%–79% and 0.7%–4.1%, respectively. For the irrigation system, using solar PV for water pumping, from an optimal threshold of 28˚C, for each 1˚C increase in temperature, there will be a decrease of 0.45% in efficiency.

For more information, Tables 16, 17, 18 clearly display those results.

- **Results**

Impact of temperature increases on crop yields (Zhao, et al., 2017):

Zhao et al. (2017) investigate "the impacts of temperature on yields of four crops by compiling extensive published results from four analytical methods: global grid-based and local point-based models, statistical regressions, and field-warming experiments." The four crops analyzed are wheat, rice, maize, and soybean, which are the most important crops for global food supply. The "results from the [four] different methods [demonstrated] negative temperature impacts on global crop yields" (effects without carbon dioxide fertilization, effective adaptation, and genetic improvement): "each degree Celsius increase in global mean temperature would, on average, reduce global yields of:

- Wheat by 6.0%,
- Rice by 3.2%,
- Maize by 7.4%,
- Soybean by 3.1%"
  (Zhao et al., 2017)

The "results are heterogeneous across crops and geographical areas"; sometimes increasing temperatures even have positive impacts. Projected changes in yield due to temperature changes by the end of the 21st century are shown in Table 16. (confidence intervals of 95% are given in square brackets) (Zhao et al., 2017).

Table 5. Projected changes in yield due to changes in temperature

	Yield changes (%) due to temperature changes by the end of century				
Scenario	Wheat	Rice	Maize	Soybean	Mean
RCP2.6	-6.9 [-15.0, -1.4]	-3.3 [-9.2, 0.8]	-8.6 [-18.6, -1.8]	-3.6 [-11.2,1.7]	-5.6 [-14.4, -0.1]
RCP4.5	-11.4 [-21.7, -3.9]	-5.5 [-13.8, 1.0]	-14.2 [-27.9, -4.9]	-5.9 [-17.0, 3.1]	-9.2 [-21.2, -0.3]
RCP6.0	-14.0 [-25.7, -5.1]	-6.8 [-16.8, 1.3]	-17.4 [-33.1, -5.8]	-7.2 [-20.2, 3.6]	-11.3 [-25.6, 0.1]
RCP8.5	-22.4 [-40.2, -8.5]	-10.8 [-25.3, 2.4]	-27.8 [-50.4, -9.7]	-11.6 [-31.0, 6.0]	-18.2 [-38.6, -0.7]

Source: Zhao et al., 2017

According to Zhao et al. (2017), the impacts of increasing temperatures differ considerably for the four crops modelled. Impacts also differ in the crop's main producer countries.

The yield lost for each 1°C increase is largest for maize: −7.4 ± 4.5% per 1°C. This impact varies in the four largest maize producer countries: "United States (−10.3 ± 5.4% per 1°C), China (−8.0 ± 6.1% per 1°C), Brazil (−5.5 ± 4.5% per 1°C), and India (−5.2 ± 4.5% per 1°C)" (Zhao et al., 2017).

For wheat, yields are modelled to decrease by 6.0 ± 2.9% per 1°C increase in temperature. Impacts are very heterogeneous in space: "United States (−5.5 ± 4.4% per 1°C), France (−6.0 ± 4.2% per 1°C), India (−9.1 ± 5.4% per 1°C), Russia (−7.8 ± 6.3% per 1°C), and China (-2.6 ± 3.1% per 1°C)" (Zhao et al., 2017).

The impact of temperature increases on rice is smaller than for maize or wheat. Yields might decrease by 3.2 ± 3.7% per 1°C. We see a large impact in India (−6.6 ± 3.8% per 1°C) (Zhao et al., 2017)

"The impact of rising temperatures on soybean yields (-3.1% per °C) is not statistically significant due to large uncertainties in each method. Impacts in Brazil, Argentina, and Paraguay might be similar to the -3.1% per °C. The largest reduction is in the United States (−6.8 ± 7.1% per °C)" Zhao et al., 2017) .

Water use efficiency (Djaman et al., 2018)

In the southwest United States, Djaman et al. (2018) assess "crop water use for water management and planning under conservation agriculture." Precisely, they assess maize water use and water productivity under full irrigation from 2011–2014 and 2017 in the Four Corners region of New Mexico. The result was that (Djaman et al., 2018):

- Maize crop water use efficiency ranged from 1.3 to 1.9 kg/m^3 and averaged 1.53 kg/m^3.
- Evapotranspiration water use efficiency values were higher than crop water use efficiency and varied from 2.0 to 2.3 kg/m^3, averaging 2.1 kg/m^3.
- Maize irrigation water use efficiency varied with years and averaged 1.74 kg/m^3

Yield depending on available water (Mirgol et al., 2020)

The study investigated "the impact of climate change on the future irrigation water requirement (IR) and yield of three crops: winter wheat, barley, and fodder maize." The study analyzed these impacts specifically for the semi-arid Qazvin Plateau in Iran for the periods 2016–2040, 2041–2065, and 2066–2090. For the projection of the monthly minimum and maximum temperatures as well as the regional monthly precipitation, Mirgol et al. (2000) used the Canadian Earth System Model (CanESM2) and applied the Intergovernmental Panel on Climate Change (IPCC) scenarios RCP 2.6, RCP 4.5, and RCP 8.5 (Mirgol et al., 2020).

Mirgol et al. (2000) discovered that "precipitation will decrease (1%–13%) under all scenarios in all months of the future periods (except August, September, and October)."

"The [irrigation water requirement] of winter wheat and barley will increase by 38%–79% (scenarios RCP 2.6 and RCP 8.5)." The increase in "the IR of fodder maize will be very slight (0.7%–4.1%)." For more details on the irrigation water requirements, see Table 17 (Mirgol et al., 2020).

"The yield of winter wheat and barley will decrease by ~50%–100% (scenarios RCP 2.6 and RCP 8.5). … The reduction in the yield of maize will be about 4%" (Mirgol, 2020). For details on the yield, see Table 18.

Table 6. Change of irrigation water requirements

Table 6. Change values of the irrigation water requirement (IR) of winter wheat under scenarios rcp2.6 and rcp8.5 for periods 2016–2040, 2041–2065, and 2066–2090 versus the baseline period.

Scenario	Periods	Feb	Mar	Apr	May	Jun	Total (%)
rcp2.6	2016–2040 vs. observed	635	50.5	37.9	29.4	21.2	38
rcp2.6	2041–2065 vs. observed	895	96.1	42.4	43.8	32.9	55
rcp2.6	2066–2090 vs. observed	1300	127.9	59.7	48.7	34.9	69
rcp8.5	2016–2040 vs. observed	625	72.4	37.4	32.8	20.8	42
rcp8.5	2041–2065 vs. observed	1025	103.9	46.8	48.5	36.6	60
rcp8.5	2066–2090 vs. observed	1180	139.3	61.1	64.4	41.6	79

Source: Mirgol, 2020.

Table 18. Change of yields

Table 9. Results of the change percentage of the crops under scenarios rcp2.6 and rcp8.5 in periods 2016–2040, 2041–2065, and 2066–2090 versus the baseline period in the Qazvin Plateau.

Scenario		Winter Wheat	Barley	Fodder Maize
rcp2.6	%(2016–2040) vs. obs	−58.24	−48.48	−3.20
	%(2041–2065) vs. obs	−75.10	−65.78	−1.47
	%(2066–2090) vs. obs	−89.86	−80.72	1.99
rcp8.5	%(2016–2040) vs. obs	−62.86	−53.21	0.18
	%(2041–2065) vs. obs	−80.69	−71.57	−3.22
	%(2066–2090) vs. obs	−99.02	−89.92	−6.70

Source: Mirgol, 2020.

Solar-powered irrigation systems (Schnetzer & Pluschke, 2017)

Air temperature has an influence on solar-powered irrigation systems: the "the optimum performance of PV panels is an average of ~28°C with a decrease in efficiency of 0.45% for every degree above optimum temperature as rule of thumb." A second factor is "the depth of the water source relative to the altitude where the water is utilized (pumping head; typically up to 70 m, but greater heads are technically feasible)." Citing three sources (Ould-Amrouche et al., 2010; Gesellschaft für Internationale Zusammenarbeit [GIZ], 2016; Parliamentary Office of Science and Technology [POST], 2011), they report the emissions of CO_2 for solar, diesel, and grid efficiency (Schnetzer & Pluschke, 2017) (see Table 19).

Table 19. Carbon dioxide emissions from three different technologies

	Unit	Solar PV	Grid electricity	Diesel
GIZ 2016	g CO^2-eq/kWh	16-32	600	1000
POST 2011	g CO^2-eq/kWh	75-116	488-990	-
Ould-Amrouche et al. 2010	g CO^2/m^3	0	-	480-2230

Source: Schnetzer & Pluschke, 2017.

- **Methodology**

1. Irrigation water requirement (Mirgole et al., 2020)

$$NWA = PR + DP + Ro – Pe / Eff$$

Whereby:
NWA = net water available in mm per month
PR = pre-irrigation, soil moisture change between t0 and t-1 in mm per month
DP = deep percolation in mm per month
Ro = runoff in mm per month
Pe = monthly precipitation in mm per month
Eff = efficiency of the centre pivot installed within the field

2. Crop yield depending on irrigation water requirement changes (Mirgol et al., 2020)

Migrol et al. (2020) used the Stewart model "to estimate the effect of irrigation water requirement changes on the yield of the crops":

$$1 - \frac{Y_a}{Y_m} = K_y\left(1 - \frac{ET_a}{ET_m}\right)$$

"Where Y_a is the actual yield (tonne ha^{-1}), Y_m is the maximum yield (tonne ha^{-1}), ET_a is the actual evapotranspiration (mm d-1), ET_m is the maximum evapotranspiration, and K_y is the coefficient of the reaction of crop yield to water stress. … Y_m and K_y. Higher K_y numbers indicate higher sensitivity to water stress" (Mirgol et al., 2020). See more in Doorenbos & Kassam (1979)

Table 20. Maxiumum yield and reaction coefficient

Table 4. Total cultivation area, maximum yield (Y_m), and the coefficient of the reaction of crop yield to water stress (K_y) for winter wheat, barley, and fodder maize in the Qazvin Plateau (Najarchi et al., 2011).

Crop	Total Cultivated Area (ha)	Y_m (ton ha^{-1})	K_y
Winter wheat	66000	6	1.2
Barley	36358	4.7	1.1
Fodder maize	28621	10	1.5

Higher K_y numbers indicate higher sensitivity of the crop to water stress.

3. Estimation of the water pumping energy demand (Ould-Amrouche et al., 2010)

The peak power of the PV generator is given by Ould-Amrouche et al. (2010):

$$P_{pv} = E_{pv}\frac{G}{E_s}$$

"Where G is the peak solar radiation intensity (1 kW/m^2) and E_s is the annual average of solar radiation on a horizontal surface (5.5 kW h/ m^2 day)" (Ould-Amrouche et al., 2010).

4. Pumping water energy cost calculator (Engineering ToolBox, 2009):

The energy cost per hour for pumping water can be calculated in imperial units as

C = 0.746 Q h c / (3960 μ_p μ_m) *(1)*

where

C = cost per hour (USD/hour, EUR/hour, ...)

Q = volume flow (US gpm)

h = differential head (ft)

c = cost rate per kWh (USD/kWh, EUR/kWh, ...)

μ_p = pump efficiency (0 - 1)

μ_m= motor efficiency (0 - 1)

Alternative calculation in metric units

$$C = q\,\rho\,g\,h\,c\,/\,(3.6\,10^6\,\mu_p\,\mu_m)$$

$$= q\,p\,c\,/\,(3.6\,10^6\,\mu_p\,\mu_m) \qquad (2)$$

where

q = volume flow (m^3/h)

ρ = density (1000 kg/m^3)

h = differential head, height (m)

g = acceleration of gravity (9.81 m/s^2)

5. Solar PV water pumping (Maupoux, 2010)

Estimation of requirements for effective water pumping from a solar PV system (Maupoux, 2010):

i. The hydraulic energy required (kWh/day) = volume required (m^3/day) x head (m) x water density x gravity / (3.6 x 106) = 0.002725 x volume (m^3/day) x head (m)
ii. The solar array power required (kWp) = Hydraulic energy required (kWh/day) / Av. daily solar irradiation (kWh/m^2/day x F x E)

Where:

- F = array mismatch factor = 0.80 on average (a safety factor for real panel performance in hot sun and after 10–20 years)
- E = daily subsystem efficiency = 0.25 - 0.40 typically

Considerations for integration into the CDS Toolbox

1. Water delivery from precipitation (mm/month):

Parameter in the model = total water from precipitation

$$Pmonth = (TPt - TPt\text{-}1) * 1{,}000$$

Pmonth = monthly precipitation
TPt = total precipitation in month t
TPt-1 = total precipitation in month t-1
1,000 = conversion from m to mm per month

2. Runoff (mm/month):

Parameter in the model = Runoff

$$E\ month = (Rt - Rt\text{-}1) * 1{,}000$$

R month = monthly runoff
Rt = total runoff in month t
Rt-1 = total runoff in month t-1
1,000 = conversion from m to mm per month

3. Rainfall per month (mm/month):

Parameter in the model = seasonal precipitation

Pmonth1 = SUM (precipitation fluxmonth1)

Pmonth1 = monthly precipitation in month 1 (January)
Precipitation fluxmonth1 = total rainfall in month 1 (January)

4. Long-term average precipitation (mm/month):

Parameter in the model = Long-term average precipitation

LTMPt0 = Average (Pmonth1-12 over the last 20 years)

LTMPt0 = long-term monthly precipitation at time t

5. Rainfall per day (mm/day):

Parameter in the model = daily precipitation

Pday1 = SUM (precipitation fluxday1)

Pday1 = daily precipitation in day 1
Precipitation fluxday1 = total rainfall during day 1.

The same approach applies to all other days of the month.

6. Rainy spell

Parameter in the model = Consecutive days of rain

Consecutive days with raint0 = IF "Rainfall per day"t0 > 0,
THEN "1 + Consecutive days with raint-1", ELSE "0"

Rainfall per dayt0 = the indicated rainfall for today
Consecutive days with raint-1 = previous consecutive days with rain (if any)

Data inputs

- Soil moisture (%) – Soil moisture gridded data from 1978 to present
- Runoff (m) – ERA5-Land monthly averaged data from 1981 to present
- Precipitation (m) – ERA5-Land monthly averaged data from 1981 to present

3.1.1.2 Efficiency (evapotranspiration)

- **Climate impact**

Irrigation efficiency represents the percentage of water extracted that effectively reaches the destination desired (e.g. 100 litres are extracted, but 80 are lost and 20 reach the fields, hence 20% efficiency) (Brouwer et al., 1989).

- **Results**

The Food and Agriculture Organization of the United Nations indicates that, "depending on the type of irrigation method surface, sprinkler, drip, field efficiency will vary from 60% to 75% and 90% respectively" (Brouwer et al., 1989).

- **Methodology**

Method 1 (Brouwer et al., 1989)

"The scheme irrigation efficiency can be subdivided into"(Brouwer & Heibloem, 1986):

1. The conveyance efficiency (ec), which represents the efficiency of water transport in canals
2. The field application efficiency (ea), which represents the efficiency of water application in the field

$$NIRcrop = ETcrop / IE / WCE$$

- NIRcrop = net irrigation requirements in mm per hectare per month
- Etcrop = crop evapotranspiration in mm per month
- IE = irrigation efficiency in %
- WCE = water conveyance efficiency in %

Net irrigation water demand depends on the application efficiency of irrigation systems and the WCE. For the examples of irrigation methods provided below, WCE will be kept constant (0.9) due to a lack of information on the length of the irrigation channels.

A calculation of IE is provided (Brouwer et al., 1989):

$$e = \frac{ec \times ea}{100}$$

with

e = scheme irrigation efficiency (%)
ec = conveyance efficiency (%)
ea = field application efficiency (%)

A scheme irrigation efficiency of 50-60% is good; 40% is reasonable, while a scheme Irrigation efficiency of 20-30% is poor.

We also extracted Table 21 and Table 22:

Table 7 Field application efficiency

Irrigation methods	Field application efficiency
Surface irrigation (border, furrow, basin)	60%
Sprinkler irrigation	75%
Drip irrigation	90%

Source: Brouwer et al., 1989.

Table 8 Conveyance efficiency

	Earthen canals			Lined canals
Soil type	Sand	Loam	Clay	
Canal length				
Long (> 2000m)	60%	70%	80%	95%
Medium (200-2000m)	70%	75%	85%	95%
Short (< 200m)	80%	85%	90%	95%

Source: Brouwer et al., 1989.

Method 2 (Das et al., 2018)

If the crop is more environmentally friendly (organic), we can use this formula (Das et al., 2018):

$$NIRcrop\ organic = NIRcrop \times (irrigation\ system) \times 0.86$$

- NIRcrop organic = net irrigation requirements organic crops in mm/ha/month
- NIRcrop (irrigation system) = net irrigation requirements conventional crops for flood, sprinkler, and drip irrigation in mm/ha/month
- 0.86 = multiplier reducing irrigation requirements by 14%.

Considerations for integration into the CDS Toolbox

Evapotranspiration (Brouwer & Heibloem, 1986)

1. "The crop water need (ET crop) is defined as the depth (or amount) of water needed to meet the water loss through evapotranspiration. In other words, it is the amount of water needed by the various crops to grow optimally" (Brouwer & Heibloem, 1986).

2. "The crop water need [and factor (Kc)] depend on" (Brouwer & Heibloem, 1986):

- The climate: in a sunny, hot climate, crops need more water per day than in a cloudy, cool climate.

- The crop type: crops like maize or sugarcane need more water than crops like millet or sorghum.
- The growth stage of the crop: fully grown crops need more water than crops that have just been planted.

“The influence of the climate on crop water needs is given by the reference crop evapotranspiration (ETo). The ETo is usually expressed in millimeters per unit of time, e.g. mm/day, mm/month, or mm/season” (Brouwer & Heibloem, 1986).

We estimate the crop water need (ET crop) in mm/day with its evapotranspiration (ETo) in mm/day and its factor (Kc) (Brouwer & Heibloem, 1986):

$$ETcrop = ETo * Kc$$

Kc estimation (Brouwer & Heibloem, 1986):
Step 1 – Determination of the total growing period of each crop
Step 2 – Determination of the various growth stages of each crop
Step 3 – Determination of the Kc values for each crop for each of the growth stages

Climate adjusted Kc (Brouwer & Heibloem, 1986):

- Kc climate = Kcbase + IF u< 2: AND: RH >80% THEN "-0.05" ELSE "0" + IF u>5: AND: RH<50% THEN "0.05"ELSE "0"Kcbase = Baseline crop factor based on crop and development stage
- u = wind speed (m/s)
- RH = relative humidity

“Kc values should be reduced by 0.05 if the relative humidity is high (RH > 80%) and the wind speed is low (u < 2 m/sec), e.g. Kc = 1.15 becomes Kc = 1.10. The values should be increased by 0.05 if the relative humidity is low (RH < 50%) and the wind speed is high (u > 5 m/sec), e.g. Kc = 1.05 becomes Kc = 1.10” (Brouwer & Heibloem, 1986).

Climate adjusted Kc (includes plant height) (Djaman et al., 2018):

$$\text{Kc Stage} = \text{KcStage} + [0.04(u_2 - 2) - 0.004(\text{RHmin} - 45)]\left(\frac{h}{3}\right)^{0.3}$$

- KcStage is the standard value according to FAO-56 approach (Allen et al., 2006)
- U_2 is the value for daily wind speed at 2 m height over grass during the growth stage (m/s)
- RHmin is the value for daily minimum relative humidity during the growth stage (%)
- H is the plant height for each growth stage (m) (0.1 m–10 m)

Increased evapotranspiration due to temperature (dimensionless) (Kosa, 2011)

Parameter in the model = Effect of temperature on evapotranspiration

$$Eto = -0.028x^2 + 1.7608x - 22.932$$

Eto = actual daily evapotranspiration
x = daily temperature in °C

This model is based on Kosa (2011) and has a R^2 value of 0.987, which could be used to establish a multiplier for evapotranspiration based on a set point (say 17°C).

Data required:

- Evapotranspiration (m of water equivalent): ERA5-Land monthly averaged data from 1981 to present
- Wind speed (m/s): ERA5 monthly averaged data on single levels from 1979 to present
- Humidity (%): ERA5 monthly averaged data on pressure levels from 1979 to present
- Evapotranspiration (m of water equivalent): ERA5-Land monthly averaged data from 1981 to present

3.2 Integration of the Literature Review with the CDS Datasets

See general instructions in the energy section.

Datasets:

- ERA5 monthly data on single level
- CMIP5 monthly data on single level
- ERA5 daily data on single level

Indicators created:

- **Precipitation**:
  - Units: mm per month
  - Frequency: monthly
  - ERA5 variable: “mean total precipitation rate”
  - CMIP5 variable: “mean precipitation flux“
  - Note different: original units in mm/s
- **Evaporation**
  - Units: mm per month
  - Frequency: monthly
  - ERA5 variable: “Mean evaporation rate”
  - CMIP5 variable: “Evaporation“
  - Note different: original units in mm/s, sign convention in ERA5 adjusted to CMIP5 convention (positive)
- **Runoff**

    - Units: mm per month
    - Frequency: monthly
    - ERA5 variable: “mean runoff rate”
    - CMIP5 variable: “runoff“
    - Note different: original units in mm/s
- **Air temperature**
    - Units: degrees Celsius
    - Frequency: monthly
    - ERA5 variable: “2 m temperature”
    - CMIP5 variable: “2 m temperature“
    - Note different: original units in Kelvin
- **Relative humidity**
    - Units: %
    - Frequency: monthly
    - ERA5 variable: calculated from “2 m temperature” and “2 m dewpoint temperature”
    - CMIP5 variable: “near_surface_relative_humidity“
    - Note: see energy asset for more information
- **Daily maximum temperature**
    - Units: degrees Celsius
    - Frequency: monthly
    - ERA5 variable: “2m_temperature” aggregated from hourly data
    - CMIP5 variable: “near_surface_relative_humidity“
    - Note: optional asset (implemented but not added by default to the asset bundle because it takes a long time to calculate)

More detailed information about precipitation variable in ERA5/CMIP5 can be found in the road asset (“road runoff”).

3.3 Integration of Climate Indicators Into the SAVi Irrigation Model

Figure 5 shows the CLD of the SAVi Irrigation model, including indicators developed for the CDS Toolbox (highlighted in pink). CDS Toolbox climate indicators related to irrigation include seasonal precipitation (including extreme events), net crop water requirements, and available surface water supply.

Figure 5. CLD for the irrigation sector (CDS variables included in pink)

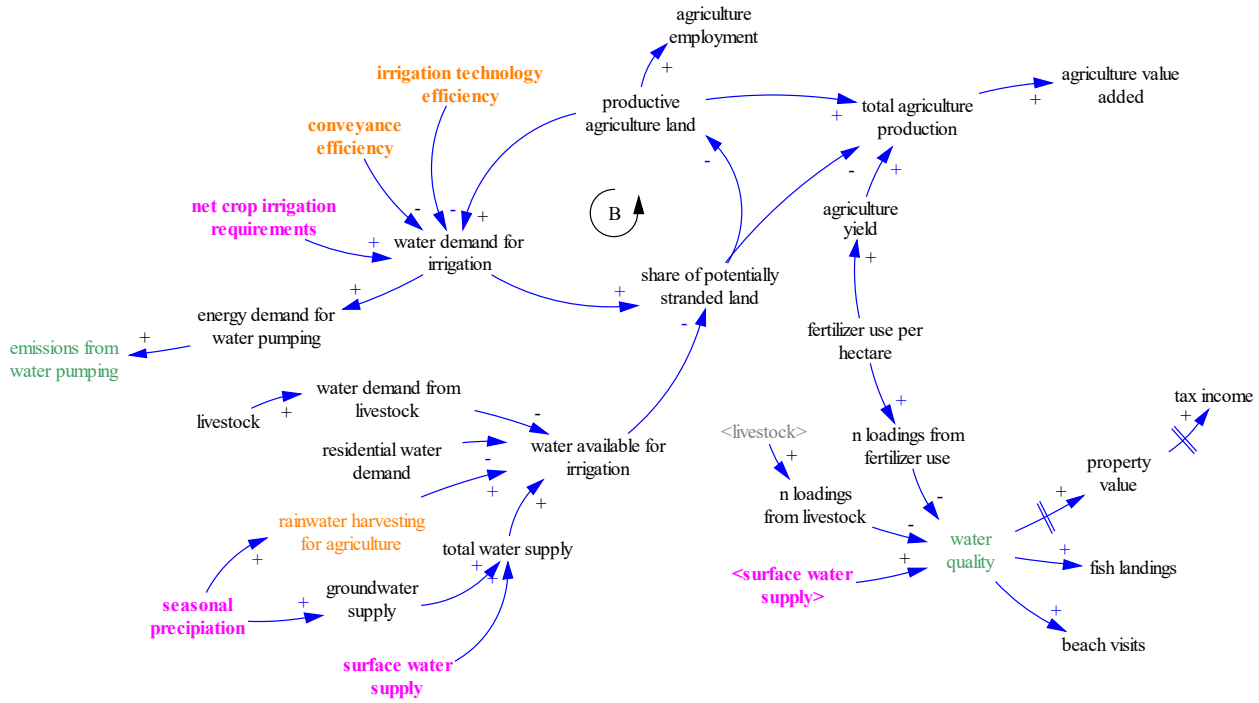

The CDS indicator seasonal precipitation refers to the precipitation per month in a given geographical context. Data on seasonal precipitation obtained from the CDS Toolbox will hence provide location-specific information concerning total rainfall and extreme weather events, such as floods or droughts. Further, data will be available with monthly time steps, allowing the estimate of changes in the rainy season where relevant and related impacts on the growing season and suitability of crops.

Net irrigation requirements in the CDS Toolbox provide information about the amount of water required for irrigation to ensure maximum yields. This parameter accounts for crop water requirements, precipitation, and evaporation and hence provides net irrigation requirements per hectare, depending on the type of crop. It will support the assessment of required investments in irrigation.

Available surface water supply depends on total rainfall, evaporation, and groundwater recharge, all of which are obtained from the CDS database. In the SAVi model, available water supply from surface water is used to calculate the water supply and demand balance and to analyze potential conflicting uses for water (e.g., potable use versus irrigation).

3.4 Behavioural Impacts Resulting from the Integration of Climate Variables

The use of the seasonal precipitation indicator obtained from the CDS replaces the less dynamic formulation concerning precipitation in the SAVi model with location-specific information. This supports assessing irrigation requirements by providing more accurate data on precipitation, both historical and future, and by allowing the generation of forecasts using a variety of climate

scenarios. Precipitation will affect crop productivity, with and without irrigation, production, and revenues, and will determine the economic viability of agriculture production.

Obtaining net irrigation requirements from the CDS Toolbox leads to improved forecasts or total irrigation requirements and potential future water shortages on a monthly or seasonal basis. This will impact the total water used for irrigation, irrigation-related energy use and total irrigation cost (total capacity requirement, related capital and O&M costs, and employment creation). Further, the implementation of this indicator into the CDS Toolbox can enable the replacement of existing variables and equations in the SAVi model, making projections more accurate.

The estimation of surface water supply allows for a system-wide analysis of water scarcity impacts going beyond irrigation. It will inform whether a reduction in agricultural land will emerge because of lower yields, leading to a loss of employment. The use of this CDS indicator in the SAVi model will affect water availability for potable, industrial, and agricultural use and affect water available for irrigation, depending on water resource allocation.

3.5 Simulation Results

Required irrigation and related water use are heavily dependent on climate variables such as precipitation and temperature. Four indicators were developed for the integration of climate variables from the CDS database into SAVi Irrigation: (1) irrigation requirements per hectare, (2) total irrigation requirements per hectare (including water conveyance loss), (3) indicated surface water supply, and (4) indicated groundwater supply.

3.5.1 Net and Total Irrigation Requirements

In the SAVi model, irrigation requirements refer to the amount of water that is required for irrigation accounting for evaporation and precipitation. Total irrigation requirements refer to the total amount of water required per hectare considering the efficiency of water conveyance infrastructure and installed irrigation systems. Both formulations use monthly precipitation and monthly crop water requirements to estimate the water required for irrigation. The equation used for net irrigation requirements is based on the crop water requirements indicated in Table 23.

Table 23. Indicated crop water requirements per month, in mm per hectare

Jan	Feb	Mar	Apr	May	Jun	Jul	Aug	Sep	Oct	Nov	Dec
120	60	0	0	0	0	0	80	120	120	120	120

The equation used for calculating the irrigation requirements per crop uses the indicated crop water requirements and an evaporation fraction based on local data (e.g., 45%).

*Net irrigation requirements per hectare = MAX(0, Indicated crop water requirement per hectare – (monthly precipitation * (1 – Evaporation fraction)))*

The MAX function is applied to prevent net irrigation requirements from taking negative values in case that monthly precipitation exceeds the required crop water supply. The risk of floods is analyzed separately.

The total amount of water needed to irrigate crops depends, in addition to rainfall and evaporation, on the efficiency of water conveyance infrastructure and the efficiency of irrigation technologies. To obtain the total irrigation requirements per hectare (or water demand for irrigation), an average irrigation efficiency multiplier of 50% (assuming flood irrigation) and an average water conveyance efficiency of 95% are applied to the net irrigation water demand per hectare. The equation used is documented below.

Total irrigation requirements per hectare = Net irrigation requirements per hectare / Efficiency of irrigation technology / Efficiency of water conveyance infrastructure

The results for net irrigation requirements per hectare are presented in monthly averages per decade and based on the Institut Pierre Simon Laplace (IPSL) RCP 8.5 scenario. The results for the average net irrigation required per month for maize is presented in Table 24 for each decade from 1980–1990 to 2090–2100.

Table 24. Net irrigation requirements, monthly averages per decade

Decade	Jan	Feb	Mar	Apr	May	Jun	Jul	Aug	Sep	Oct	Nov	Dec	**Total**	*relative to 1980-1990*
1980-1990	33.2	14.7	0.0	0.0	0.0	0.0	0.0	72.7	103.8	62.5	51.5	44.5	**382.8**	
1990-2000	56.2	17.9	0.0	0.0	0.0	0.0	0.0	71.1	100.0	59.4	51.3	44.7	**400.6**	*4.6%*
2010-2020	48.8	14.7	0.0	0.0	0.0	0.0	0.0	72.1	105.5	81.4	61.4	60.6	**444.5**	*16.1%*
2040-2050	55.9	10.5	0.0	0.0	0.0	0.0	0.0	71.1	105.8	80.9	59.8	50.2	**434.2**	*13.4%*
2070-2080	54.9	17.8	0.0	0.0	0.0	0.0	0.0	77.3	104.5	74.8	60.8	48.5	**438.5**	*14.6%*
2090-2100	65.7	32.3	0.0	0.0	0.0	0.0	0.0	77.8	103.1	77.8	56.4	57.7	**470.8**	*23.0%*

The results in Table 24 indicate a relative increase of 4.6% between the decades 1980–1990 and 1990–2000. By 2090–2100, the net irrigation requirements per hectare are projected to increase by 23% compared to 1980–1990, driven by the decline in precipitation. The absolute increase between 1980–1990 and 2090–2100 is 88 mm per year, which is equivalent to 880,000 litres per hectare per year in additional water requirements. Figure 6 illustrates the development of net irrigation requirements per hectare for the area of Johannesburg.

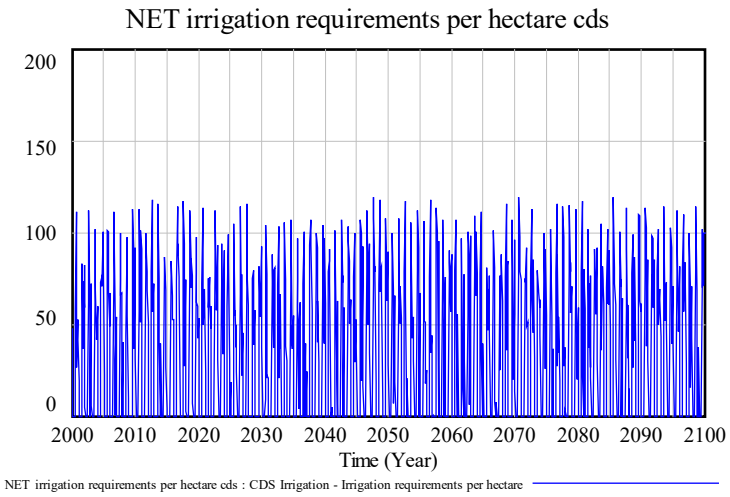

Figure 6. Net irrigation requirements per hectare for Johannesburg, IPSL RCP8.5 scenario

The trend in total irrigation water requirements per hectare is identical to the trend in irrigation requirements per hectare, unless there is a change in irrigation efficiency or the efficiency of water conveyance infrastructure. Table 25 shows how total irrigation water requirements compare to irrigation requirements in each decade. For months without irrigation, the value is 1. During the decade 1980–1990, total irrigation water requirements are on average 2.11 times higher than crop water requirements. By 2090-2100, total irrigation water requirements are an average of 2.97 times higher than during the decade 1980–1990. Considering the monthly crop water demand during the decade 2090–2100, the results indicate that irrigation requirements may be almost five times as high (February) as net irrigation requirements.

Table 25. Relative water use total irrgation requirements vs net irrigation requirements

	Jan	Feb	Mar	Apr	May	Jun	Jul	Aug	Sep	Oct	Nov	Dec
1980–1990	2.11	2.11	1.00	1.00	1.00	1.00	1.00	2.11	2.11	2.11	2.11	2.11
1990–2000	3.56	2.56	1.00	1.00	1.00	1.00	1.00	2.06	2.03	2.00	2.10	2.12
2010–2020	3.09	2.11	1.00	1.00	1.00	1.00	1.00	2.09	2.14	2.74	2.51	2.87
2040–2050	3.54	1.50	1.00	1.00	1.00	1.00	1.00	2.06	2.15	2.73	2.44	2.38
2070–2080	3.48	2.55	1.00	1.00	1.00	1.00	1.00	2.24	2.12	2.52	2.48	2.30
2090–2100	4.16	4.62	1.00	1.00	1.00	1.00	1.00	2.25	2.09	2.62	2.31	2.73

Between 1979 and 2100, the cumulative difference between net and total irrigation requirements is 55,871 mm per hectare, which is equivalent to 550,871,000 litres or 4,667,467 litres per hectare per year on average. If an irrigation efficiency of 75% is assumed, the cumulative difference declines from 55,871 mm per hectare to 20,398 mm per hectare, which is a net reduction of 63.5% in irrigation water use compared to the scenario with 50% irrigation efficiency.

3.5.2 Surface and Groundwater Supply

Surface and groundwater supply indicate the amount of renewable surface and groundwater sources available per hectare. Both indicators are calculated based on monthly precipitation, the

evaporation fraction, and the percolation fraction (the share of precipitation that reaches groundwater aquifers). The equations used for the calculation of the indicated surface and groundwater supply are presented below.

*Indicated surface water supply = Monthly precipitation * Evaporation fraction * (1 - Percolation fraction)*

*Indicated groundwater supply = Monthly precipitation * Evaporation fraction * Percolation fraction*

The results indicate the monthly availability of groundwater and surface water, respectively. Simulation results for indicated surface water supply and indicated groundwater supply are presented in Figures 7 and 8, respectively, using the IPSL RCP 8.5 projections for Johannesburg.

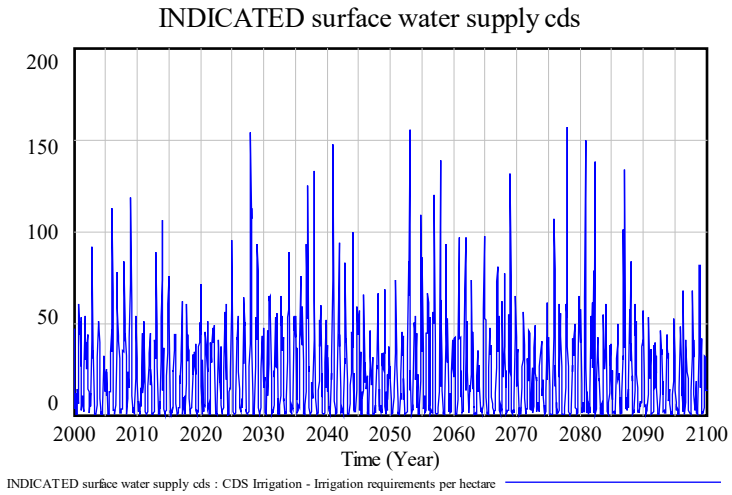

Figure 7. Indicated surface water supply per hectare, IPSL RCP8.5 scenario

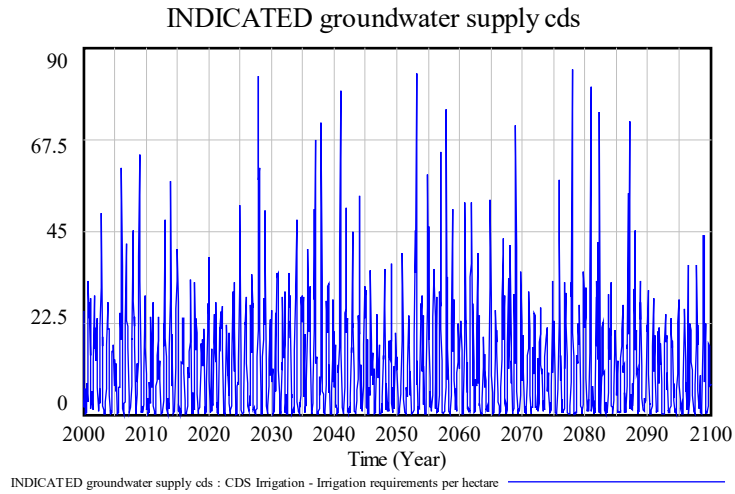

Figure 8. Indicated groundwater supply per hectare, IPSL RCP8.5 scenario

4 Wastewater Treatment Infrastructure

4.1 Literature Review

4.1.1 Capacity Utilization

The amount of water treated by a wastewater treatment facility (WWTF) is primarily a function of capacity and technical efficiency. On the other hand, there are several climate-related factors that affect both the extent to which the WWTF can be used and how effectively. Impacts that reduce effectiveness include, among others, high rainfall, which can lead to overflow; increased temperature, resulting in the growth of algae; and climate-induced power cuts, which reduce the operation time of the WWTF.

4.1.1.1 Precipitation

- **Climate impact**

Precipitation impacts WWTFs in various ways: it can lead to overflow due to runoff, affecting the efficiency of water treatment and the cost of operations or excessive water flow can lead to the shutdown of the facility.

4.1.1.2 Runoff

- **Methodology**

The equation used in many articles to calculate runoff is (Poullain, 2012):

$$Q = C * i * A$$

Q = peak rate of runoff in cubic feet per second,
C = runoff coefficient, a dimensionless unit
i = average intensity of rainfall in inches per hour
A = the watershed area in acres

A typical range for runoff coefficients is provided by Bengtson (2020) (see Table 26):

Table 26. Runoff coefficients

Type of Area	Typical Range for Runoff Coefficient
Concrete Pavement	0.70-0.95
Park or Cemetary	0.10-0.25
Downtown Business	0.70-0.95
Single Family Residential Area	0.30-0.50

Source: Bengtson, 2020

Considerations for integration into the CDS Toolbox

- ERA5-Land monthly averaged data from 1981 to present
- CMIP5 monthly data on single levels

4.1.1.3 Overflow

- **Methodology**

Precipitation can cause overflow of wastewater, given that sewage systems are created to manage wastewater rather than total runoff. “Literature shows that several categories of damages to road infrastructures can be related to distinct degrees of extreme precipitation” (Nemry & Demirel, 2012). Specifically, the Extreme Weather impacts on European Networks of Transport (EWENT) project indicates the following, (Nemry & Demirel, 2012):

- 50 mm/24h: flooded roads, reduced pavement fraction.
- 100 mm/24h: the sewer system fills up; water rises up the streets from drains; rainwater fills the underpasses and lower laying streets; drain well covers may become detached and cause danger to street traffic; reduced visibility.
- 150 mm/24h: road structures may collapse; bridges may be flooded; vehicle motors are damaged and vehicles can be flooded; roads might be covered by water or transported debris. As a result, a non-linear function generating an index of severity of the rainfall events, based on precipitation per day, could be created.

Severity of rainfall = [(0, 0), (50, 1), (100, 2), (150, 3)] (precipitation per day).

4.1.1.4 Temperature

- **Climate impact**

Changes in the temperature of wastewater treatment change the efficiency of pollutant removal. Higher water temperatures allow the creation of algae and other parasites that reduce the efficiency of treatment and increase the amount of time required to treat the same quantity of water. At the same time, higher temperatures lead to the reduction of the concentration of other pollutants, increasing efficiency. Impacts vary depending on the pollutant to be removed.

Higher temperatures have a second possible impact—on water quantity. If higher temperatures reduce water availability, the facility will have to stop operations.

- **Summary of results**

For precision: SS = suspended solids; COD = chemical oxygen demand; PO_4^{3-} = phosphate; NO^-_3 = nitrate; NH^+_4 = ammonium.

Removal efficiency of nutrients varies in wastewater treatment with refuse cement or concrete. The first one (refuse cement) for [SS; COD; PO_4^{3-}; NO^-_3; NH^+_4] removal efficiency from 20˚C to 40˚C has an increase for a median particle size of 0.43 of [29%; 51%; 1%; -33%; 20%], respectively. For the second one (concrete), with the same parameters, removal efficiency change is [11%; 14%; -34%; 5%; 15%].

Specifically for nitrogen (N), from a base case of influent sewage temperature of 7–10 ˚C and removal efficiency of 75–80%, a change of -1.5 to +5˚C impacts N removal efficiency by -6% per 1˚C in influent sewage temperature.

- **Results**

Ahsan et al. (2005) estimated the removal efficiency of a wastewater plant for different pollutants when there are increasing temperatures (see Table 27).

Table 27. Pollutant removal efficiency and temperature

Table 1 Effect of temperature on the wastewater treatment with refuse cement and refuse concrete

Treatment medium	Pollutant	Temperature (°C)	Removal efficiency (%)			
			Particle diameter (mm)			
			0.30	0.35	0.43	0.60
Refuse cement	SS	20	95	82	71	73
		40	97	92	100	94
	COD	20	40	25	24	29
		40	74	77	75	84
	PO_4^{3-}	20	92	90	89	92
		40	90	90	90	89
	NO_3^-	20	23	25	33	20
		40	0	0	0	0
	NH_4^+	20	34	10	10	34
		40	35	29	30	36
Refuse concrete	SS	20	92	77	87	71
		40	98	96	98	93
	COD	20	53	47	46	35
		40	65	57	60	62
	PO_4^{3-}	20	90	47	70	50
		40	54	30	36	20
	NO_3^-	20	32	26	28	28
		40	43	40	33	38
	NH_4^+	20	58	58	12	24
		40	24	30	27	13

$n=3$

Source: Ahsan et al., 2005.

In a case study about Norway, Plósz et al. (2009) report that, “at low daily air mean temperatures, heat transported by the influent sewage into the WWTP can be characterized with liquid temperatures between 7 and 10˚C, and with high biological nitrogen removal efficiencies (75–80%). Moreover, during temporary increases of air temperature (-1.5 to + 5C), nitrogen removal efficiency decreases by 6% per 1˚C degree decrease in the influent sewage temperature.”

In China, Yuan et al. (2013) have studied the efficiency of three soil wastewater infiltration systems (SWIS) under different temperatures. All the SWISs were operated at a hydraulic loading of 26 cm/day and a COD of 233 mg/L for 10 weeks at the influent wastewater temperature of 7°C, 13°C, 18°C, 25°C, and 33°C, respectively.

- COD decreased sharply when the temperature was less than 13°C; meanwhile, the removal efficiency of COD was between 83.3% and 95.0% in the treatment of the soil column. When the operation temperature increased to 33°C, the effluent COD concentration decreased gradually to a very low level, and the COD removal efficiency could reach as high as 98.3%.
- NH3-N (ammoniacal nitrogen): At 7°C, the average removal efficiency was below 85%, and the NH3-N concentration of effluent from the experimental soil column was about 4.0 mg/L. When the temperature was about 13°C, the NH3-N concentration of effluent decreased from 4.0 mg/L to 1.0 mg/L, and the average removal rate could reach as high as 97.1% when the SWIS operation temperature was higher than 13°C.

- TN (total nitrogen): When the operation temperature of the SWIS was lower than 25°C, the removal efficiency of TN was between 60.0% and 75.0%. Furthermore, the highest removal efficiency of TN could reach 85.0% when the SWIS was operated at 33°C.
- TP (total phosphorus): No effect

- **Methodology**

Method 1 (Singh & Tiwari, 2019)

Rate of biological reaction (sedimentation) (Singh & Tiwari, 2019): k = k20Θ T-20

K = reaction rate constant at temperature, T
k20 = reaction rate constant at 20˚C
Θ = temperature coefficient
T = temperature of biological reaction.

Considerations for integration into the CDS Toolbox

- ERA5-Land monthly averaged data from 1981 to present
- CMIP5 monthly data on single levels

Method 2 (Zsirai et al., 2012)

Impact of temperature on viscosity: "The change in the viscosity of water (in mPa s, millipascal-second) with temperature within the limits of 5 and 35°C can, within an R2 value of 0.9995, be represented by the following quadratic equation" (Zsirai et al., 2012):

$$\mu_w = 5.829 \times 10^{-5} T^2 - 4.868 \times 10^{-2} T + 0.00174$$

Roorda and van der Graaf (2000) cite another regression:

$$\mu = 497 \left(T + 42.5\right)^{-1.5}$$

Considerations for integration into the CDS Toolbox

- ERA5-Land monthly averaged data from 1981 to present
- CMIP5 monthly data on single levels

4.2 Integration of the Literature Review with the CDS Datasets

See Section 1.2 for explanations about how we selected the indicators to implement in the CDS Toolbox. Similarly to Section 1.2, each variable is available in two versions: ERA5 re-analysis (single level, monthly) for past data (2000–2019) and CMIP5 (single level, monthly) for future data (2006–2100).

The work performed with the CDS Toolbox is available at these links:

- Source code: https://cds.climate.copernicus.eu/toolbox-editor/27053/indicator-download
- App: https://cds.climate.copernicus.eu/apps/27053/indicator-download

Datasets:

- ERA5 monthly data on single level: 2000 to 2019
- CMIP5 monthly data on single level: 2006 to 2100

Indicators created:

- **Precipitation**:
  - Units: mm per month
  - Frequency: monthly
  - ERA5 variable: “mean total precipitation rate”
  - CMIP5 variable: “mean precipitation flux“
  - Note: original units in mm/s
- **Runoff**
  - Units: mm per month
  - Frequency: monthly
  - ERA5 variable: “mean runoff rate”
  - CMIP5 variable: “runoff“
  - Note: original units in mm/s
- **Air temperature**
  - Units: degrees Celsius
  - Frequency: monthly
  - ERA5 variable: “2 m temperature”
  - CMIP5 variable: “2 m temperature“
  - Note: original units in Kelvin

4.3 Integration of Climate Indicators Into the SAVi Wastewater Model

CDS climate indicators related to wastewater include impacts on wastewater volumes in the sewage system, wastewater treatment efficiency, and capacity depreciation. The CLD of the SAVi Wastewater model is presented in Figure 9.

Figure 9. CLD for the wastewater sector (CDS variables included in pink)

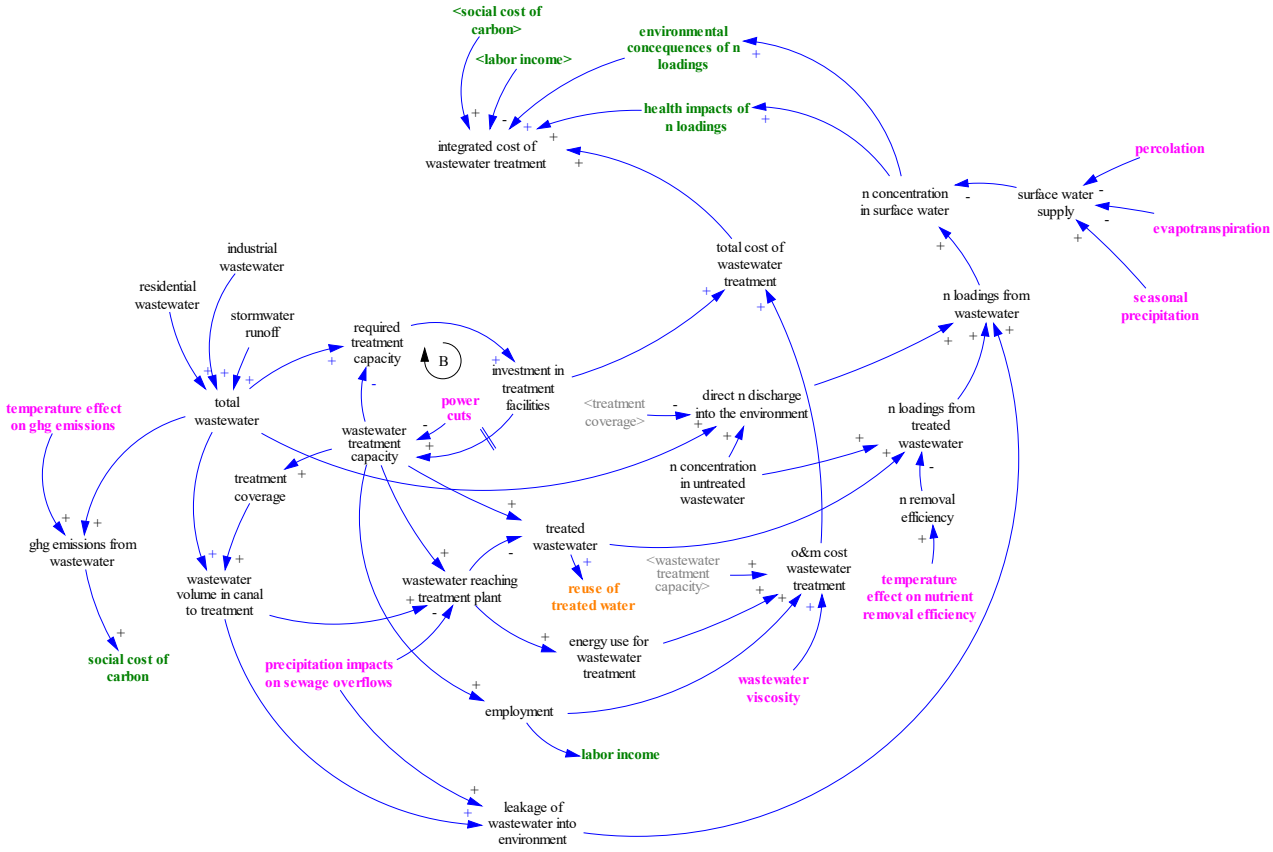

Climate change impacts on wastewater volumes refer to (i) sewage overflows due to excessive water flow during precipitation events, (ii) a reduction in total sewage flow volume due to decreases in water volume, while pollution loads remain the same, and (iii) increased viscosity of water. During sewage overflows, vast amounts of water enter the sewage system within a short period of time. The stormwater mixes with the sewage, and once the total wastewater and stormwater volume exceeds sewage capacity, wastewater is flushed into the streets and leaks into the environment. On the other hand, low precipitation may reduce the flow of water and the amount that is effectively treated. In addition, low precipitation and higher temperatures, combined with no reduction in pollution, increase the viscosity of wastewater. This reduces flow speed in the sewage system and causes increased system corrosion in sewers and wastewater treatment plants, also resulting in higher operation and maintenance costs.

The wastewater treatment efficiency indicator developed from the CDS Toolbox refers to impacts on nutrient removal efficiency in treatment plants. Warmer temperatures benefit nutrient removal efficiencies and are a requirement for the use of certain wastewater treatment technologies.

4.4 Behavioural Impacts Resulting From the Integration of Climate Variables

The sewage overflow indicator obtained from the CDS Toolbox forecasts seasonal changes in stormwater loads and the occurrence of sewage overflows. This allows an improved estimate of

leakage in the SAVi model and better represents the concentration of pollutants in waterbodies, related environmental impacts, and costs.

Furthermore, wastewater treatment efficiency is reduced during peak flow events that exceed the capacity of WWTFs because of the lower amount of water treated and the reduced concentration of pollutants in the wastewater treated.

The CDS Toolbox will also support the estimation of wastewater treatment efficiency using seasonal data. This is important due to the higher impact of wastewater and related pollutants during months with warm climate and months with low precipitation. Viscosity affects maintenance costs, and nutrient removal impacts energy use for treatment, which then affects the operation costs of WWTFs. In addition to operations costs, removal efficiency determines the total capacity requirement of a wastewater system.

The CDS Toolbox indicator on sewage viscosity specifically is used to forecast accelerated depreciation of wastewater treatment infrastructure (sewers and treatment plants). An increase in viscosity leads to increased settlement of sludge in sewers, increasing maintenance cost for dredging. The accelerated depreciation leads to a shorter asset lifetime and increased replacement capital cost.

4.5 Simulation Results

The dynamics of wastewater treatment and its efficiency depend on wastewater loads remaining within the capacity of sewers and sewage treatment plants. The following additions were implemented into the SAVi Wastewater treatment model: (1) urban flood indicator and (2) stormwater runoff per hectare. While the flood indicator enables a forecast of the number of months with extreme stormwater loads, the actual stormwater runoff per hectare provides information about the forecasted total loads that occur during one month. The total area considered for the results presented below is 10 hectares.

4.5.1 Impact of Heavy Precipitation on Urban Flooding

Heavy precipitation events cause urban flooding and contribute to sewage overflows. Sewage overflow is caused by vast stormwater and wastewater loads into sewers that exceed their capacity.

The urban flood indicator is based on the precipitation thresholds provided by Nemry and Demirel (2012) (see Table 28)

Table 28. Precipitation thresholds and their impact on urban flooding

Precipitation (mm/hr)	**Expected impact**
50 mm–100 mm	Flooded roads
100 mm–150 mm	Sewer overflows and potential impacts on traffic
>150mm	Severe flooding; roads may collapse and bridges flood; vehicle damages will occur

Source: Nemry & Demirel, 2012.

The SAVi model is operationalized using monthly precipitation data, therefore relative monthly precipitation is used to determine the potential flooding that may occur. The thresholds for relative precipitation used for this illustration are listed in Table 29.

Table 29. Thresholds for relative precipitation used for the operationalization of urban flooding in the SAVi Wastewater model

Relative precipitation	**Projected impact**
0-2	No impacts
2-3	Flooded roads
3-4	Sewer overflows and potential impacts on traffic
>5	Severe flooding; roads may collapse and bridges flooded; vehicle damages will occur

The equation used for the calculation of the urban flood indicator is described below.

Urban flood indicator = IF THEN ELSE (Relative precipitation > Threshold for urban flooding, Relative precipitation / Threshold for urban flooding, 1)

The urban flood indicator is used as a multiplier in the model, indicating that a value of 1 will result in no flooding impact, while any month during which precipitation exceeds the threshold value will see an increased risks of floods. The resulting flood indicator values for Johannesburg are presented in Figure 10 for the period 1979 to 2100.

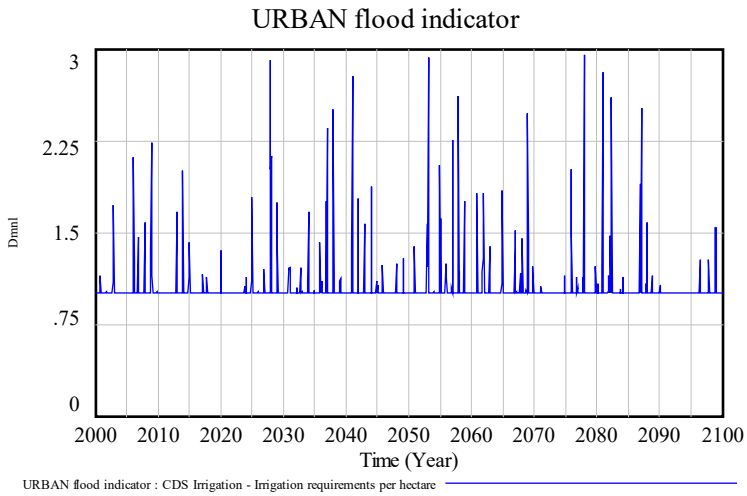

Figure 10. Flood indicator for Johannesburg IPSL RCP 8.5 scenario

The effect of urban flooding on sewage overflows is implemented using the flood indicator and an assumption about the percentage that flows out with each 1 point increase of the flood indicator. The percentage assumed for this simulation is 10%, indicating that, if the flood indicator value increases from 3 to 4, and additional 10% will flow out of sewers during that month. An IF THEN ELSE function is used to ensure that there is no outflow if the indicator has a value of 1 (default value in case of no impacts). The amount of water that flows out of the sewers is presented in Figure 11.

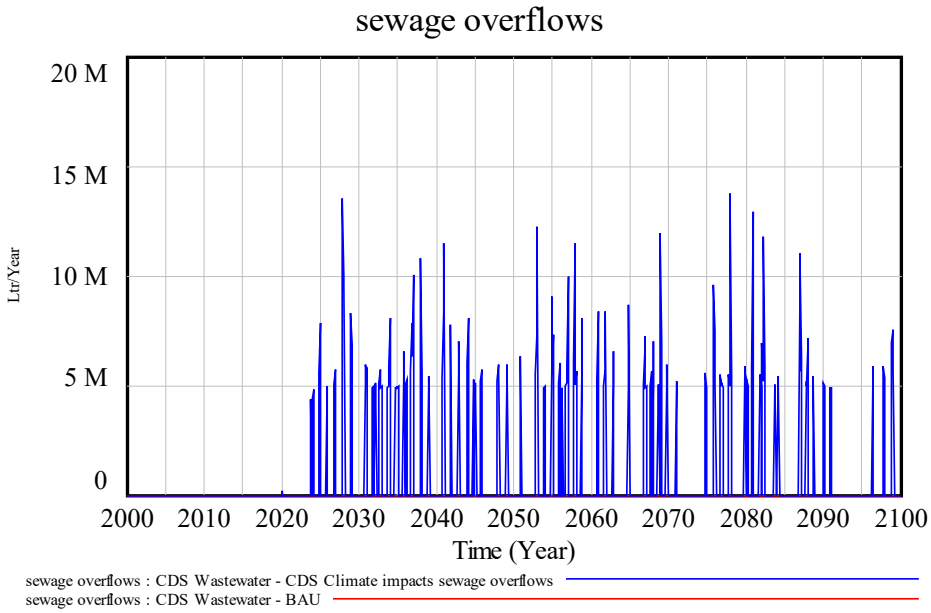

Figure 11. Projected sewage overflows Johannesburg

The simulation results indicate higher energy use in the sewage overflow scenario, resulting in higher energy costs and energy-related emissions. Between 2020 and 2080, the cumulative energy use for wastewater treatment in the CDS climate-impact scenario is projected to be 2.25%

higher, which is equivalent to 679 MWh over 80 years, or approximately 8.5 MWh per year on average. The model indicates that, despite the reduction in the share of wastewater treated induced by the sewage overflow formulation, the total amount of N removed is 2.25% higher.[4]

Energy costs are assumed at 20 cents per kWh, and emissions are estimated using total energy use for N removal and an average grid emission factor of 0.7 tonnes per MWh. Emissions are valued using the social cost of carbon, based on Nordhaus (2017), using USD 31 per tonne of carbon dioxide equivalent (CO_2e) without escalation. In addition, sewage overflows cause wastewater to leak into the environment, which can have detrimental consequences for ecosystems and land productivity (United Nations Environment Programme, 2015).[5] A value of USD 4.9 per kg N is applied to estimate the additional cost of N leaking into the environment and the avoided environmental damages through wastewater treatment. Table 30 provides an overview of the economic performance for selected indicators of the wastewater treatment sector.

Table 30. Monetized impacts of sewage overflows

Indicator	No impacts	(1) Sewage overflow	(1) vs. no impact
Energy cost for wastewater treatment	6,036,634	6,172,436	135,803
Cost of N leaching into the environment	0	204,343	204,343
Social cost of carbon from wastewater treatment	654,975	669,709	14,735
Total costs and externalities	**6,691,608**	**7,046,488**	**354,880**
Avoided environmental damages through wastewater treatment	5,915,901	6,048,988	133,087
Net societal cost of wastewater treatment	**775,707**	**997,500**	**221,793**

4.5.2 Climate Impacts on Urban Runoff

Information about urban runoff is important for urban infrastructure planners to ensure the capacity adequacy of sewage system capacity and potential mitigation requirements. The stormwater runoff per hectare in urban areas is calculated using the following equation:

*Runoff quantity = Average intensity of monthly rainfall * runoff coefficient * conversion from mm to liters per hectare*

Figure 12 presents the simulation results for stormwater runoff in urban areas in the no-climate-impact and the CDS climate-impact scenarios. The results show a significant difference in variability and magnitude of stormwater runoff in the CDS climate-impact scenario.

[4] The difference in energy use is mainly driven by two factors: (1) new precipitation inputs obtained from the CDS database (pushing energy consumption higher relative to the no-impact scenario), and (2) the impact of sewage overflows (reducing energy consumption).

[5] A value of USD 4.9 per kg N (EUR 4.6) released into the environment is assumed for the estimation of N-related environmental damages and the avoided environmental cost of disposing N into the environment. The values indicated in United Nations Environment Programme (2015) range from EUR 4.6 per kg N released into the open sea to EUR 65.2 per kg N released into wetlands.

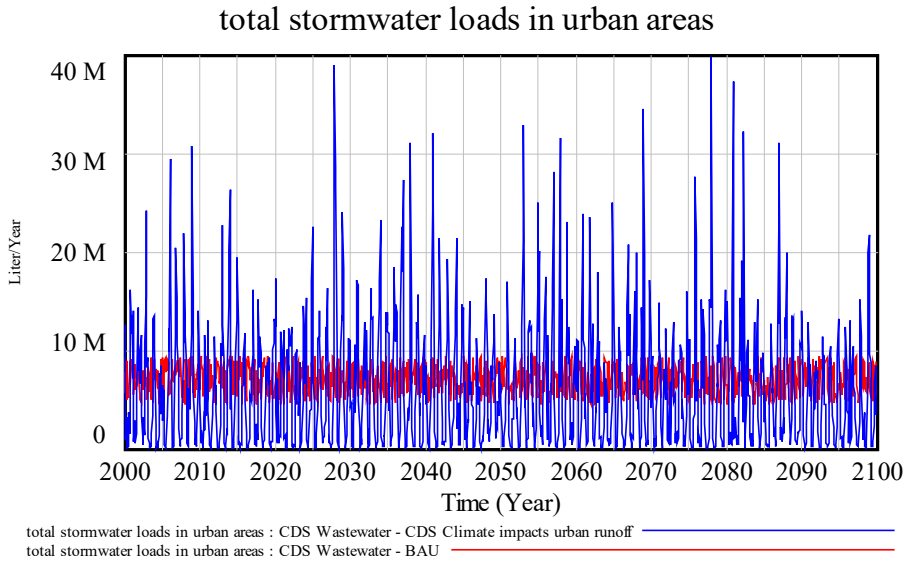

Figure 12. Urban stormwater runoff per hectare

The results indicate a cumulative total stormwater load of 6.7 billion litres and 5.83 billion litres in the no-climate-impact and climate-impact scenarios, respectively, between 2020 and 2100. The change in simulation results is equivalent to a reduction of 13% in cumulative stormwater loads in the CDS climate-impact scenario compared to the no-impact scenario. The above indicates that the updated formulation allows for introducing extreme precipitation events into the analysis while estimating stormwater loads more accurately. For example, the maximum monthly stormwater load projected in this example is 37.8 million litres in the CDS climate-impact scenario, which is more than four times the amount of the 9.5 million litres indicated in the no-impact scenario.

The increased stormwater loads increase the total energy use of the wastewater treatment system. Compared to the no-impact scenario, total energy use is projected to be 5.4% higher, which is equivalent to 20.33 MWh per year or approximately 1,627 MWh over 80 years. Consequently, the energy cost and social cost of carbon are higher in the CDS climate-impact scenario compared to the no-impact scenario. This CDS climate-impact scenario assumes that the urban stormwater runoff does not cause sewage overflows, hence, no additional cost of N reaching the environment incurs.

Table 31. Monetized impacts of urban stormwater runoff

Indicator	No impacts	(2) Urban flooding	(2) vs. no impact
Energy cost for wastewater treatment	6,036,634	6,362,023	325,390
Cost of N leaching into the environment	0	0	0
Social cost of carbon from wastewater treatment	654,975	690,280	35,305
Total costs and externalities	**6,691,608**	**7,052,303**	**360,695**
Avoided environmental damages through wastewater treatment	5,915,901	6,234,783	318,882
Net societal cost of wastewater treatment	**-775,707**	**-817,520**	**-41,813**

5 Buildings

5.1 Literature Review

5.1.1 Energy Demand and Efficiency

5.1.1.1 Heating and Cooling Degree Days

Higher temperature increases the demand for cooling days. Lower temperature increases the need for heating days. Depending on the level of the building's thermal insulation, more energy will be required for indoor thermal regulation.

- **Climate impact**

The heating degree day (HDD) index represents the number of days in which heating is required in a building. The cooling degree day (CDD) index indicates how many days cooling is required. Both have an impact on energy demand and building isolation efficiency.

- **Summary of results**

A case study in Los Angeles, California, estimates that, for every 1˚C increase in temperature, electricity demand would increase in the range of 2%–4% for the whole network.

Another study of Guangzhou, China, found that, on average, an increase of 1˚C would lead to an increase of electricity demand between 0.015% and 0.02% per capita during the year, with fluctuations between summer and winter.

- **Results**

Akbari (2005) found that, "on a clear summer afternoon, the air temperature in a typical city is as much as 2.5K higher than in the surrounding rural areas." The author showed "that peak urban electric demand rises by 2–4% for each 1K rise in daily maximum temperature above a threshold of 15–20°C. Thus, the additional air-conditioning use caused by this urban air temperature increase is responsible for 5–10% of urban peak electric demand."

In rural China, Zhang et al. (2019) found out that, "by using the statistics of counties from 2006 to 2015 in a fixed-effect panel model, the results indicate that a one-degree temperature increase in summer days may lead to 0.015% more electricity consumption per capita, and this correlation may be weaker as income increases. Moreover, a one-degree temperature decrease in winter days may lead to 0.002% more electricity consumption. The northern region may consume 0.021% more electricity than the southern region when facing the same temperature drop"

The threshold for cooling and heating degree days is set at 5°C for heating and 26°C for cooling (Zhang et al., 2019).

In Guangzhou, China, Zheng et al. (2020) estimate that, "with a higher temperature of 1 °C, total electricity consumption would increase by 2.7%, and the residential one would increase by 0.9%. In addition, the projected impacts of climate change on electricity consumption would depend on the emissions of greenhouse gases. In other words, electricity consumption would vary significantly under four RCPs, with the impacts being increased gradually from RCP2.6 to RCP8.5."

- **Methodology**

Method 1 (De Rosa et al., 2014)

The degree days method is based on the assumption that energy consumption is proportional to the difference between external and internal temperatures (De Rosa et al., 2014):

1. Therefore, assuming a global building transmission coefficient H in W/K, the monthly energy consumption Em can be calculated as follows:

$$E_m = \frac{H \cdot DD_m \cdot t_h}{\eta_{hs/cs}}$$

"Where t_h is the heating time in a day (which can be assumed equal to 24 h if a continuous heating/cooling is provided), $\eta_{hs/cs}$ is the efficiency of the equipment, and DD_m is the total heating or cooling degree days of a month" (De Rosa et al., 2014).

$$\text{Heating}: \quad DD_m = \text{HDD}_m = \sum_{d=1}^{D_m} (T_{b,hs} - \overline{T}_{e,d})^+$$

$$\text{Cooling}: \quad DD_m = \text{CDD}_m = \sum_{d=1}^{D_m} (\overline{T}_{e,d} - T_{b,cs})^+$$

"$T_{e,d}$ represents the mean of the daily maximum and minimum external air temperature of a day d
$T_{b,hs}$ and $T_{b,cs}$ are the base temperatures for heating and cooling respectively, which represent the temperature set point of the inner heated/cooled zones
The sign + indicates that only positive values are added. Different approaches can be adopted to calculate the degree days, depending on the type of data available for the external temperature" (De Rosa et al., 2014).

Cooling degree days modified for low values (De Rosa et al., 2014):

"In order to restore the validity of CDDs for low values, a simple correction is introduced. Starting from the standard CDD" (De Rosa et al., 2014):

$$\text{CDD}^* = \text{CDD} + \chi \cdot I_{t0,y}$$

"Where $I_{t0,\,y}$ is the total horizontal solar irradiation of each locality, computed by summing the daily values only when a cooling demand is necessary, while χ is the correction factor, which is adjusted in order to minimize the deviation of the linear regression" (De Rosa et al., 2014).

Mourshed (2012) gives a short review of the different techniques, while a simple application can be found in another article by Büyükalaca et al. (2001).

Method 2 (Eurostat, 2019)

HDD (Eurostat, 2019): If Tm ≤ 15°C Then [HDD = ∑i(18°C - Tim)] Else [HDD = 0] where Tim is the mean air temperature of day i.

CDD (Eurostat, 2019): If Tm ≥ 24°C Then [CDD = ∑iTim - 21°C)] Else [CDD = 0] where Tim is the mean air temperature of day i.

Considerations for integration into the CDS Toolbox

- Air temperature (K): ERA5-Land hourly data from 1981 to present and CMIP5 daily data on pressure levels can be used to estimate the previous equations.

5.1.1.2 Albedo/Temperature of a Surface

- **Climate impact**

"High temperatures are responsible for the increase of energy demand for air conditioning in buildings and photochemistry effects that increase atmospheric pollution, as well as increasing environmental impacts due to the demand of energy generation. Materials with high albedo and emittance attain lower temperatures when exposed to solar radiation, reducing the transference of heat to the environmental air" (Prado & Ferreira, 2005).

- **Methodology**

The equation for determining the temperature for a surface under the sun (Prado & Ferreira, 2005):

$$(1 - a)I = \sigma \times \varepsilon \times (T^4_s - T^4_{sky}) + h_c \times (T_s - T_a)$$

"where a is the albedo or solar reflectance; I the incident solar radiation on the surface (W/m2); ε the emittance of the surface; σ the constant of Stefan–Boltzmann (5.67×10^{-8} W/m^2 K^4); T_s the balance temperature of the surface (K or ˚C); T_{sky} the radiating temperature of the sky (K or ˚C); h_c the convection coefficient (W/m^2 K or W/m^2 ˚C); T_a the temperature of air (K or ˚C)" (Prado & Ferreira, 2005).

Considerations for integration into the CDS Toolbox

- Albedo: Dimensionless – ERA5-Land monthly averaged data from 1981 to present

- Solar radiation: J /m^2 – ERA5-Land monthly averaged data from 1981 to present
- Temperature of air: K – ERA5-Land monthly averaged data from 1981 to present

5.1.1.3 Soil Temperature and Moisture

- **Climate impact**

Soil temperature and moisture have an impact on how much energy is evacuated through soils and hence affect indoor temperature and related cooling and heating needs.

- **Methodology**

In a paper by Janssen et al. (2004), the influence of "soil moisture transfer on building heat loss via the ground is investigated by comparing fully coupled simulations with linear thermal simulations. The observed influences of coupling are" (Janssen et al., 2004):

- The larger amplitude of surface temperature
- The variation of thermal conductivity with moisture content
- The advection of sensible heat by liquid transfer.

Surface heat balance ($q_{h,se}$) and moisture balance ($q_{m,se}$) are given (Janssen et al., 2004):

$$q_{\mathrm{h,se}} = H + R_{\mathrm{t}} + \mathrm{LE} + \mathrm{HP},$$

$$q_{\mathrm{m,se}} = E + P.$$

Where "heat exchange (H), solar and long-wave radiation (R_t), and the transfer of sensible and latent heat by evaporation (LE) and precipitation (HP). … Precipitation (P) and evaporation.(E)" (Janssen et al., 2004).

<u>Considerations for integration into the CDS Toolbox</u>

- Radiation, evaporation, precipitation: ERA5 monthly averaged data on single levels from 1979 to present

5.1.2 Rainwater harvest

Rainwater harvest is a common feature of buildings, either new ones or those located in areas prone to drought.

5.1.2.1 Precipitation

- **Climate impact**

Precipitation and the roof area of buildings are the main determinants of rainwater harvesting.

- **Methodology**

Method 1 (Pande & Telang, 2014)

Estimation of mean rainwater supply that could be used for buildings or any other infrastructure (Pande & Telang, 2014):

Mean rainwater supply in m^3 =
Mean annual rainfall in m/year × Surface area of catchment in m^2 × Run-off coefficient

Considerations for integration into the CDS Toolbox

- Rainfall: m – ERA5 monthly averaged data on single levels from 1979 to present
- Runoff: m – ERA5-Land monthly averaged data from 1981 to present

Method 2 (Diaz et al., 2015)

"This method supplements existing climate analysis tools by defining a scale and benchmarks that easily link potential water requirements of buildings with water availability from precipitation." Further, "it is necessary to associate the units of precipitation with those of water demand. […]The relation of precipitation and water demand scales is influenced by the runoff efficiency of the roof or other element from which the water is collected" (Diaz et al., 2015).
.

Precipitation Benchmark: "minimum level of precipitation required for a building to fully meet its demand of rainwater, and any amount above this level is exceeding precipitation which could be stored by the building for future needs" (Diaz et al., 2015):

$$PB = (Dt \times 30 \text{ days}) / ([CRa/HFa] \times C) \quad (1)$$

PB = precipitation benchmark (mm or L/m^2)
Dt = total water demand (L/m^2 day)
CRa = collectable roof area (m^2)
HFa = habitable floor area (m^2)
C = runoff coefficient (dimensionless)
The denominator in equation *(1)* is termed the building factor (BF), because all its variables depend on the configuration of the building. The minimum precipitation required to satisfy the water demand of the building will vary according to its BF (the requirement increases when BF is 1).

"If water is required for different purposes (e.g. laundry, toilets, EC, etc.) DT [total water demand] must be calculated previously with the formula" (Diaz et al., 2015):

$$Dt = De + (Da/HFa) \quad (2)$$

De = Water demand for EC (L/m² day)
Da = Supplementary water demand (L/day)

"This water demand may vary according to the climate and the specific needs of each building. Even very similar buildings may have differences in the amounts of water required (e.g. due to orientation, surrounding influences, etc.). Thus, the particular demand of a building must be individually calculated" (Diaz et al., 2015).

Considerations for integration into the CDS Toolbox

- ERA5 monthly averaged data on single levels from 1979 to present
- ERA5-Land monthly averaged data from 1981 to present

5.1.3 Climate Hazards

A building (a type of physical infrastructure) is impacted by extreme events related to wind, water, and temperature. Depending on the type of building and technology, construction materials, and strength of construction, impacts will vary.

5.1.3.1 Flood Discharge

- **Climate impact**

Floods have an impact on buildings due mainly to water penetration and flooding.

- **Methodology**

Assessing the impact of flood damage (JICA, 2003):

$$Q_p = \frac{ciA}{3.6}$$

Where: Q_p = maximum flood discharge (m^3/s)
c = dimensionless runoff coefficient
i = rainfall intensity within time t_c
A = catchment area (km^2)

"The computed peak rate of runoff at the outlet point is a function of the average rainfall rate during the time of concentration, i.e., the peak discharge does not result from a more intense storm of shorter duration, during which only a portion of the watershed is contributing to the runoff at the outlet" (JICA, 2003).

"The time of concentration employed is the time for the runoff to become established and flow from the most remote part of the drainage area to the outlet point. Rainfall intensity is constant throughout the rainfall duration" (JICA, 2003).

Considerations for integration into the CDS Toolbox

- ERA5 monthly averaged data on single levels from 1979 to present
- ERA5-Land monthly averaged data from 1981 to present

5.1.3.2 Wind pressure

- **Climate impact**

"Overhangs from a building are affected by wind pressure acting from underneath. These combined with pressures (or suctions) on the top surface often create a severe design condition" (Krishna et al., 2002).

- **Methodology**

"The wind pressure at any height above mean ground level shall be obtained by the following relationship between wind pressure and wind speed" (Krishna et al., 2002):

$$P_z = 0.6 \times V_z^2$$

"Where P_z = wind pressure in N/m2 at height z, and V_z = design wind speed in m/s at height z. The relationship between design wind speed V_z and the pressure produced by it assumes the mass density of air as 1.20 kg/m^3, which changes somewhat with the atmospheric temperature and pressure" (Krishna et al., 2002).

Considerations for integration into the CDS Toolbox

- Wind speed: m/s – ERA5 monthly averaged data on single levels from 1979 to present

5.1.3.3 Lightning

- **Climate impact**

Lightning can cause damage to a building's infrastructure. Material damages and electrical damages to cables and electricity infrastructure might cause a power shutdown.

- **Summary of results**

Literature is very scarce, but we found that, "for every 1˚C rise in global temperatures, there will be an increase of 12% in the frequency of lightning strikes" (Sollatek, 2016).

- **Results**

According to Vought (2019), damages from lightning in the United States "costs about $1,200 per year or $100 per month" for facility lightning protection; "yet [lighting protection] can prevent infrastructure failure costing as much as $100,000 per hour." Lightning events are likely to increase, as shown with the following equation (Vought,2019):

$$F = \text{constant} \times P \times CAPE$$

With F = flash rate per area; P=precipitation rate; CAPE = convective potential available energy (potential electrical energy of that area increases with higher temperatures, as reflected by the ability of air to rise more rapidly into the upper atmosphere).

Sollatek (2016), a firm specialized in lightning equipment, shows that, "for every 1˚C rise in global temperatures, there will be an increase of 12% in the frequency of lightning strikes. With that said we can expect to see a 50% rise in the next 100 years. For every two lightning strikes in 2000, there will be three lightning strikes in 2100."

5.2 Integration of the Literature Review with the CDS Datasets

See section 1.2 for explanations about how we selected the indicators to implement in the CDS Toolbox.

Datasets:

- ERA5 monthly data on single level
- CMIP5 monthly data on single level
- ERA5 hourly data on single level

Indicators created:

- **Air temperature**
  - Units: degrees Celsius
  - Frequency: monthly
  - ERA5 variable: "2 m temperature"
  - CMIP5 variable: "2 m temperature"
  - Note: original units in Kelvin
- **Precipitation**:
  - Units: mm per month
  - Frequency: monthly
  - ERA5 variable: "mean total precipitation rate"
  - CMIP5 variable: "mean precipitation flux"
  - Note different: units scaling was necessary
  - CMIP5 variable: "2m_temperature"
- **Minimum daily temperature**

- Units: degrees Celsius
- Frequency: monthly
- ERA5 variable: “2m temperature”
  - Daily minimum and monthly mean from hourly temperature
- CMIP5 variable: “minimum_2m_temperature_in_the_last_24_hours “

- **Maximum daily temperature**
  - Units: degrees Celsius
  - Frequency: daily
  - ERA5 variable: “2m temperature”
    - Daily maximum and monthly mean from hourly temperature
  - CMIP5 variable: “maximum_2m_temperature_in_the_last_24_hours “
- **Wind**
  - Units: m/s
  - Frequency: monthly
  - ERA5 variable: “10 m wind speed”
  - CMIP5 variable: “10 m wind speed“

Additional information
Daily temperature indices may be useful to determine HDD and CDD indices.

5.3 Integration of Climate Indicators into the SAVi Buildings Model

The climate indicators developed in and extracted from the toolbox include impacts on heating and cooling, lighting, rooftop solar generation, and rainwater harvesting. We have also estimated climate hazards related to flood and wind pressure. The CLD for buildings is presented in Figure 13.

Figure 13. CLD for the buildings sector (CDS variables included in pink)

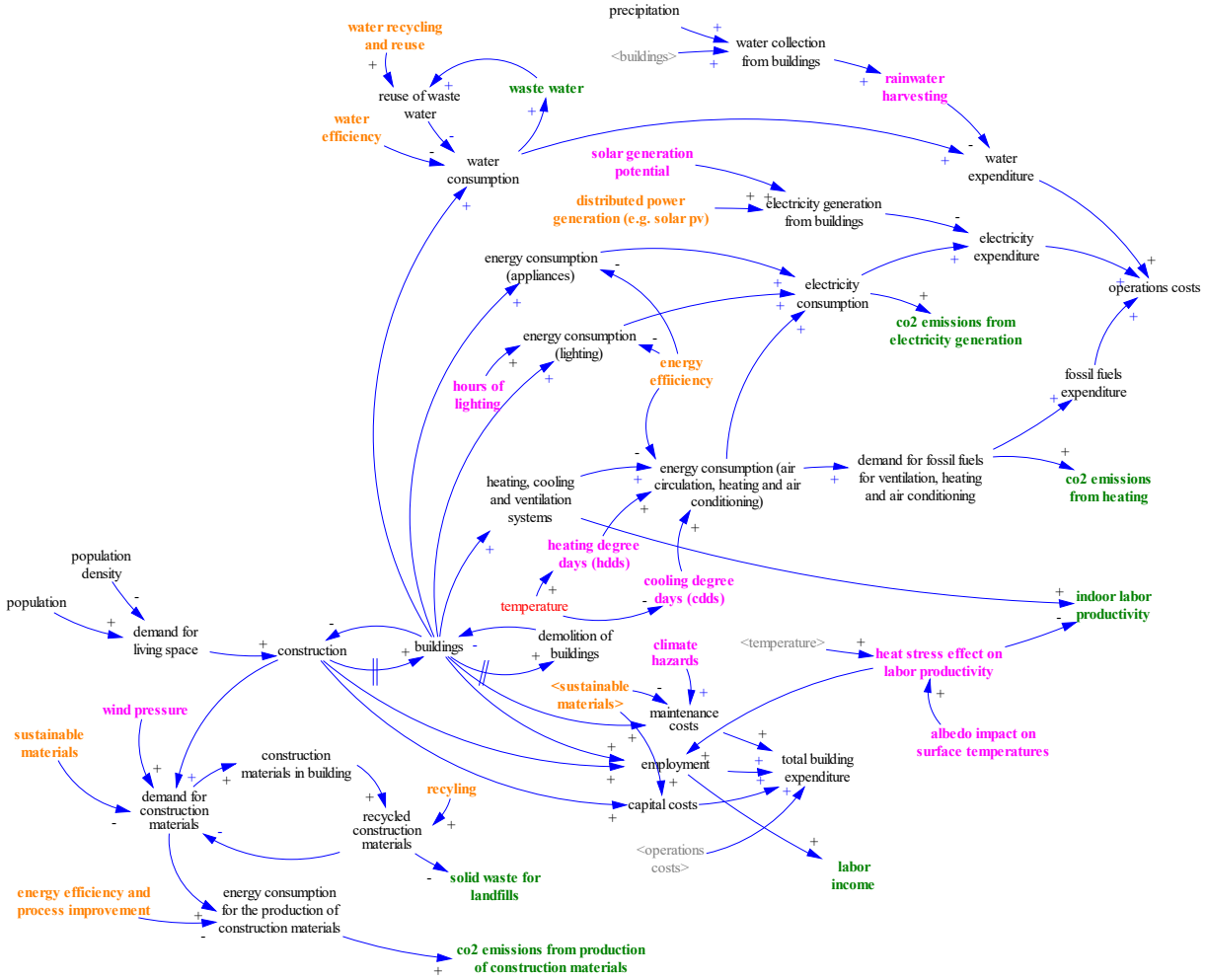

The time duration of heating and cooling in the SAVi model is defined as a function of HDDs and CDDs, which are obtained from the CDS Toolbox. In the model, HDDs determine the days of the year that buildings are heated. CDDs, on the other hand, determine the number of days that air conditioning is required. HDD and CDD therefore affect energy consumption, energy costs, and emissions (depending on the technology used) and have an impact on both operation cost and societal costs.

The hours of lighting, used to determine energy consumption for lighting, are obtained from the CDS Toolbox. The further away from the equator the project is located, the more seasonal and total difference in lighting hours have to be considered. The energy requirements for lighting affect energy costs, and hence the cost of operation of the building and, indirectly, emissions (depending on the technology and energy source used to produce electricity).

The rooftop solar power generation potential represents the amount of electricity that can be generated using rooftop solar PV. Solar generation depends on solar radiation (resulting from location, sunshine hours, and cloud cover). The CDS Toolbox provides the projected solar power generation potential by location, and the SAVi model uses it to determine the specific electricity

generation for the project considered. This takes into account the size of the PV installation, and reduces the purchase of electricity, its cost, and emissions.

The rainwater harvesting potential is the amount of water that could be harvested by a building, given a specific technology and related efficiency. Rainwater harvesting reduces building water demand and contributes to lowering potable water use. The rainwater harvesting potential is estimated by the CDS Toolbox and used as an input to SAVi.

The impact of floods and wind pressure are considered to determine the integrity of the building and any potential damage to physical infrastructure and related costs.

5.4 Behavioural Impacts Resulting From the Integration of Climate Variables

Obtaining HDDs and CDDs from the toolbox enables the projection of future heating and cooling requirements and seasonal peaks more accurately. This improves both the estimation of capacity requirements for heating and cooling and related costs. It further allows a more accurate assessment of the effectiveness and economic viability of different solutions for heating and cooling as well as thermal insulation.

Information concerning the hours of lighting enables the modelling of lighting requirements and related energy consumption and costs more accurately. Changes in lighting requirements also lead to changes in the use of light bulbs, hence improving the estimation of replacement rates and related cost.

Location-specific forecasts of solar power generation potential improves the projection of rooftop PV power generation and economic viability in the SAVi model. Changes in solar generation potential affect revenues from feed-in tariffs as well as the amount of grid-based electricity that is consumed. Grid-based electricity consumption affects user costs and total building-related CO_2e emissions.

The rainwater harvesting potential generated by the CDS Toolbox improves estimates of monthly water requirements and purchases from water utilities. It also allows SAVi to make use of various climate change forecasts with daily/weekly/monthly time steps, a new feature for the estimation of this indicator. This greatly enhances the potential for SAVi to be used in areas prone to drought and to assess the climate resilience of buildings more fully.

Floods and extreme wind pressure support the estimation of extraordinary maintenance costs in the model. This information will highlight how constructing new buildings in disaster-prone areas may not be financially viable.

5.5 Simulation Results

The literature review above has shown that climate impacts buildings in various ways. Three CDS-based climate variables were integrated into the SAVi Buildings model: (1) rainwater harvesting

potential per m^2, (2) heating and cooling degree days, and (3) the effect of temperature on rooftop solar PV generation.

5.5.1 Rainwater Harvesting Potential

Rainwater harvesting potential refers to the amount of rainwater that can be collected given that infrastructure for rainwater harvesting is in place. In most cases, the collected rainwater is used to substitute potable water for a variety of uses, such as gardening, toilet flushing, and others.

The amount of rainwater that can be collected depends on the available area (in m^2) for rainwater harvesting, the runoff coefficient of the roof surface, and seasonal precipitation. The following equation is used for calculating potential rainwater harvesting yield based on CDS data, based on Biswas (2014).

*Rainwater harvesting potential = Monthly precipitation * Runoff coefficient * Conversion mm to liter per m^2*

Table 32 provides an overview of runoff coefficients for various roofing materials, as provided by Biswas (2014). For the results presented below, a runoff coefficient of 0.8 is applied.

Table 32. Rainwater runoff coefficients for various roofing materials

Type	Runoff coefficient
Galvanized iron sheet	>0.9
Corrugated metal sheet	0.7–0.9
Tiles	0.8-0.9
Concrete	0.6–0.8
Brick pavement	0.5-0.6
Rocky natural catchment	0.2–0.5
Soil with slope	0.0–0.3
Green area	0.05–0.1

Source: Biswas, 2014.

The results of rainwater harvesting potential in the no-climate-impact and climate-impact scenarios are presented in Figure 14. The results show that the previous formulation used in SAVi significantly underestimates the potential for rainwater harvesting.

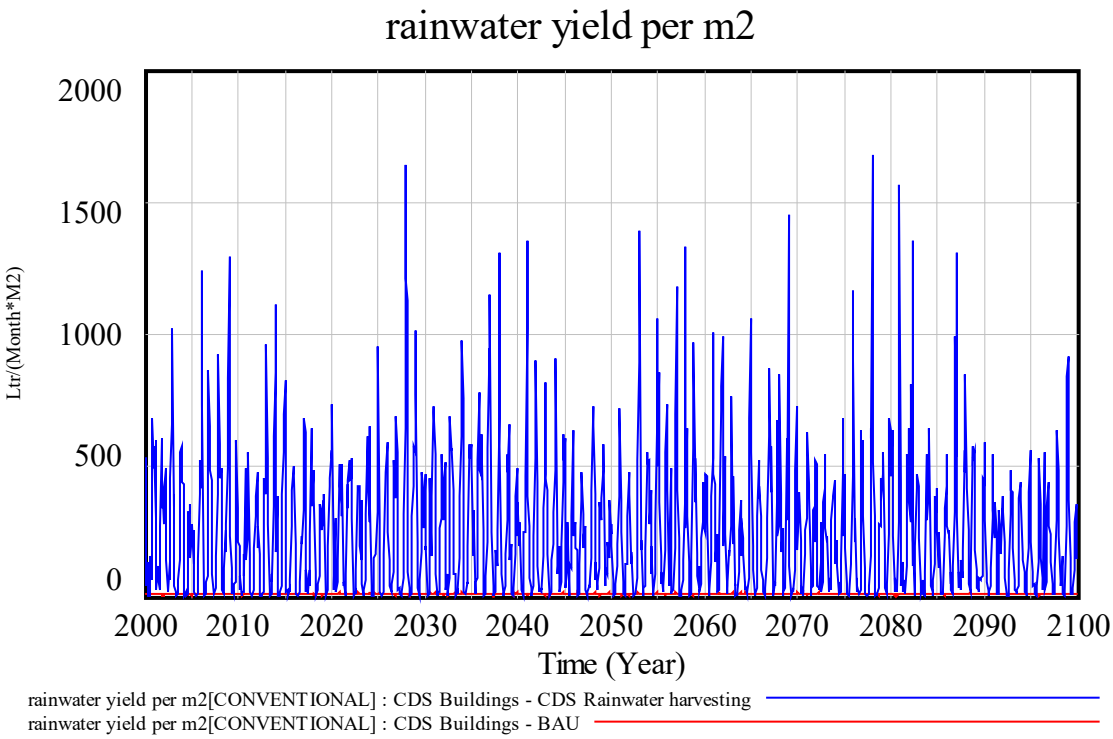

Figure 14. Rainwater harvesting yield per m^2 of roof surface

The use of climate data to forecast rainwater harvesting yields compared to using constant seasonal precipitation values in the no-climate-impact scenario yields significant differences. Between 2020 and 2100, the average annual rainwater harvesting yield is 134.7 litres/m^2 in the no-climate-impact scenario and 3,068.6 litres/m^2 in the CDS climate scenario. The difference in annual averages indicates that the yield forecasted by climate data-based formulations is almost 23 times higher compared to the no-climate-impact scenario.

Furthermore, the maximum monthly value for rainwater harvesting yields indicated in the no-climate-impact and CDS climate-impact scenario are 15.2 litres/m^2 and 1,674.9 litres/m^2, respectively. Table 33 compares the average monthly rainwater harvesting yields in the CDS climate and the no-climate-impact scenario respectively.

Table 33. Average rainwater harvesting yield per decade

Rainwater yield in liter per m^2	2020-2030	2030-2040	2040-2050	2050-2060	2060-2070	2070-2080	2080-2090	2090-2100
CDS climate scenario	275.41	286.10	247.46	272.25	270.34	235.02	258.96	196.39
CDS relative to 2020-2030	*0.0%*	*3.9%*	*-10.1%*	*-1.1%*	*-1.8%*	*-14.7%*	*-6.0%*	*-28.7%*
No climate scenario	11.48	11.49	11.01	10.83	11.17	11.54	10.81	11.37
No climate relative to 2020-2030	*0.0%*	*0.0%*	*-4.1%*	*-5.7%*	*-2.8%*	*0.5%*	*-5.8%*	*-1.0%*

Between 2020 and 2100, the cumulative amount of rainwater that can potentially be harvested is 10,774 litres/m^2 in the no-climate-impact scenario and 245,491 litres/m^2 in the CDS climate-impact scenario, respectively. Assuming that one litre of water costs 0.5 cents, the projected net savings in water expenditure over 80 years total EUR 53.87 and EUR 1,227.50 per m^2 in the no-

climate-impact and CDS climate-impact scenarios, respectively. These savings are equivalent to average annual savings of EUR 0.67 and EUR 15.34 per m^2 in the no-climate-impact and climate-impact scenarios, respectively.

5.5.2 Impacts on Rooftop Solar PV Generation

Similar to the energy sector, the load factor of rooftop solar PV generation potential is affected by the surrounding air temperature. As temperatures increase beyond the threshold of optimal functioning for rooftop solar PV systems, their efficiency decreases and so does the potential generation.

The equation used for estimating temperature impacts on rooftop solar PV load factor is described below.

*Temperature effect on rooftop solar PV load factor = 1 - IF THEN ELSE (Mean annual temperature > Temperature threshold for optimal functioning, (Mean annual temperature - Temperature threshold for optimal functioning) * 0.01, 0)*

Figure 15 presents the forecasted generation of 1,000 kW of rooftop solar capacity in kWh in the no-climate-impact (red line) and CDS climate-impact scenarios (blue line). The reductions in generation occur during warmer periods of the year as a consequence of air temperature exceeding the threshold for optimal functioning of solar PV systems.

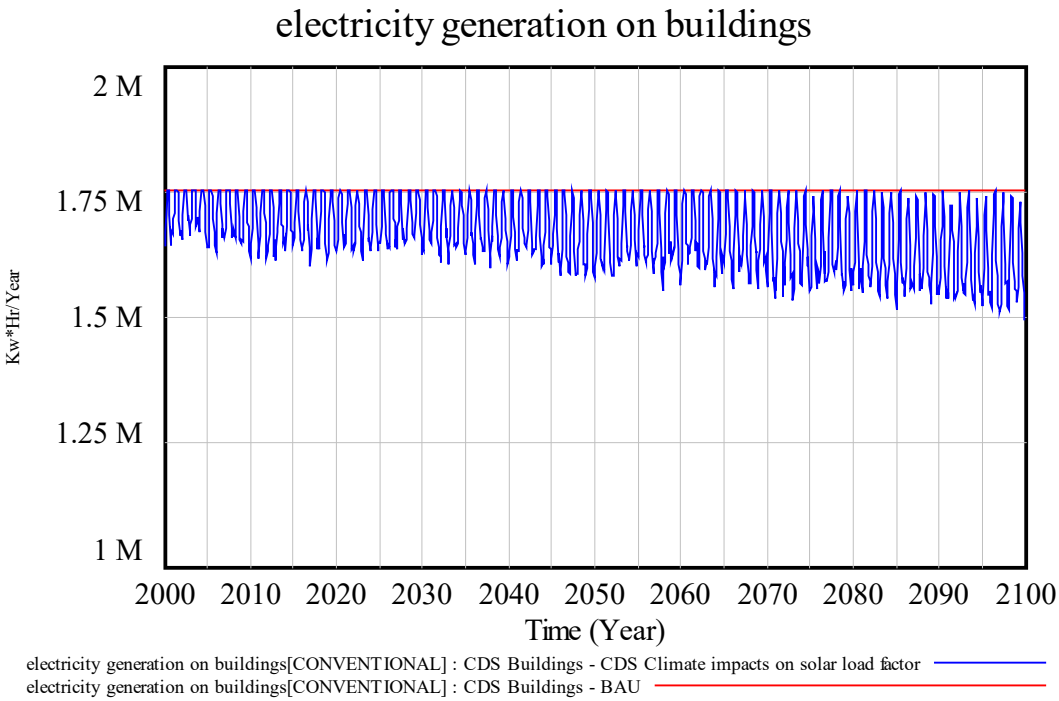

Figure 15. Solar PV generation on buildings for 1 MW of installed capacity

Between 2020 and 2080, the forecasted cumulative generation is 1,683.7 GWh in the no-climate-impact scenario and 1,593.5 GWh in the CDS climate-impact scenario. The cumulative reduction

in generation induced by climate impacts is 90.21 GWh over 80 years or 1.128 GWh per year on average. This difference in cumulative generation indicates that the average reduction in the load factor of solar PV is 5.4% compared to the no-impact scenario.

Assuming a price of 20 cents per kWh, the cumulative savings in electricity cost from using solar energy over 80 years total EUR 336.73 million and EUR 318.69 million in the no-climate-impact and CDS climate-impact scenarios, respectively. This is equivalent to average annual reductions in electricity costs of EUR 4.21 million (no-climate-impact scenario) and EUR 3.98 million (CDS climate-impact scenario). Considering 1 kW of capacity, the cumulative savings over 80 years are equivalent to EUR 336,730 and EUR 318,690, respectively.

5.5.3 Impact of Climate on Heating and Cooling Degree Days

Heating and cooling degree days determine the capacity utilization of heating and cooling systems and, hence, directly affect heating- and cooling-related energy use and emissions. The approach used for estimating the number of heating and cooling degree days is based on a formula by Eurostat (2019). The formulation proposed by Eurostat compares daily temperature values to a minimum threshold to obtain HDD and a maximum threshold to obtain CDD. The following formulations are provided (Eurostat, 2019):

Heating Degree Days =
If Tm ≤ 15°C Then [HDD = ∑i(18°C - Tim)] Else [HDD = 0] where Tim is the mean air temperature of day i.
Cooling Degree Days = If Tm ≥ 24°C Then [CDD = ∑iTim - 21°C)] Else [CDD = 0]

Where Tim is the mean air temperature of day i.

Due to the use of monthly data, the number of HDDs and CDDs is estimated using the monthly average daily temperature and the Eurostat thresholds. The equations below describe how climate data is processed to obtain the number of HDDs and CDDs respectively.

Heating Degree Days = IF THEN ELSE (Tair < 15°C, 30, 0)
Cooling Degree Days = IF THEN ELSE (Tair > 24°C, 30, 0)

The above formulations assume that, if the monthly average daily temperature falls under or exceeds the defined thresholds, heating or cooling will be considered for the whole month. Figure 16 presents the forecasts for HDD and CDD in Johannesburg, using the IPSL RCP 8.5 scenario. The results indicate that CDDs will increase, starting around 2046, while the number of HDDs will decrease gradually between 2040 and 2085, after which heating seems to occur only in specific months, no longer a season.

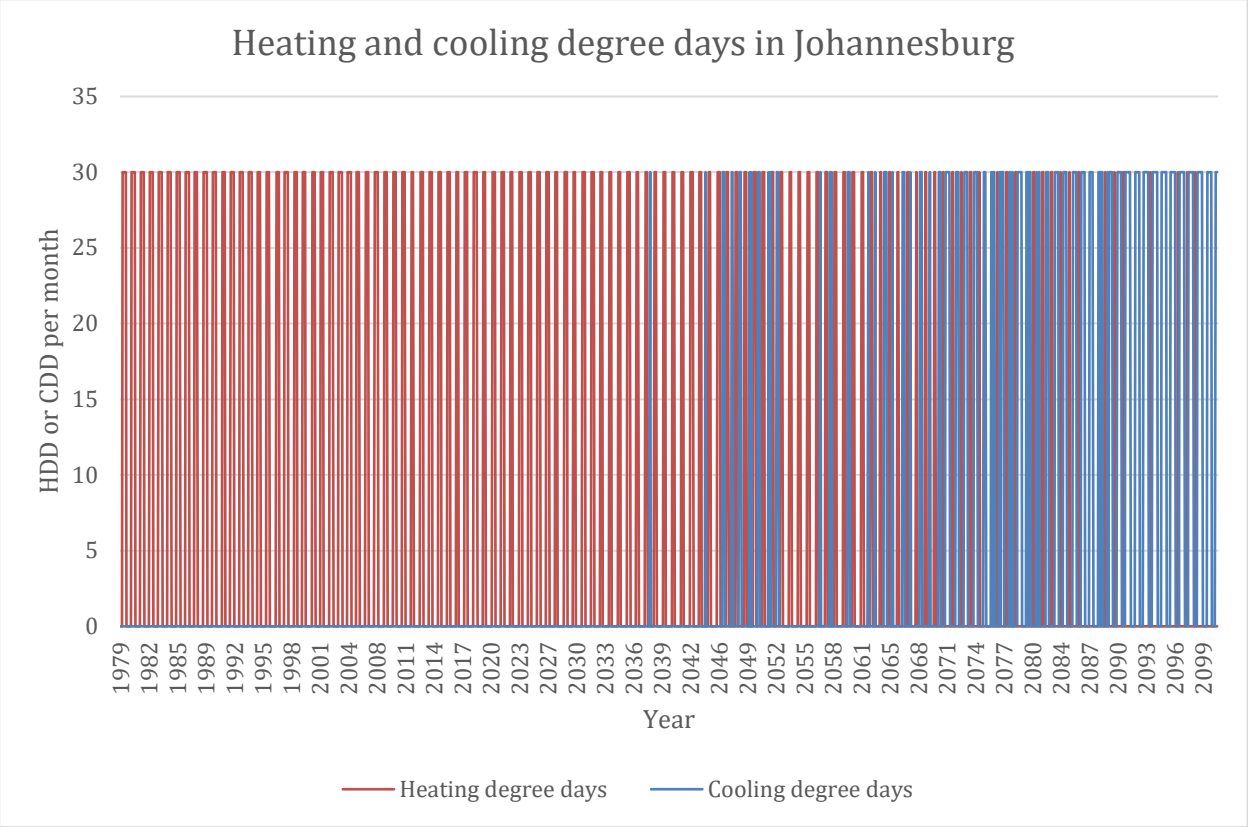

Figure 16. Forecasted HDDs and CDDs in Johannesburg

Table 34 provides information about the forecasted HDDs and CDDs for Johannesburg in the IPSL RCP 8.5 scenario. Compared to 2020–2030, the number of HDDs is forecasted to decline by 82% over the next 80 years as a consequence of increasing temperatures. The number of CDDs increases from zero (no cooling) to 204 days per year over the next 80 years.

Table 34. Average heating and cooling degree days per decade

Indicator	2020–2030	2030–2040	2040–2050	2050–2060	2060–2070	2070–2080	2080–2090	2090–2100
Heating degree days								
Climate-impact scenario	111	99	99	90	66	39	36	18
Relative to 2020–2030	*0%*	*0%*	*0%*	*-9%*	*-33%*	*-61%*	*-64%*	*-82%*
No-impact scenario	168	168	168	168	168	168	168	168
Cooling degree days								
Climate-impact scenario	0	3	40	33	51	138	144	204
Relative to 2020-2030	*0%*	*0%*	*1224%*	*988%*	*1588%*	*4489%*	*4689%*	*6691%*
No-impact scenario	95	95	95	95	95	95	95	95

The changes in HDDs and CDDs indicated above lead to changes in energy consumption and emissions. Results for key indicators affected by the change in the formulation of heating and cooling degree days are presented in Table 35. Results are presented in cumulative million USD between 2020 and 2100. The results show that the initial setup of the SAVi model was overestimating energy use and related costs and emissions for both heating and cooling. The most

significant impact can be seen in the heating sector, where the indicated energy expenditure is 58.5% lower in the CDS climate-impact scenario compared to the no-impact scenario. For cooling, the reduction in energy cost is 19.2% compared to the no-impact scenario.

Table 35. Key indicators affected by Heating and Cooling Degree Days (in million USD)

Indicator	Heating			Cooling		
	No impact	Climate impact	Climate impact vs. no impact	No impact	Climate impact	Climate impact v.s no impact
Energy expenditure	183.55	76.20	-58.5%	6.73	5.44	-19.2%
Social cost of carbon	0.57	0.24	-57.2%	3.96	3.19	-19.3%
Total costs	**184.12**	**76.45**	**-58.5%**	**10.68**	**8.63**	**-19.2%**
CO_2e emissions	18,421	7,888	-57.2%	127,659	103,036	-19.3%
Energy demand	614.16	21.25	-96.5%	182.37	147.19	-19.3%

6 Roads

6.1 Literature Review

6.1.1 Infrastructure Impacts

The impacts of climate variables on roads vary depending on how they are built and the materials used. Precipitation, snow, and high temperatures imply higher costs of maintenance (operating costs). If maintenance is not timely, the reduced quality of roads can lead to the emergence of structural problems and increase the probability of accidents.

6.1.1.1 Precipitation

- **Climate impact**

High amounts of precipitation can damage roads, depending on surface permeability and materials used. Surface runoff is an indicator commonly used to determine the extent to which a road is exposed to damage due to precipitation.

- **Summary of results**

Runoff holding capacity for interlocking block pavement with gravel (IBPG) is 136 mm per rainfall depth. For porous concrete pavement (PCP), the normalized volume reduction was $2.81 \times 10^{-3} \pm 0.67 \times 10^{-3}$ $m^3/m^2/mm$ (Alam et al., 2019).

One study concluded that, for every 10 cm of monthly rainfall, rut depth would increase by 3 mm (Chinowsky et al., 2013).

- **Results**

Chinowsky et al. (2013) estimated that, for the maintenance of roads in the United States, “rut depth over a road’s lifecycle increases by approximately 3mm with every 10 cm increase in mean monthly rainfall. This implies higher road maintenance with heavy rainfall.”

When considering runoff efficiency, Alam et al. (2019) showed that “IBPG was capable of holding runoff from rainfall depths up to 136 mm prior to flooding. PCP (Porous Concrete Pavement) was the most satisfactory in reducing surface runoff (NVR (normalized volume reduction): $2.81 \times 10^{-3} \pm 0.67 \times 10^{-3}$ m^3 /m^2 /mm), which was significantly higher than the traditional pavement” (Alam et al., 2019).

- **Methodology**

6.1.1.2 Runoff Efficiency

Alam et al. (2019) examined "the hydrologic and environmental performance of three types of permeable pavement designs: PCP, permeable interlocking concrete (PICP), and IBPG in the semi-arid South Texas."

"Equations (1)–(5) show the approach used to calculate the total inflow volume into the pavement surface, % peak flow reduction, total outflow volume at the pavement's outfall, total volume stored into pavements, and normalized volume reductions (NVR) from monitored permeable and traditional pavements" (Alam et al., 2019).

1. Total inflow volume (Alam et al., 2019):

$$V_i = R\left(A_p + C_1A_1 + C_2A_2 + C_3A_3 \ldots\ldots\right) \quad (1)$$

V_i = total inflow volume onto pavement surface (m^3)
R = rainfall depth (mm)
A_p = permeable pavement area (m^2)
A1, A2, A3 = areas from surrounding drainage sources (m^2)
C1, C2, C3 = runoff coefficients of surrounding drainage sources

2. The % peak flow reduction for all monitored permeable pavements (Alam et al., 2019):

$$\%\ Peak\ Flow\ Reduction = \left(\frac{TP_{PF} - PP_{PF}}{TP_{PF}}\right) \times 100 \quad (2)$$

TP_{PF} = Normalized peak flow rate at the outfall of traditional pavement (m^3/s)
PP_{PF} = Normalized peak flow rate at the outfall of alternative pavement (m^3/s)

3. Volume of runoff (Alam et al., 2019):

$$V_o = q_0 \times t \quad (3)$$

V_o = total runoff volume (m^3)
q_0 = outflow rate (m^3/s)
t = flow duration (s)

4. Storage volume (Alam et al., 2019):

$$S = V_i\ (1) - V_o\ (3)$$

5. Normalized volume reduction (Alam et al., 2019):

$$\left(\frac{m^3}{m^2 \cdot mm}\right) = \frac{V_i - V_o}{A_p \times R} \quad (5)$$

Considerations for integration into the CDS Toolbox

- ERA5 hourly data on single levels from 1979 to present

6.1.1.3 Flood Risk

See section 5.1.3.1 on flood risk for buildings, proposing the creation of a non-linear function based on a report by Nemry and Demirel (2012).

6.1.1.4 Temperature and Freeze–Thaw

According to Chinowsky et al. (2013) freeze–thaw effects are worst in moderate freeze areas. When a former moderate freeze area transitions to a low freeze area due to higher temperatures, this reduces rutting of the road and therefore maintenance costs. Increased temperatures also cause some areas to change from high freeze to moderate freeze, which increases rutting and maintenance costs. Moderate freeze areas are defined to have 50–400 freeze days per year; high freeze areas have more than 400 freeze days per year. Freezing degree days are usually calculated as a sum of average daily degrees below freezing for a specified time period (National Snow & Ice Data Center, n.d.). Rut depths in moderate freeze areas and high freeze areas are approximately 3.25 and 2.75 mm higher, respectively, than in no-freeze zones (Jackson & Puccinelli, 2006).

6.1.1.5 Temperature

As presented in Chinowsky et al. (2013), higher temperatures imply higher stress for paved roads, as the asphalt becomes more susceptible to cracking. Cracking can be avoided by using a different binder in the surface asphalt.

6.1.2 Maintenance

6.1.2.1 Precipitation

- **Summary of results**

Regarding specific changes in precipitation, a review of the literature indicates that maintenance costs are affected by precipitation. Specifically, the increase in cost is approximately 0.8% for every 1% increase in maximum monthly precipitation.

Degradation of 5.625 points per millimetre of rutting is related to precipitation per year, and 7.83 points per millimetre of rutting is related to freeze–thaw.

- **Results**

Method 1 (Chinowsky et al., 2013)

Chinowsky et al. (2013) propose an equation based on a study conducted on the U.S. road network, taking rutting (or rut depth) as a measure of road depreciation. The approach assumes that higher rutting leads to shorter maintenance intervals and, hence, overall maintenance costs. For paved roads, they included three climate-related effects on roads: (1) rutting from precipitation, (2) rutting caused by freeze–thaw cycles, and (3) cracking during periods of high temperatures. For unpaved roads, only the erosion from precipitation was calculated.

There are different estimates of the rutting occurring over a road's life cycle: N.D. Lea International (1995) estimates 8 mm of rutting over a road's life cycle, while Lavin (2003) estimates 5.75 mm of rutting. Based on these values, degradation of 5.625 points per millimetre of rutting is estimated related to precipitation and 7.83 points per millimetre of rutting related to freeze–thaw (Chinowsky et al., 2013). According to Chinowsky et al. (2013):

> To estimate RC, we draw from prior studies examining the rutting associated with precipitation and freeze– thaw, and subsequently assess the changes in pavement condition index associated with these rutting impacts. N.D. Lea International (1995) indicates that rut depth over a road's lifecycle increases by approximately 3 mm with every 10 cm increase in mean monthly rainfall. In addition, U.S. DOT (2006) shows that rut depths in moderate freeze areas (50–400 freeze days per year) and high freeze areas (more than 400 freeze days per year) are approximately 3.25 and 2.75 mm higher, respectively, than in no-freeze zones.

Equation: Based on the above, the equation proposed is the following

$$\text{Impact of precipitation on road maintenance} = 1 + (\text{Precipitation} - \text{Mean precipitation})/100 * 0.375$$

Method 2 (Chinowsky, et al., 2011)

This approach "is based on the cost of preventing a reduction in lifespan that may result from changes in climate-related stress" (Chinowsky et al., 2011). Authors assume that "a reduction in lifespan is equal to the percent change in climate stress (scaled for the stressor's effect on maintenance costs)" (Chinowsky et al., 2011).

According to Miradi (2004), "maintenance for paved roads that is precipitation-related accounts for 4% of maintenance costs and temperature-related maintenance accounts for 36% of costs."

The "costs of avoiding a reduction in lifespan is calculated by the product of (1) the potential percent reduction in lifespan and (2) the base construction costs of the asset." This means that a "10% potential reduction in lifespan causes an estimated increase in maintenance costs of 10% of the construction costs" (Chinowsky, et al., 2011).

Unpaved roads are strongly influenced by precipitation. According to Ramos-Scharron & MacDonald (2007), "80% of unpaved road degradation can be attributed to precipitation and the

remaining 20% to traffic rates and other factors. Given this 80% attribution to precipitation, maintenance costs increase by 0.8% with every 1% increase in the maximum monthly precipitation values projected for any given year."

Considerations for integration into the CDS Toolbox

- ERA5 monthly averaged data on single levels from 1979 to present

6.1.2.2 Temperature

- **Summary of results**

In present value terms, costs emerging from higher temperatures range from USD 140 per mile under a global action scenario, which means a 1.2% increase in costs, to USD 475 per mile under a business-as-usual (BAU) scenario, resulting in means a cost increase of 2.7%. Annual adaptation costs would be in the range of USD 3,000–3,600 for 2006 through 2080 per lane mile (Chinowski et al., 2013).

- **Results**

Higher temperatures imply higher stress for road materials that can melt, crack, and be affected by the daily flow of road traffic. Higher temperatures can also change the freeze–thaw effects. Precipitation influences a road's maintenance costs, especially in case of unpaved roads.

In the United States, Chinowsky et al. (2013) estimate that, if unchecked, "if unchecked, will increase the annual costs of keeping paved and unpaved roads in service by $785 million in present value terms by 2050. When not discounted, this figure increases to $2.8 billion." They "estimate annual adaptation costs ranging from $140 per lane mile in 2025 under the global action scenario and $475 per lane mile in 2075 under the business as usual scenario. This suggests a 1.2% increase in costs in 2075 under global action scenario and a 2.7% increase under the business as usual case."

Chinowsky et al. (2013) compare their results to a study from Larsen et al. (2008) about adaptation costs for roads in Alaska. Chinowsky et al. (2013) base the comparison on converting the Larsen et al. (2008) estimates to year 2010 USD and expressing these estimates on a cost-per-lane-mile basis, assuming two lanes per road. Thus, the annual adaptation costs per lane mile are estimated to be USD 3,000–3,600 for 2006 through 2080. Larsen et al.'s (2008) results imply a 5.6%–5.8% increase in road construction and maintenance costs during the 2006–2080 period. The higher estimates in Larsen et al. (2008) can be attributed to stronger climate changes in Alaska and the additional consideration of costs related to flooding and the melting of permafrost.

- **Methodology**

Method 1 (Chinowsky et al., 2013)

Costs are estimated "under a baseline scenario in which annual mean global temperature increases by 1.5 degree Celsius in 2050 relative to the historical average, and a mitigation scenario under which this increase in mean temperature is limited to 1.0 degree Celsius" (Chinowsky et al., 2013).

To assess the cost of adapting roadways to changes in temperature, they "examine the implications of climate change for the design specifications of asphalt pavements. In areas where maximum temperatures increase due to climate change, asphalt pavements will become susceptible to increased cracking" (Chinowsky et al., 2013).

1. The cost (savings) of adapting paved roads to higher (lower) temperatures is estimated as the incremental cost of repaving with a higher (lower) grade binder:

As an initial step in this process, the daily pavement temperature is estimated under current climate and under each climate change scenario (based on Lavin, 2003):

$$T_P = 0.9545(T_A - 0.00618L^2 + 0.2289L + 42.2) - 17.78 \qquad (5)$$

where T_P is the pavement temperature (°C), T_A is the air temperature (°C) and L is the latitude.

2. Seven-day pavement temperatures are used "to determine the level of adaptation of asphalt binder" (Lavin, 2003). We can use an average function and average the last 7 days of this variable to determine the extra cost of maintenance.

Effect of heat on road maintenance costs (binder, based on variable above):

Additional cost for road maintenance = f(Tp Max 7 day)

The indicated cost of binder use is illustrated in the "additional data" tab, based on 7-day pavement temperatures. This applies to construction as well if we are assuming that binders in planned roads will be already updated.

Considerations for integration into the CDS Toolbox

- Air temperature (K) – ERA5-Land hourly data from 1981 to present

Method 2 (Zhao et al, 2018)

The temperature adaptability of asphalt pavements is very important due to its potential influence on pavement structure design, particularly in areas that experience significant temperature differences.

To calculate pavement radiation and convection, the precondition is to identify the pavement surface temperature. Here, we refer to Tang (2012):

$$T_{sur} = 1.0852\,T_{air} - 0.0684\,h + 4.29, \qquad (6)$$

where T_{sur} (°C) is the pavement surface temperature, T_{air} (°C) is the air temperature, and h (m) is the pavement depth.

Hourly surface temperature requires an assumption on pavement depth.

Considerations for integration into the CDS Toolbox

- Air temperature (K) – ERA5-Land hourly data from 1981 to present

6.1.3 Accidents

Rainfall and temperature can have an impact on accidents. Literature shows that accidents are more frequent with higher rainfall. Also, fatal accidents seem to be more frequent when temperatures are high, while fatality is the lowest when the weather is bad or icy roads are found. This points to the importance of the driver (attention and skills) in addition to the quality of the road.

6.1.3.1 Temperatures/Precipitation

- **Climate impact**

"Weather conditions are considered to be a factor that affects the number of road accidents and casualties significantly, with different effects according to the type of road (motorways, rural roads or urban roads). Moreover, as the weather also affects mobility, it is to be expected that the effects of weather on the number of injury accidents and casualties are partly due to the changes in mobility occurring at the same time" (Bergel-Hayat et al., 2013).

- **Summary of results**

When rainfall increases by 100 mm per month, the probability of a road accident increases by 0.2%–0.3%. For monthly temperature, an increase of 1˚C is equal to an increase in road accident probability of 1%–2%. Finally, 1 day of frost more per month is equal to an increase in road accident probability of 0.3%–0.6% (Bergel-Hayat et al., 2013).

- **Results**

A study regrouping datasets for France, the Netherlands, and the City of Athen has been analyzed "to highlight the link between weather conditions and road accident risk at an aggregate level and on a monthly basis" (Bergel-Hayat et al., 2013).

Results at a national level indicate that "100 mm of additional rainfall during a month increases the number of injury accidents in that month by 0.2–0.3% (NED/FR);[…] 1°C of additional average temperature during a month increases the number of injury accidents in that month by 1–2%;

[…]and 1 additional day of frost during a month decreases the number of injury accidents in that month by 0.3–0.6%" (Bergel-Hayat et al., 2013).

- **Methodology**

Injury accident multiplier = 1 + (RF - mean RF)/100 * 0.002 + IF THEN ELSE (Time > March: AND: Time < October, (ST - mean ST) * 0.02, 0) + IF THEN ELSE (Time > October: AND: Time < March, (WT - mean WT) * 0.006,0)) + (DF - mean DF) * 0.006

RF = monthly precipitation
Mean RF = mean precipitation (for each month)
ST = monthly summer temperature (March–September)
Mean ST = mean temperature for summer months (by month)
WT = monthly winter temperature (October–February)
Mean WT = mean temperature for winter months (by month)
DF = days of frost (per month)
Mean DF = mean days of frost per month

The data used is based on the general conclusions for national highway networks. The numbers used relate to the Netherlands and France, but geographical factors matter. It was, for example, also found that ice causes more frequent but less deadly accidents due to driver anticipation.

Considerations for integration into the CDS Toolbox

- ERA5-Land monthly averaged data from 1981 to present
- ERA5 monthly averaged data on single levels from 1979 to present

6.2 Integration of the Literature Review with the CDS Datasets

See section 1.2 for a general introduction.

Datasets:

- ERA5 monthly data on single level
- CMIP5 monthly data on single level
- ERA5 hourly data on single level

Indicators created:

- **Monthly 2-m temperature**
  - Units: degrees Celsius
  - Frequency: monthly
  - ERA5 variable: "2 m temperature"
  - CMIP5 variable: "2 m temperature"
  - Note: original units in Kelvin
- **Monthly precipitation**:

- Units: mm per month
- ERA5 variable: “mean total precipitation rate”
- CMIP5 variable: “mean precipitation flux“
- Note : original units in mm/s

- **Monthly evaporation**
  - Units: mm per month
  - ERA5 variable: “mean evaporation rate”
  - Note: original units in mm/s
- **Monthly surface runoff**
  - Units: mm per month
  - ERA5 variable: “mean surface runoff rate”
  - Note: original units in mm/s

6.3 Integration of Climate Indicators Into the SAVi Roads Model

CDS climate indicators developed for the roads sector include climate impacts on road lifetime, stormwater management, and road safety. Figure 17 presents the CLD for the SAVi Roads asset model.

Figure 17. CLD for the roads sector (CDS variables included in pink)

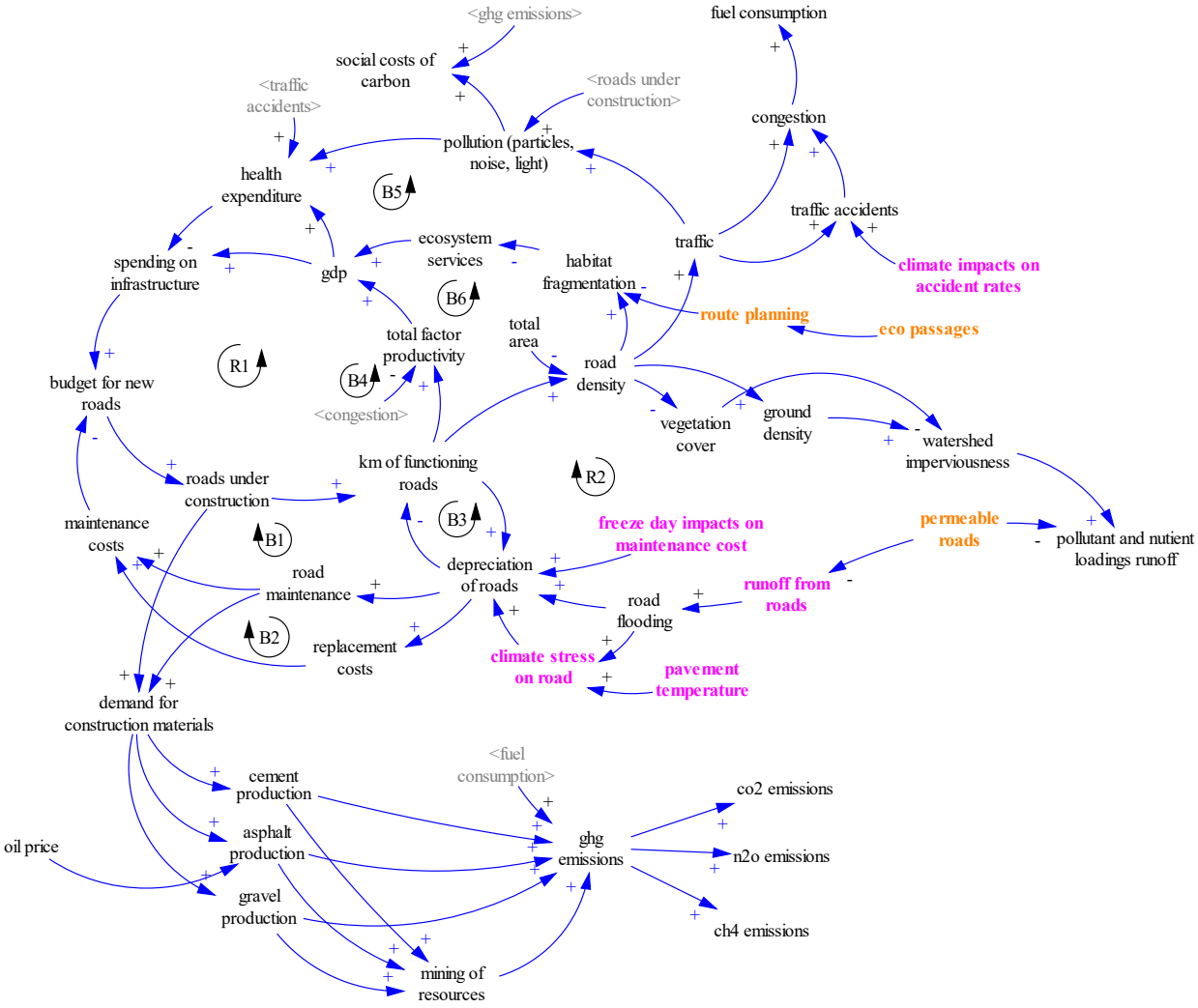

Weather has impacts on the road lifetime, increasing depreciation of the road surface as a consequence of temperature extremes (both increasing temperatures and more frequent freezing days) and precipitation. CDS indicators developed for the model include the impact of precipitation on pavement lifetime as well as the impact of air temperature on pavement integrity. Increases in mean precipitation cause the road surface to depreciate at a higher rate. Similarly, heat stress impacts are captured using pavement temperature. In both cases, CDS impacts lead to a reduced operational lifetime for roads, additional maintenance required, and, as a consequence, material use.

The stormwater indicator developed in the CDS Toolbox provides information about the water runoff from road surfaces during precipitation events. Stormwater, if not properly managed, can cause traffic disruptions and a multitude of environmental impacts due to the pollutants that are carried off the road into the environment (creating a direct connection with stormwater management).

The CDS Toolbox indicator for road safety refers to changes in accident rates based on weather conditions. Variables such as precipitation, temperature, icy days, and sunshine hours have an impact on traffic patterns and accidents. Depending on the change of climate variables, accident rates will increase or decrease.

6.4 Behavioural Impacts Resulting From the Integration of Climate Variables

Climate impacts on the operational lifetime of roads and pavement layers cause higher maintenance frequency and, hence, increase material use and maintenance costs (both due to higher temperature and freezing days). Changes in maintenance frequency further affect energy use for road maintenance and road-related greenhouse gas emissions. The use of CDS data allows for a more precise and location-specific assessment of road performance, with a more reliable estimate of maintenance costs.

The CDS indicator related to pavement temperature affects road construction and maintenance related costs by affecting the type of binder required. The indicator provides information about changes in cost related to the requirement of using a specific binder.

Obtaining stormwater quantities directly from the CDS Toolbox improves the ability to capture seasonal changes in stormwater loads and stormwater management-related costs. This improves the modelling of mitigation measures, required stormwater management capacity, and related investment and maintenance costs.

Climate impacts on accidents affect the number of accidents per million vehicle kilometres travelled, causing changes in the total number of accidents and related health costs. This indicator contributes to improving the modelling of seasonal accident patterns and informs decisions about the type pavement used (e.g., depending on desired permeability) to avoid societal costs. The information obtained can support the road management and design process, depending on the forecasted magnitude of climate impacts on accidents.

6.5 Simulation results

Three impacts were integrated into the SAVi Roads model, based on climate data obtained from the CDS data base: (1) precipitation effect on road lifetime, (2) weather effect on injury accidents, and (3) precipitation-based road runoff.

6.5.1 Impact of Precipitation on Road Lifetime

According to the literature (N.D. Lea International, 1995; Lavin, 2003), precipitation is responsible for approximately 37.5% of road depreciation, also expressed as rutting depth. The equation used for operationalizing the impacts of precipitation on road maintenance is:

*Impact of precipitation on road maintenance = 1 + (Precipitation - Mean precipitation)/100 * 0.375*

Simulation results comparing the no-climate-impact simulation to the simulation with CDS indicators are presented in Figure 18. The left figure illustretes the simulation results for road lifetime and the right figure provides information about the replacement rate of roads; both compare the no-climate-impact scenario (red) to the CDS integration (blue).

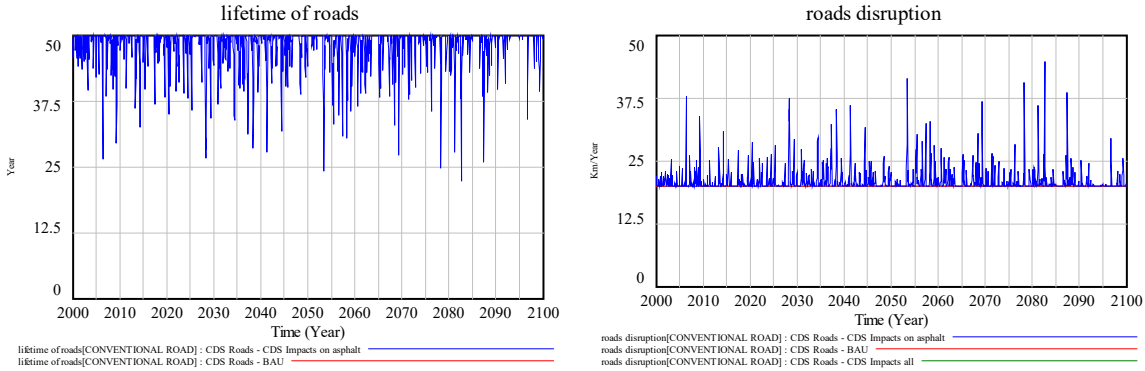

Figure 18. Impact of precipitation on roads lifetime (left) and road disruption rate (right) in the BAU and CDS scenario

Reductions in road lifetime are simulated on a monthly level, leading to a change in road disruption and, consequently, required road works. The monthly changes in lifetime and road disruption provide a more nuanced perspective on the impacts of severe events and the seasons during which the highest impacts occur. In the no-climate-impact scenario (red), the road lifetime is forecasted to be 50 years constant.

Over an 80-year period (2020–2100), the forecasted additional disruption for 1,000 km of road resulting from the integration of CDS climate data is 5.45% or 87.26 km. In the no-climate-impact scenario, the cumulative reconstruction of roads is 1,601.67 km over 80 years, while the forecasted cumulative disruption of roads in the CDS scenario is 1,688.9 km.

6.5.2 Impact of Weather on Accidents

Weather affects driving behaviour and the number of injury accidents occurring during specific seasons of the year. For example, when the roads are icy, studies indicate a reduction in injury accidents resulting from more careful driving behaviours. The same applies for higher temperatures, which have been found to cause more aggressive driving behaviours.

Bergel-Hayal et al. (2013) describe the relationship between climate variables (precipitation and temperature) and accident frequency. A 100 mm increase in monthly precipitation yields a 0.2%–0.3% increase in accidents, and a 1°C increase in mean monthly temperature increases accidents by 1%–2% (Bergel-Hayat et al., 2013). The equation used for estimating the impacts of weather on accidents is described below.

*Injury accident multiplier = 1 + (RF - mean RF)/100 * 0.002 + IF THEN ELSE (Time > March: AND: Time < October, (ST - mean ST) * 0.02, 0) + IF THEN ELSE (Time > October: AND: Time < March, (WT - mean WT) * 0.006,0)) + (DF - mean DF) * 0.006*

RF = monthly precipitation
Mean RF = mean precipitation (for each month)
ST = monthly summer temperature (March–September)
Mean ST = mean temperature for summer months (by month)
WT = monthly winter temperature (October–February)
Mean WT = mean temperature for winter months (by month)
DF = days of frost (per month)
Mean DF = mean days of frost per month

The difference in injury accidents between the BAU (red line) and including CDS climate impacts (blue line) is presented in Figure 19.

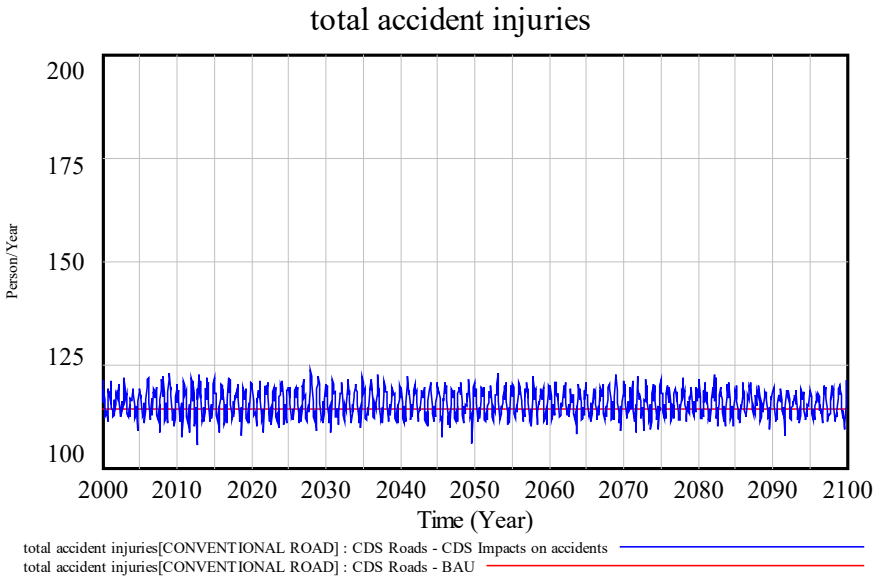

Figure 19. Injury accidents in the BAU and the CDS climate scenario

Compared to the no-climate-impact scenario, we observe an increase in injury accidents during the summer and a decline in injury accidents during the winter season. This change in accidents leads to a change in physical and economic damages resulting from traffic accidents throughout the year (and the whole simulation).

Between 2020 and 2100, the forecasted number of injury accidents is 1.2%, or 1,324 accidents higher in the CDS scenario compared to the no-climate-impact scenario. On average, this corresponds to approximately 16.5 additional traffic accidents per year over a period of 80 years. As a consequence of more injury accidents, injury accident-related damages will be 1.2% higher as well.

6.5.3 Runoff and Stormwater Management

Road runoff and resulting stormwater loads pose a challenge to asset managers, especially in urban environments. The need to mitigate stormwater loads to maintain traffic and prevent flood damages requires an accurate forecast of stormwater loads from roads.

Stormwater runoff from roads depends on the total amount of rainfall and the runoff coefficient of roads, whereby the latter indicates their permeability and capacity to store water. The equation for estimating stormwater runoff from roads is described as:

*Runoff from roads = Monthly precipitation * Runoff coefficient for roads * Conversion from mm per hectare to liters*

The change in road runoff and resulting stormwater in the CDS integration scenario is presented in Figure 20. The results show a significant difference between the initial setup of the SAVi model and the results obtained from the CDS integration.

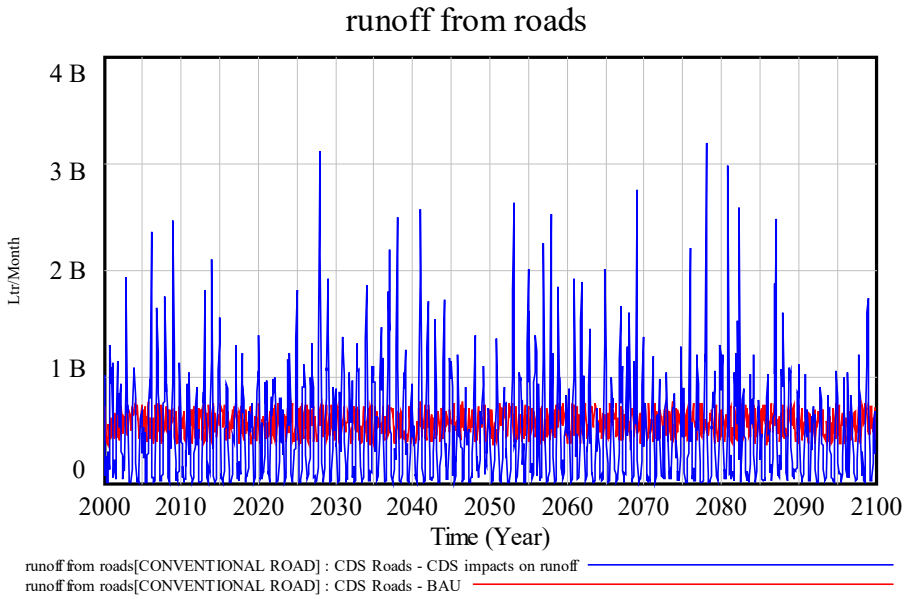

Figure 20. Runoff from roads CDS scenario compared to the BAU sceario

While runoff is relatively constant in the no-climate-impact scenario, the CDS integration shows differences both in terms of seasonality and magnitude of stormwater loads. In terms of the magnitude of impacts, the maximum monthly stormwater loads forecasted in the no-climate-impact scenario is 758.63 million liters, and the cumulative amount of stormwater between 2020 and 2100 is 466.43 billion liters for 1,000 km of road. In comparison, the maximum monthly stormwater load resulting from the integration of CDS climate variables is 3,182.3 million litres, and the cumulative amount over an 80 year period is 534.48 billion litres. The highest difference in monthly maximum values is 319%, and the difference in observed minimum runoff during the dry period is 99.92%, meaning that the simulation indicates 0.08% of BAU runoff during the dry period.

The above indicates that the previous formulation used for estimating stormwater runoff from roads underestimated the total maximum loads and overestimated stormwater loads during periods with low precipitation. In summary, the results indicate that the BAU simulation underestimated total cumulative runoff by around 68.05 billion litres over 80 years.

6.5.4 Economic Impacts Resulting From the Integration of CDS Climate Variables

The physical impacts resulting from the integration of CDS-based climate impacts leads to a change in road management costs and related externalities. The integrated CBA presented in Table 36 provides an overview of the cumulative costs for each scenario. The results presented provide cumulative figures for the period 2020 to 2100 in USD million.

Impacts related to asphalt indicate an increase in capital expenditure for road construction and the cost of road maintenance. Over an 80 year period, the additional cost of road construction totals USD 9.4 million, while additional maintenance costs are projected to be in the range of USD 87,000. The additional labour income generated from employment related to road construction and maintenance is forecasted at USD 25.8 million between 2020 and 2100. At a system level, these impacts yield positive results (net positive impacts of USD 8 million) if the labour income generated by the additional construction and maintenance is considered.

The integration of weather into the equation for injury accidents indicates that the additional economic cost of traffic accidents is USD 21.9 million between 2020 and 2100 or USD 272,500 per year on average.

The most significant difference in economic cost results from the updated formulation for stormwater runoff. Based on the differences in stormwater loads described above, the additional cost of stormwater management is projected at USD 2.06 billion over 80 years. This is equivalent to an additional annual cost of USD 25.58 million on average.

Considering all impacts at the same time (scenario 4 in CBA), the total difference between the no-climate-impact scenario and the CDS climate-impact scenario totals USD 2.08 billion between 2020 and 2100, out of which the largest share comes from stormwater management. This analysis assumes that all stormwater is conveyed and treated, which is not necessarily a realistic assumption.

Table 36. Integrated CBA assessing the differences between the BAU and the CDS integration

Indicator	Unit	0. No Climate	1. Impacts on asphalt	*1. vs no imapct*	2. Impacts on accidents	*2. vs no impact*	3. Impacts on runoff	*3. vs no impact*	4. All impacts	*4. vs no impact*
Investment and cost										
Capital cost	mln USD	185.0	194.4	*9.4*	185.0	*0.0*	185.0	*0.0*	194.4	*9.4*
O&M costs	mln USD	34.9	35.0	*0.087*	34.9	*0.000*	34.9	*0.000*	35.0	*0.1*
Total cost	mln USD	219.9	229.4	*9.5*	219.9	*0.0*	219.9	*0.0*	229.4	*9.5*
Externalities										
(1) Positive										
Labor income	mln USD	1,348.8	1,374.6	*25.8*	1,348.8	*0.0*	1,348.8	*0.0*	1,374.6	*25.8*
(2) Negative										
Cost of traffic accidents	mln USD	759.5	761.4	*1.9*	781.5	*21.9*	759.5	*0.0*	783.4	*23.9*
Social cost of carbon	mln USD	14.7	14.7	*0.0*	14.7	*0.0*	14.7	*0.0*	14.7	*0.0*
Stormwater management cost	mln USD	2,423.6	2,429.9	*6.3*	2,423.6	*0.0*	4,481.1	*2,057.5*	4,492.8	*2,069.2*
Cost of N removal	mln USD	1.6	1.6	*0.0*	1.6	*0.0*	1.6	*0.0*	1.6	*0.0*
Net sum of externalities (1) - (2)	mln USD	1,850.5	1,833.0	*-17.5*	1,872.5	*21.9*	3,908.0	*2,057.5*	3,917.9	*2,067.3*
Total integrated cost	**mln USD**	**2,070.4**	**2,062.4**	***-8.0***	**2,092.4**	***21.9***	**4,127.9**	***2,057.5***	**4,147.3**	***2,076.8***

7 Nature-Based Infrastructure

7.1 Literature Review

7.1.1 Definitions

7.1.1.1 Natural Infrastructure

Natural infrastructure is defined as “ecosystems that provide infrastructure through services that are inherent to such ecosystems, while also perpetuating active conservation efforts and the enhancement of the environments they are embedded in” (Bassi et al., 2019).

7.1.1.2 Green-Grey infrastructure

Green-grey infrastructure is an urbanized natural infrastructure. It tends to hybridize natural and grey infrastructure into easily implementable structures to urban environments (e.g., permeable pavements, green spaces) (Bassi et al., 2019).

7.1.2 Precipitation: Rainfall Harvesting and Runoff

- **Climate impact**

Precipitation is one of the main climate variables that impacts natural and green-grey infrastructure. It affects rainwater harvesting, water management, and water absorption through vegetation or soils. Natural and green-gray infrastructures can reduce extreme event impacts on buildings (reducing flood impact), curb demand for water (rainwater harvesting), and improve the performance of wastewater plants. They are also good to treat and absorb high precipitation as well as wastewater through constructed or natural wetlands and mangroves, among others.

- **Summary of results**

Green roofs have a capacity to retain 75% of a 24.5 mm storm and 85% from a 50.8 mm storm (depending on location; results are for Chicago and Milwaukee, respectively). Green roofs recorded precipitation of 323 mm on average compared to 587 mm for asphalt roofs; they retained 52.6% and 14.1%, respectively. For pavements, we found that the efficiency of retaining a 1-hour storm is 3 mm.

For a combined sewer overflow (CSO), there would be a reduction in discharge of 2.8391 litres (0.75 U.S. gallons) per increase of 3.7854 litres (1 U.S. gallon) of stormwater when green infrastructure is installed near the water inflow.

A study in Spain that compares seasonal efficiency removal in constructed wetlands in Barcelona and Leon found that for [total suspended solids (TSS); COD; ammonium], their efficiency in summer is [97.4%; 97.1%; 99.9%] and winter [83.5%; 73.2%; 19%] for Barcelona and [97.8%; 96.2%; 88.9%] and winter [74.4%; 60.6%; 1NA] for Leon. Influent average TSS mass loading rate

was 2.84 g m^{-2} d^{-1}, and for average influent biological oxygen demand (BOD), it was of 4.72 g m^{-2} d^{-1}.

- **Results**

In Chicago, green roofs helped "retain over 75 percent of the volume from a one-inch storm, preventing the water from reaching the combined sewer system." In Milwaukee, green roofs "green roofs will be able to retain 85 percent of a two-inch downpour. The remaining 15 percent of the water is directed to rain gardens and a retention basin for on-site irrigation" (Dunn, 2007).

In the United States, a report published under the Natural Resources Defense Council by Kloss and Calarusse (2011) established that "permeable pavement in a typical alley can infiltrate 3 inches of rainwater from a 1-hour storm with an infrastructure life expectancy of 30 to 35 years. It is typically designed with the capacity to manage a 10-year rain event within a 24-hour period."

Under the Environmental Protection Agency (EPA), in an analysis that covers the United States, Berghage et al. (2009) report that, "for 683 mm of recorded precipitation, there is a corresponding mean value of 323 mm with a standard deviation of 71 mm of green roof runoff compared to a mean of 587 mm with a calculated standard deviation of 43 mm for the flat asphalt roofs. The green roofs retained 52.6% while flat asphalt roofs retained 14.1% of the precipitation."

In Lancaster, Pennsylvania, a project managed by the Green Infrastructure Technical Assistance Program and the EPA estimated that, "for every 1 gallon of stormwater captured by green infrastructure, (Combined Sewer Overflow) CSO discharges will be reduced by 0.75 gallons. Based on these assumptions, the green infrastructure installed within the CSS area will capture an average of 706 million gallons of stormwater runoff annually, and reduce CSO discharges by an average of 529 million gallons/year" (EPA, 2014).

In Spain, Garfi et al. (2012) estimated the removal efficiency of two experimental constructed wetlands in Leon and Barcelona. The "two constructed wetland systems had the same experimental set-up. Each wetland had a surface area of 2.95 m^2, a water depth of 25 cm and a granular medium of D60=7.3 mm, and was planted with *Phragmites australis*. Both systems were designed in order to operate with a maximum organic loading rate of 6 gDBO m^{-2} d^{-1}. Experimental systems operated with a hydraulic loading rate of 28.5 and 98 mm d^{-1} in Barcelona and León, respectively. Total suspended solids, biochemical oxygen demand, and ammonium mass removal efficiencies followed seasonal trends, with higher values in the summer (97.4% vs. 97.8%; 97.1% vs. 96.2%; 99.9% vs. 88.9%, in Barcelona and León systems, respectively) than in the winter (83.5% vs. 74.4%; 73.2% vs. 60.6%; 19% vs. no net removal for ammonium in Barcelona and León systems, respectively)."

"Influent average TSS mass loading rate was 2.84 g m^{-2} d^{-1} (7.58 g m^{-2} d^{-1}, ranging from 0.41 to 7.95 g m^{-2} d^{-1} in Leon). Average influent BOD was 4.72 g m^{-2} d^{-1} (6.11 g m^{-2} d^{-1} in Leon), ranging from 3.5 to 5.1 g m^{-2} d^{-1} in winter and summer respectively, which fits quite well in the range of 4–6gm^{-2} d^{-1}" (Garfi et al., 2012).

- **Methodology**

Many papers are based on the same methodology: the StormWaterManagement Method (SWMM) (Nazahiyah et al., 2007). Zoppou (2001) lists all the urban stormwater models. One of the first model examples comes from Tsihrintzis and Hamid (1998). This approach measures the amount of pollutants absorbed through runoff that are probably not treated. "Pollutant loadings are calculated as the product of event mean concentration (EMC)" (Tsihrintzis & Hamid, 1998):

$$\mathrm{EMC} = \frac{M}{V} = \frac{\sum Q_i C_i \Delta t}{\sum Q_i \Delta t}$$

"where M is total mass of pollutant over the entire event duration (g), V is total volume of flow over the entire event duration (m3), t is time (min), Qi(t) is the time-variable flow (m3 /min), Ci is the time-variable concentration (mg/l) and Dt is the discrete time interval (min) measured during the runoff event" (Tsihrintzis & Hamid, 1998).

Considerations for integration into the CDS Toolbox

- ERA5-Land monthly averaged data from 1981 to present
- CMIP5 monthly data on single levels

Method 2 (Cronshey, et al., 1986; Gajbhiye et al., 2013)

This method is based on the Soil Conservation Service curve number (CN) method, a well-established technique for estimating event runoff depths from various urban and agricultural land uses. The CN method uses an infiltration loss model to estimate direct runoff from storm rainfall based on soil type, land use/land cover, surface conditions, and antecedent moisture conditions (Cronshey, et al., 1986; Gajbhiye et al., 2013):

$$VR = \frac{(P - Ia)^2}{P - Ia + S} \cdot A_d \cdot C$$

and

P = total event precipitation depth, [in]
$S = \frac{1000}{\mathrm{CN}} - 10$
CN = curve number, set at 98 for impervious urban surfaces
Ia = initial abstraction, $0.2\,S$
A_d = Drainage area (m^2)
C = conversion factor from inches to m.

"Initial abstraction (Ia) is all losses before runoff begins. It includes water retained in surface depressions, water intercepted by vegetation, evaporation, and infiltration. Ia is highly variable but generally is correlated with soil and cover parameters. Through studies of many small

agricultural watersheds, Ia was found to be approximated by the following empirical equation: Ia = 0,2S" (Cronshey, et al., 1986).

"The major factors that determine CN are the hydrologic soil group (HSG), cover type, treatment, hydrologic condition, and antecedent runoff condition" (Cronshey, et al., 1986).

Considerations for integration into the CDS Toolbox

- ERA5-Land monthly averaged data from 1981 to present
- CMIP5 monthly data on single levels

7.1.3 Vegetation: Rainfall absorption, temperature, soil erosion, and climate mitigation

- **Climate impact**

Vegetation has an impact on natural and green–grey infrastructure, depending on the type of vegetation, country, latitude, and canopy coverage. Vegetation helps to mitigate climate risks for infrastructure and provides an efficient way of increasing air quality, reducing flood risks, absorbing high precipitation levels, and reducing the demand for cooling.

- **Summary of results**

Our references mainly come from studies in the United States, China, and England. Trees are important in mitigating flood and wastewater treatment costs by their rainfall absorption capacity. Trees can absorb as much as 6.6 m^3/tree and reduce costs by USD 3.60/tree (based on a study in Santa Monica, California). "Trees also act as an air cleaner by reducing air pollutants. Some studies found trees could reduce particulate matter ($PM_{2.5}$) by ~64.5 tonnes (Atlanta). Trees can also remove ~312.03 tonnes (Guangzhou) of N, sulfur dioxide, and total suspended particulates, depending on location." For example, "a 10 x 10 km grid in London with 25% tree cover could remove 90.4 tonnes of PM_{10} per year" (Demuzere et al., 2014).

We learned that vegetated areas are 3% cooler than non-vegetated areas (Kumamoto, Japan). For example, an area containing 30% vegetation can be cooler by 6˚C, retain 2˚C of warmth at night, and reduce wind speed by 2–6.7 m/s (Davies, California). Vegetation also prevents soil erosion. For a 1% annual increase in vegetation cover, soil erosion could be reduced by 456 $t/km^2/a^{-1}$ (China).

On average, vegetation can absorb 18–31.6 t/˚C/ha of carbon particles (depending on location) for urban areas and as much as 1.66-7.6 t/˚C/ha for domestic gardens (Leicester). Removal efficiency (depending on location) for the removal of PM_{10}/year ranges from 852 to 2,121 tonnes (Seattle and Hangzhou).

- **Results**

In Santa Monica, California, Xiao and McPherson (2002) assess the rainfall absorption capacity of urban trees to mitigate wastewater treatment costs and flood costs. Results show that the "annual rainfall interception by the 29,299 street and park trees was 193,168 m^3 (6.6 m^3/tree), or 1.6% of total precipitation … Longtime average annual precipitation is 569.5 mm and the dominant land use over the 21.8 km^2 study area is residential (66.0%). Commercial, industrial, and park land uses account for 15.9%, 7.0%, and 2.6%, respectively. The remaining 8.5% of land has other uses … Inventory data was limited to 29,229 public trees, of which 87% were street trees and 13% were park trees. The majority of trees were broadleaf evergreens (59.9%), 11.1% were conifers, and 22.6% were palms."

"The annual value of avoided stormwater treatment and flood control costs associated with reduced runoff was $110,890 ($3.60/tree). Interception rate varied with tree species and sizes" (Xiao & McPherson, 2002).

In Kumamoto, Japan, Saito et al. (1990) estimated the impact of vegetation coverage on air temperature. "Temperature difference is on average 3% lower compared to non-vegetated areas. Three areas were analyzed …The Kengun Shinto Shrine area has a scale of about 150m × 150 m and it is covered with coniferous trees and bamboos … The Izumigaoka Park has a scale of about 60m × 40 m and it is covered with"broad-leaved trees … The total area of tree crowns is ~25,900 m^2 in Kengun Shinto Shrine and ~2,300 m^2 in Izumigaoka Park."

In Davis, California, Taha et al. (1991) estimated "that a vegetative cover of 30% could produce a noontime oasis of up to 6°C in favorable conditions, and a nighttime heat island of 2°C. Wind speed was reduced by ~ 2 m/s in mild conditions and by as much as 6.7 m/. The measurements were taken from October 12–25, 1986. These meteorological variables were measured 1.5 m above ground along a transect of seven weather stations set up across the canopy and the upwind/downwind open fields. These variables were averaged every 15 minutes for a period of two weeks so we could analyze their diurnal cycles as well as their spatial variability" (Taha et al., 1991). In the canopy, the cumulative leaf-area index (LAI), integrated over the foliage depth, was about 3. This LAI was uniform across the entire canopy except near the middle of the tree stand where a slight discontinuity in cover brought the LAI down to about 2. The tall trees at the south end of the stand, on the other hand, had a cumulative LAI between 4.5 and 5 (Taha et al., 1991).

In China, Zhou et al. (2006) assessed the evolution "of vegetation and soil erosion at the watershed of Zhifanggou from 1987 to 1996. Vegetation coverage increased linearly with a speed of 1.84% per year and soil erosion decreased by 757 t km^{-2} per year. The amount of soil erosion was closely negative correlated with the degree of vegetation coverage ($r = -0.99$***). Regression of soil erosion with vegetation coverage indicated that a 1% increase in vegetation coverage in a year could decrease soil erosion by 456 t km^{-2} a^{-1}."

Demuzere et al. (2014) also report existing evidence on the role of green infrastructures in mitigating climate change. For carbon dioxide reduction, "Davies et al. (2011) report the total average carbon stored within the above-ground vegetation across the city to be 31.6 t C/ha of urban area and 7.6 t C/ha alone for domestic gardens" (Demuzere et al., 2014).

"This is similar to the results of Zhao et al. (2010) in the Hangzhou downtown area, where they reported 30.25 t C/ha and 1.66 t C/ha/year as the average carbon storage and sequestration rate, and a little higher than along three sample transects radiating from the Seattle (the USA) central urban core (18 ± 13.7 t C/ha) (Hutyra et al., 2011)" (Demuzere et al., 2014).

Concerning air quality, "the evidence based on modelling studies is much broader compared to the results from empirical studies. In London, green areas are estimated to remove 852–2,121 tonnes of PM_{10} annually, which equates to 0.7–1.4% PM10 reduction (Tiwary et al., 2009). Tallis et al. (2011) have found that a 10 x 10 km grid in London with 25% tree cover could remove 90.4 tonnes of PM_{10} per year" (Demuzere et al., 2014).

"A recent analysis in 10 U.S. cities showed that the mass of fine particles ($PM_{2.5}$) removed by trees annually could be up to 64.5 tonnes in Atlanta (Nowak et al., 2013). In Guangzhou, China, the annual removal of N, sulfur dioxide, and total suspended particulates could be 312.03 tonnes (Jim & Chen, 2008)" (Demuzere et al., 2014).

- **Methodology**

Considerations for integration into the CDS Toolbox

- ERA5-Land monthly averaged data from 1981 to present
- ERA5 monthly averaged data on single levels from 1979 to present
- Land-cover classification gridded maps from 1992 to present derived from satellite observations
- ERA5-Land monthly averaged data from 1981 to present
- Leaf area index and fraction absorbed of photosynthetically active radiation 10 daily gridded data from 1981 to present

7.1.4 Air Temperature and Solar Radiation

- **Climate impact**

Green roofs and green gardens, among other options, can provide a good alternative for cities to face higher temperatures and decrease the demand for cooling. They can also act as greenhouse gas emission regulators and contribute to the improvement of air quality.

Green–gray infrastructures also reduce solar radiation impact on buildings. They help in reducing demand for cooling systems and can even transform solar radiation energy into electricity through solar panels.

Constructed and natural wetlands are also sensitive to changes in temperatures regarding their nutrient absorption efficiency and their capacity in treating wastewater.

- **Summary of results**

An increase in albedo of 0.13 would lead to a decrease of temperature by 2–4˚C, reducing the need for air conditioning by 10% and reducing smog by 20% during the summer.

Trees help to mitigate high temperatures. By doing a simple average from all references, areas with trees are cooler by 2.15˚C (0.7°C–3.6 ˚C range of our studies) depending on location and method. Green areas also help to reduce ambient air temperature by an average of 1.635˚C (a range of 0.47°C–2.8˚C) to a maximum of 3.3°C–5.6˚C for over 25% of trees.

Green roofs have the same function as trees, reducing ambient air temperature by 0.3°C–3˚C. Facades reduce temperatures by 1°C–15˚C. Surface temperature can be lower by 21˚C, and it can reduce air temperature by 15˚C.

Regarding green infrastructure and constructed wetlands, the efficiency of water treatment also changes with temperature variation. “COD removal is relatively high at 16˚C (92%) and at 24˚C in (88%), but ranged between 58% and 69% during all other batches at 4, 8, and 16˚C. Removal rate without plants was significantly less at 4˚C than 24˚C. At 4 and 8˚C, when differences were statistically significant, planted microcosms removed 25–30% more COD on average than unplanted controls; at 16˚C, significant differences between planted and unplanted microcosms were <20%” (Taylor et al., 2011). Another study found that the average “Nitrogen uptake rate was calculated in the order of *C. indica L. > A. donax > A. calamus L.*, for 22.88 mgN/m^3 /d, 18.21 mgN/m^3 /d and 16.68 mgN/m^3 /d, respectively. NO_3-N removal rates of 95.2%, 97.2%, 96.8% and 96.2% occurred in summer (Aug. and Sep.), while 83.3%, 84.4%, 77.56% and 73.45% in autumn (Oct. to Dec.)” (Du et al., 2006).

For wetland without specific plants, “removal efficiency for SS (71.8 ± 8.4%), BOD5 (70.4 ± 9.6%), COD (62.2 ± 10.1%), total coliform (99.7%), fecal coliform (99.6%), ammonia nitrogen was relatively low (40.6 ± 15.3%)" (Song et al., 2006).

For inflow and removal efficiency, the wetland received “24 g P m^{-2} $year^{-1}$ and 130 g NO_3-N m^{-2} $year^{-1}$ and it retained 3.1 g m^{-2} $year^{-1}$ of P and 18 g m^{-2} $year^{-1}$ of NO_3-N. Annual TP reduction was 13% and NO_3-N reduction 14%. The monthly relative NO_3-N reduction was 25–82% in growing season (June–September), 7–10% in January–March and 4–6% in November–December. The highest absolute monthly reduction of NO_3–N occurred in December” (Valkama et al., 2017).

- **Results**

Taha (1996; 1997) performed simulations in the Los Angeles basin “of the effects of large-scale albedo increases and found that an average decrease of 2°C and up to 4°C may be possible by increasing the albedo by 0.13 in urbanized areas of the basin. Temperature decreases of this magnitude could reduce the electricity load from air conditioning by 10% and smog (ozone concentrations) by up to 20% during a hot summer day.”

A review of the literature shows that vegetation can reduce temperature. “Air temperature in the shade of trees was reported to be lower by 0.7–1.3°C (Souch & Souch, 1993), 1.7–3.3°C (Taha et al., 1988), up to 3.6°C (Parker, 1989) than areas with no trees. The cooling effect of parks was also investigated by several other researchers. The average air temperature in green areas was variously recorded to be lower by 0.47°C (Dhakal & Hanaki, 2002), 0.6°C (Watkins et al., 2002), and 1.5°C–2.8°C (Nichol, 1996) than surrounding areas. In another study, this temperature difference reached up to 3.3°C– 5.6°C during the summer with a 25% increase in the number of trees (Akbari et al., 1992)” (Zoulia et al., 2009).

Koc et al.’s (2018) literature review on the effects of green infrastructures for cooling urban areas found that “green roofs, when applied at the city level, may decrease average ambient temperatures between 0.3 and 3 K (Santamouris, 2014) and also that the application of green walls/facades showed a reduction of surface temperatures of building facades between 1 and 15 °C for studies in warm temperate climates (Pérez, Coma, Martorell, & Cabeza, 2014). This is just two examples among many others.”

The EPA (2003) reports that, in the United States, it is estimated that “urban air temperatures can be up to 5.6°C warmer than the surrounding countryside and, for every 0.6˚C increase in air temperature, peak utility load may increase by 2%” (U.S. Environmental Protection Agency, 2003).

In Chicago, “since completion in 2001, green roofs have saved the city USD 5,000 a year in energy costs” (City of Chicago, 2006). Monitoring of local temperatures found that the “cooling effects during the garden’s first summer showed a roof surface temperature reduction of 21°C and an air temperature reduction of 15°C” (American Society of Landscape Architects, 2003) .

Taylor et al. (2011) conducted a study on the efficiency of 19 different plants in absorbing and removing COD and sulphate from wastewater for different air temperatures. They compared treatment and control (unplanted) by varying temperatures after 20 days for 1 year. “In unplanted microcosms COD removal was relatively high at 16◦C in 2006 (92%) and at 24 ◦C in 2007 (88%), but ranged between 58% and 69% during all other batches at 4, 8, and 16 ◦C. Removal in controls was significantly less at 4◦C than 24 ◦C. … In contrast to the controls, planted microcosms showed no significant differences between the coldest and warmest temperatures with 15 species. Microcosms planted with *L.cinereus* and *P. virgatum* had significantly lower COD removal at 4 than 24 ◦C, while *C. utriculata* and *P. arundinacea* had significantly higher removal at 4 ◦C.”

“At 4 and 8 ◦C, when differences were statistically significant, planted microcosms removed 25–30% more COD on average than unplanted controls; at 16 ◦C, significant differences between planted and unplanted microcosms were <20%” (Taylor et al., 2011) (see Table 37).

Table 37. COD removal regarding influent wastwater

COD removal in wetland microcosms as percent reduction relative to influent wastewater (±standard error).

	16 °C 2006[b]	8 °C 2006	4 °C 2007	8 °C 2007	16 °C 2007	24 °C 2007	16 °C 2007	8 °C 2007	4 °C 2008	Study-long average[c]
D. cespitosa	95 ± 2	99 ± 1 ↑	99 ± 1 ↑	98 ± 1 ↑	100 ± 0 ↑	96 ± 2	95 ± 1 ↑	95 ± 1 ↑	98 ± 1 ↑	97 ± 2
C. bebbii	90 ± 2	98 ± 1 ↑	98 ± 1 ↑	98 ± 0 ↑	99 ± 0 ↑	100 ± 0 ↑	91 ± 2 ↑	99 ± 0 ↑	98 ± 1 ↑	97 ± 1
C. nebrascensis	91 ± 2	100 ± 0 ↑	96 ± 2 ↑	98 ± 1 ↑	96 ± 3 ↑	93 ± 3	95 ± 0 ↑	99 ± 0 ↑	97 ± 1 ↑	96 ± 1
C. praegracilis	96 ± 1	95 ± 2 ↑	NA	97 ± 1 ↑	95 ± 2 ↑	97 ± 3	94 ± 1 ↑	98 ± 2 ↑	97 ± 1 ↑	96 ± 1
S. acutus	87 ± 3	92 ± 5 ↑	92 ± 2 ↑	94 ± 2 ↑	97 ± 1 ↑	94 ± 2	96 ± 1 ↑	100 ± 0 ↑	99 ± 0 ↑	95 ± 2
C. aquatilis	89 ± 1	88 ± 7 ↑	90 ± 3 ↑	95 ± 2 ↑	98 ± 0 ↑	98 ± 0	95 ± 0 ↑	93 ± 1 ↑	97 ± 1 ↑	94 ± 2
C. utriculata[*,a]	93 ± 2	97 ± 1 ↑	96 ± 2 ↑	99 ± 1 ↑	90 ± 5 ↑	83 ± 1	91 ± 3 ↑	97 ± 1 ↑	99 ± 1 ↑	94 ± 2
J. torreyi	94 ± 1	95 ± 3 ↑	94 ± 2 ↑	96 ± 0 ↑	90 ± 2 ↑	92 ± 6	93 ± 2 ↑	97 ± 2 ↑	91 ± 2 ↑	94 ± 1
J. arcticus	89 ± 0	90 ± 6 ↑	89 ± 4 ↑	96 ± 0 ↑	97 ± 2 ↑	96 ± 4	94 ± 0 ↑	91 ± 3 ↑	96 ± 2 ↑	93 ± 2
C. microptera	80 ± 6 ↓	88 ± 8 ↑	83 ± 4 ↑	93 ± 3 ↑	92 ± 4 ↑	82 ± 3	82 ± 4 ↑	93 ± 3 ↑	96 ± 3 ↑	88 ± 2
P. arundinacea[*]	92 ± 1	81 ± 4 ↑	87 ± 1 ↑	89 ± 1 ↑	65 ± 3	79 ± 4	90 ± 4 ↑	88 ± 2 ↑	92 ± 4 ↑	85 ± 3
T. latifolia	79 ± 6 ↓	81 ± 6 ↑	83 ± 6 ↑	83 ± 3 ↑	85 ± 4 ↑	89 ± 4	84 ± 1 ↑	90 ± 2 ↑	92 ± 2 ↑	85 ± 2
C. canadensis	90 ± 1	65 ± 6	73 ± 11	80 ± 4 ↑	69 ± 2	94 ± 4	82 ± 2 ↑	78 ± 2 ↑	85 ± 2 ↑	80 ± 4
H. jubatum	76 ± 1 ↓	66 ± 5	71 ± 3	88 ± 4 ↑	88 ± 7 ↑	86 ± 4	87 ± 5 ↑	80 ± 4 ↑	79 ± 1 ↑	80 ± 2
P. vulgaris	81 ± 11	87 ± 6 ↑	87 ± 1 ↑	84 ± 4 ↑	62 ± 5	77 ± 8	75 ± 1	82 ± 2 ↑	74 ± 2	79 ± 3
P. virgatum[*]	70 ± 6 ↓	69 ± 4	66 ± 3	81 ± 5 ↑	75 ± 4	92 ± 2	77 ± 6 ↑	83 ± 3 ↑	71 ± 3	76 ± 3
P. australis	53 ± 2 ↓	65 ± 5	67 ± 5	73 ± 3	88 ± 5 ↑	67 ± 6 ↓	79 ± 2 ↑	87 ± 4 ↑	89 ± 1 ↑	74 ± 3
I. missouriensis	83 ± 6	63 ± 4	67 ± 5	83 ± 2 ↑	70 ± 4	92 ± 1	69 ± 2	69 ± 0	67 ± 3	74 ± 3
L. cinereus[*]	66 ± 5 ↓	62 ± 5	69 ± 2	61 ± 3	69 ± 3	79 ± 2	74 ± 1	77 ± 3 ↑	72 ± 1	70 ± 2
Control[*]	92 ± 1	62 ± 4	58 ± 1	65 ± 9	66 ± 1	88 ± 2	69 ± 2	64 ± 1	66 ± 2	70 ± 3

[a] COD removal differed significantly between 4 °C and 24 °C in treatments with an asterisk.
[b] Within each column, values followed by (↑) had significantly higher COD removal than the control; values followed (↓) by had significantly lower COD removal than the control ($p < 0.05$, planned contrast within ANOVA).
[c] Treatments are sorted in descending order of study-long average COD removal calculated as the mean of all nine batches.
[*] Repeated measures ANOVA ($p < 0.05$).

Source: Taylor et al., 2011.

In another study, Du et al. (2018) analyzed the performance of integrated vertical-flow constructed wetlands (IVCWs) in removing N for treating water. "Four sets of lab-scale IVCWs were built with a 25 L working volume. Natural sands (in the same diameter 1–2 mm) were filled into each tank as the substrate layers (35 cm). Arundo donax (A. donax), Canna indica L. (C. indica L.) and Acorus calamus L. (A. calamus L.) were selected as wetland vegetation" and planted in three sets of wetland system sequentially "with the nearby biomass."

"Results showed that IVCWs planted with vegetation generally achieved a higher Total Nitrogen removal rate than unplanted treatment, especially for *Canna indica L.* with 10.35% enhancement. … The average N uptake rate was calculated in the order of *C. indica L. > A. donax > A. calamus L.*, for 22.88 mgN/m^3 /d, 18.21 mgN/m^3 /d and 16.68 mgN/m^3 /d, respectively).

"Moreover, the microbial process proportion (83.87–87.94%) is the main Nitrogen removal pathway in IVCW, and vegetation planting could increase 8.16% of it in average. The average NO_3-N removal rates of 95.2%, 97.2%, 96.8% and 96.2% occurred in summer (Aug. and Sep.), while 83.3%, 84.4%, 77.56% and 73.45% in autumn (Oct. to Dec.)" (Du et al., 2006).

In China, Song et al. (2006) observed the seasonal efficiency of a constructed wetland for sewage treatment. The wetland has "a total area of 80 ha and treatment capability of 2.0 × 104 m^3 d^{-1} … Average seasonal temperatures for the region are: winter (from December to February), −0.1°C; spring (from March to May), 11.1°C; summer (from June to August), 22.9°C; and fall (from September to November) 14.6°C (2003 data)."

Their removal results showed that "SS (71.8 ± 8.4%), BOD5 (70.4 ± 9.6%), COD (62.2 ± 10.1%), total coliform (99.7%), fecal coliform (99.6%), ammonia N were relatively low (40.6 ± 15.3%), and

TP showed the least efficient reduction (29.6 ± 12.8%) […] Mean percent reduction was higher during spring (72.8%) and summer (74.1%) and lower during autumn (66.6%) and winter (67.8%)" (Song et al., 2006).

Kadlec and Reddy (2001) did a literature review of the impact of change in temperature on treatment efficiency of wetlands. "The temperature coefficient (Θ) varied from 1.05 to 1.37 for carbon and N cycling processes during isolated conditions. P sorption reactions are least affected by temperature, with Θ values of 1.03 to 1.12. Temperature seems to have minimal effect on biochemical oxygen demand ($0.900 < \Theta < 1.015$) and P ($0.995 < \Theta < 1.020$) removal, and a more significant effect on N removal ($0.988 < \Theta < 1.16$)" (Kadlec & Reddy, 2001). See all results tables for more precise details on each result for each reference. There is some insight on an equation description under methodology.

Land et al. (2016) focused on the efficiency of N and P removal in recreated wetlands. Their analysis was based on results from many other studies mainly across Europe and the United States. "Median removal rates of nitrogen and phosphorous were 93 and 1.2 g m^{-2} $year^{-1}$, respectively. Removal efficiency for Total Nitrogen was significantly correlated with hydrologic loading rate (HLR) and Temperature, and the median was 37 %, with a 95 % confidence interval of 29–44 %. Removal efficiency for Total Phosphorous was significantly correlated with inlet Total Phosphorous concentration, HLR, Temperatures, and Average Median Total Phosphorous removal efficiency was 46 % with a 95 % confidence interval of 37–55 %. Maximum in removal efficiency appeared at intermediate annual average temperatures (approximately 14–19 °C)" (Land, et al., 2016). For N we have a table per climate region (Aw, Cfa, Cfb, Csa, Dfa, Dfb):

Table 38. Removal efficiency depending on regional climate characteristics

	n[a]	Ln R ± 1 SE	R	Median removal efficiency (%)	95 % confidence interval
All wetlands	38	−0.46 ± 0.05	0.63	37	29–43
Climate zone					
Aw (equatorial savannah, dry winter)	1	−0.49 ± 0.21	0.61	39	7–60
Cfa (warm, fully humid, hot summer)	6	−0.47 ± 0.15	0.63	37	15–54
Cfb (warm, fully humid, warm summer)	19	−0.44 ± 0.08	0.64	36	23–46
Csa (warm, dry and hot summer)	3	−0.63 ± 0.02	0.53	47	44–50
Dfa (snow, fully humid, hot summer)	5	−0.61 ± 0.12	0.54	46	30–58
Dfb (Snow, fully humid, warm summer)	4	−0.31 ± 0.11	0.73	27	9–42

Source: Land et al., 2016.

In Sweden, Valkama et al. (2017) indicate that the "mean temperature in 2014 was 6.2◦C and precipitation 320 mm. Normal annual mean temperatures in this boreal region is 5.0 ◦C and annual precipitation is 660 mm. The coldest month was January (mean temperature −7.5 ◦C) and warmest July (mean temperature 19.1 ◦C). … The incoming and outgoing TP and NO_3–N loads were calculated and the relative and absolute reduction rates were determined."

"The wetland received 24 g P m^{-2} $year^{-1}$ and 130 g NO_3-N m^{-2} $year^{-1}$ and it retained 3.1 g m^{-2} $year^{-1}$ of P and 18 g m^{-2} $year^{-1}$ of NO_3-N .Annual TP reduction was 13% and NO_3-N reduction 14%. … The monthly relative NO_3–N reduction was 25–82% in growing season (June–September), 7–10% in January–March and 4–6% in November–December. The highest absolute monthly reduction of NO_3–N occurred in December" (Valkama et al., 2017).

- **Methodology**

  - Method 1 (Georgi & Zafiriadis, 2006)

In a study in Greece, the authors used Thom's Discomfort Index for population based on air temperature and relative humidity in order to justify the use of vegetation in mitigating solar radiation and air temperatures (equations for temperature and radiation relative impact on vegetation is also available) (Georgi & Zafiriadis, 2006):

$$DI = TEM - 0.55\,(1 - 0.01\,HUM)\,(TEM - 14.5)\ ^{\circ}C$$

where:

DI = Discomfort Index in °C (DI)
TEM = Air temperature °C.
HUM = Relative humidity (percentage) %.

"<21 degrees = no discomfort / 21-24 = under 50% population feels discomfort / 24-27 = most 50% population feels discomfort / 27-29 = Most population suffers discomfort / 29-32 = everyone feels severe stress / >32 = state of medical emergency" (Georgi & Zafiriadis, 2006).

  - Method 2 (Kadlec & Reddy, 2001)

Areal removal rate (Kadlec & Reddy, 2001):

$$k = k_{20}\theta^{(T-20)}$$

$$k_V = k_{V20}\theta^{(T-20)}$$

"Where k_{20} = areal removal rate constant at 20 °C (m/a); k_{V20} = volumetric removal rate constant at 20 °C (1/d); T = temperature (°C); Θ = temperature coefficient" (Kadlec & Reddy, 2001).

Another descriptor in the literature is Q_{10}, which measures the effect of a 10°C change in temperature and is defined as the ratio of removal rates (Kadlec & Reddy, 2001):

$$Q_{10} = \frac{\text{Rate at } (T + 10)}{\text{Rate at } T} = \theta^{10}$$

7.2 Integration of the Literature Review With the CDS Datasets

See section 1.2 for a general instruction.

Datasets:

- ERA5 monthly data on single level
- CMIP5 monthly data on single level

Indicators created:

- **Air temperature**
  - Units: degrees Celsius
  - Frequency: monthly
  - ERA5 variable: “2 m temperature”
  - CMIP5 variable: “2 m temperature“
  - Note: original units in Kelvin
- **Monthly precipitation**:
  - Units: mm per month
  - ERA5 variable: “mean total precipitation rate”
  - CMIP5 variable: “mean precipitation flux“
  - Note: original units in mm/s

7.3 Integration of Climate Indicators Into the SAVi Natural Infrastructure Model

Natural infrastructure-related indicators developed for and extracted from the CDS Toolbox include impacts on rainwater harvesting and flood risk, climate impacts on nutrient absorption in natural infrastructure assets, and vegetation impacts on temperature. The CLD representing the dynamics of the SAVi Natural Infrastructure model is presented in Figure 21.

Figure 21. CLD for natural infrastructure (CDS variables included in pink)

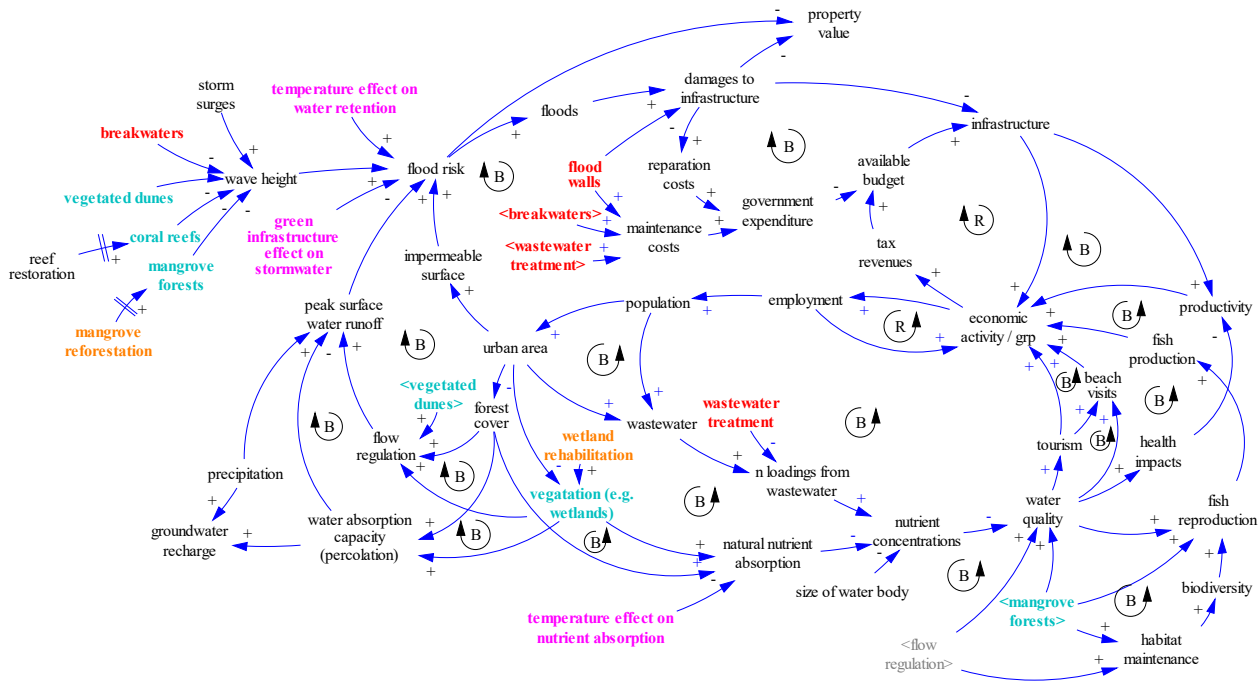

Flood risk is estimated as a function of temperature area, permeability, and peak surface water runoff. The CDS indicator “effect of temperature on water retention” refers to the ability of natural landscapes to retain water given a specific outside temperature. The “effect of green infrastructure on stormwater” refers to potential reductions in stormwater runoff through the implementation of nature-based infrastructure assets (i.e., vegetation). The implementation of green roofs, vegetation strips, and riparian buffers increases water retention on built assets and reduces flood risk by reducing peak stormwater flows during precipitation events.

The impact of temperature on the nutrient absorption of natural infrastructure developed for the CDS Toolbox refers to changes in the rate at which natural infrastructure removes nutrients such as N and P. Nutrient absorption in natural infrastructure assets such as wetlands highly depends on the type of vegetation and climatic conditions.

7.4 Behavioral Impacts Resulting From the Integration of Climate Variables

Using the CDS Toolbox to forecast the flood mitigation capacity of natural infrastructure captures the seasonality of ecosystem service provisioning for simulating the seasonal severity of flood damages in the SAVi simulations. The use of this indicator improves the forecasting of future flood risk and damages and increases the accuracy of natural infrastructure’s contribution to flood mitigation given a range of climate scenarios. This will affect the return on investment of natural infrastructure assets by changing flood damages incurred, depending on whether the natural infrastructure asset is located in favourable or unfavourable climatic conditions.

The impacts of green infrastructure on stormwater runoff developed for and extracted from the CDS Toolbox affects total peak stormwater runoff and stormwater-related management costs as well as flood risk during stormwater events. An increase in the capacity of urban areas to store rainwater and delay runoff leads to a reduction in total stormwater loads, which translates into reduced costs for stormwater management. As water is retained and released over time, natural infrastructure and nature-based infrastructure contribute to reducing flood risk and flood damage incurred in areas with improved absorption and infiltration capacity.

Nutrient absorption is an essential service provided by natural infrastructure, especially wetlands and riparian buffers. The use of the CDS indicator forecasting climate change impacts on nutrient absorption of natural infrastructure in the SAVi model has far reaching impacts on various aspects of the model and simulation results. Changes in nutrient absorption affect the asset's capacity to remove nutrients from water stored with impacts on ecosystem service delivery, the value of ecosystem services provided, and water quality. By impacting water quality, nutrient concentration further affects indicators such as chlorophyll-a concentration, water clarity, and the valuation of economic activities such as fisheries, tourism and real estate.

7.5 Simulation Results

With regard to SAVi Natural Infrastructure, different variables were developed using the CDS database. Natural infrastructure is affected by its surrounding climatic conditions and impacts its surrounding environment in various ways. An example of the former is the impact of temperature on P removal efficiency in wetlands. An example of the latter is the use of trees and urban green infrastructure to reduce the heat island effect. The following three variables were developed to incorporate data from the CDS : (1) the effect of temperature on P removal efficiency in wetlands, (2) the effect of vegetation cover on surrounding temperatures, and (3) the number of months during which heat impacts on health can occur.

7.5.1 Effect of Temperature on P Removal Efficiency in Wetlands

El-Rafaie (2010) describes the impact of temperature on the removal efficiency of the Manzala Engineerede Wetland in Egypt. The results of the study indicate that the P removal efficiency of wetland increases with temperature. The following equation is used to forecast the P removal efficiency of wetlands using CDS data:

*P removal efficiency of wetlands = (1.4035 * seasonal temperature - 10.888) / 100*

Forecasting P removal efficiency in wetlands enables an estimation of the value of nutrient removal in relation to local climatic conditions. Figure 22 presents the results for the BAU (red line) and the CDS climate-impact scenario (blue line), respectively.

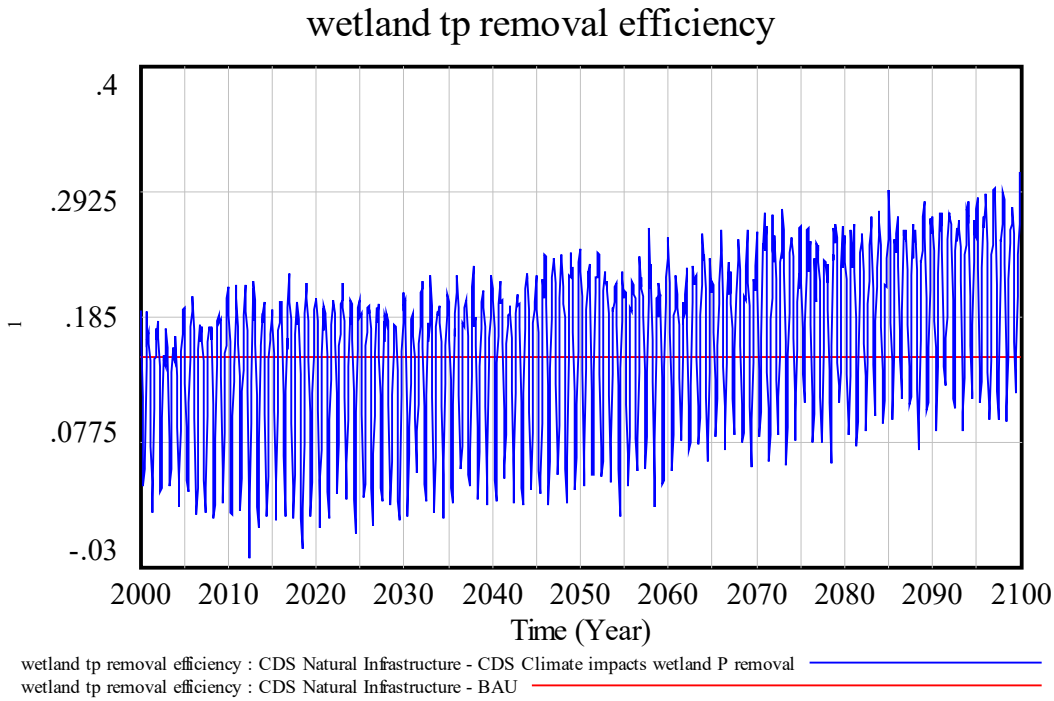

Figure 22. P removal efficiency in wetlands

Figure 22 above illustrates that the overall removal efficiency of wetlands is projected to increase in the area around Johannesburg, due to the projected increase in temperature in the IPSL RCP 8.5 scenario. The seasonal fluctuation of P removal efficiency directly affects the water quality of waterbodies that receive the effluent of the wetland. Figure 23 illustrates the P loadings in wetland effluent (water leaving the wetland) and how the constant formulation in the BAU scenario significantly underestimates P loadings from wetland effluent.

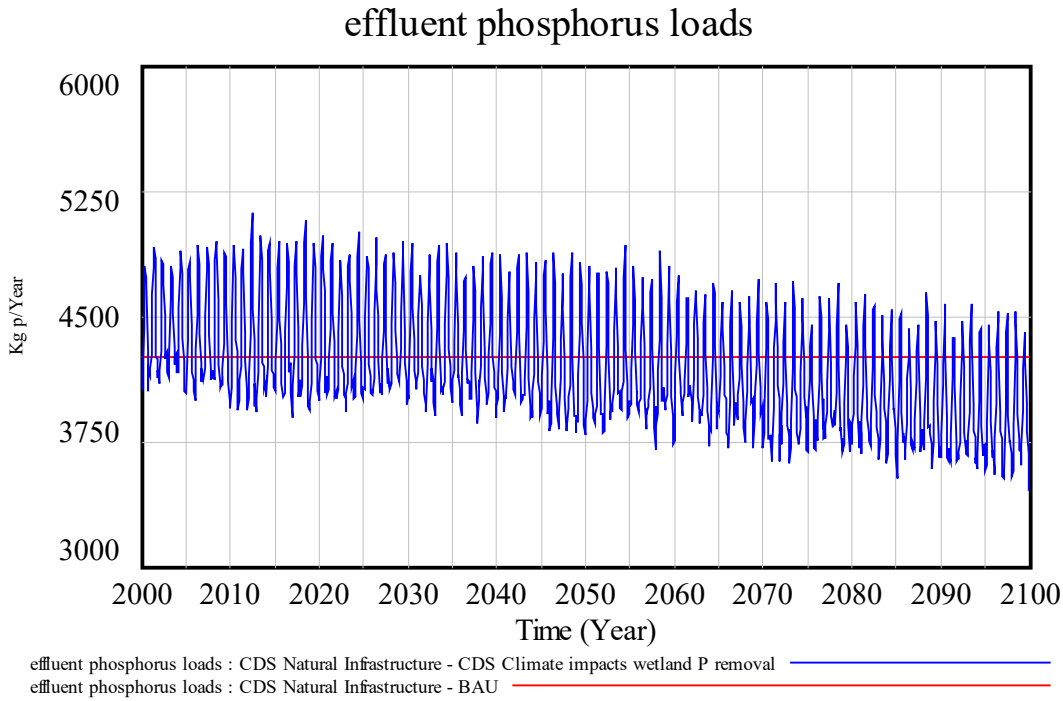

Figure 23. Wetland effluent P loads

Cumulatively, the amount of P removed by the wetland is 60.06 tonnes P and 67.29 tonnes P in the no-impact and CDS climate-impact scenarios, respectively. This is equivalent to an annual reduction of 750.58 kg P (no-impact scenario) and 841.13 kg P (CDS climate-impact scenario) per year, respectively. Assuming an average cost of P removal in wastewater treatment plants of USD 68.38 per kg P removed, the cumulative avoided cost of wastewater treatment between 2020 and 2100 totals USD 4.11 million in the no-impact scenario and USD 4.60 million in the CDS impact scenario. Both the amount of P removed and related costs in the CDS impact scenario are 12% higher compared to the no-impact scenario.

7.5.2 Effect of Temperature on Labour Productivity and Impacts of Vegetation Cover

We have assumed that working in temperatures above 25°C exposes individuals to a higher risk of suffering adverse health impacts, leading to higher health costs and the need for replacement workers. The CDS climate data is used to forecast the number of months during which adverse health impacts may occur. The following equation is used to calculate the labour productivity impact indicator:

Labor productivity impact indicator = IF THEN ELSE (Tair>25, Tair / 25, 0)

The IF THEN ELSE function assesses whether the threshold temperature (25°C) is exceeded and, hence, whether impacts may occur. Dividing air temperature by the threshold value indicates the potential strength of impacts relative to the threshold temperature. Figure 24 presents the forecasted labour productivity impact indicator for Johannesburg.

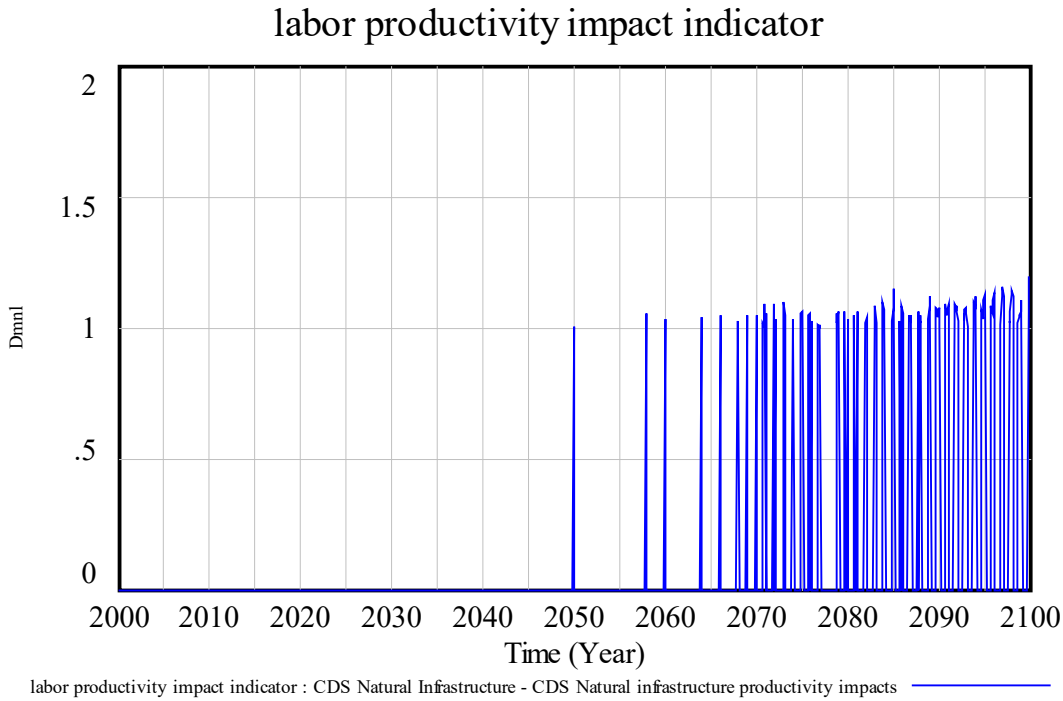

Figure 24. Labour productivity impact indicator

The forecast indicates that temperature-related labour productivity impacts start occurring around the year 2050/2060 and become frequent after 2065.

7.5.3 Impacts of Vegetation Cover on Surrounding Air Temperature

The literature review above highlights the role of trees and green spaces in temperature regulation in urban environments. Vegetation cover mitigates sun radiation and provides shade, contributing to counteracting the urban heat island effect. The average reduction for a 25% increase in vegetation cover is 1.635 °C.

In light of the temperature-related labour productivity impacts described above, three indicators were developed for assessing the potential benefits of increasing vegetation cover in Johannesburg. Table 39 provides an overview of the three indicators and their equations.

Table 39. Air temperature indicators considering vegetation cover

Indicator	Equation
Air temperature 25% vegetation cover	= T_{air} – 1.635
Air temperature 50% vegetation cover	= T_{air} – 3.27
Air temperature 75% vegetation cover	= T_{air} – 4.905

Assuming the same temperature threshold for the occurrence of temperature-related impacts on labour productivity (25°), the labour productivity impact indicator is simulated using the three different air temperature values. This simulation assumes that the vegetation cover in Johannesburg is close to 0%, for illustration purposes.

The results of the simulations using different CDS-based air temperature values are presented in Figure 25. The figure in the top left represents the simulation without vegetation cover, as already presented in Figure 24. The subsequent figures represent the months with potential labour productivity impacts considering 25% (top right), 50% (bottom left), and 75% (bottom right) vegetation cover.

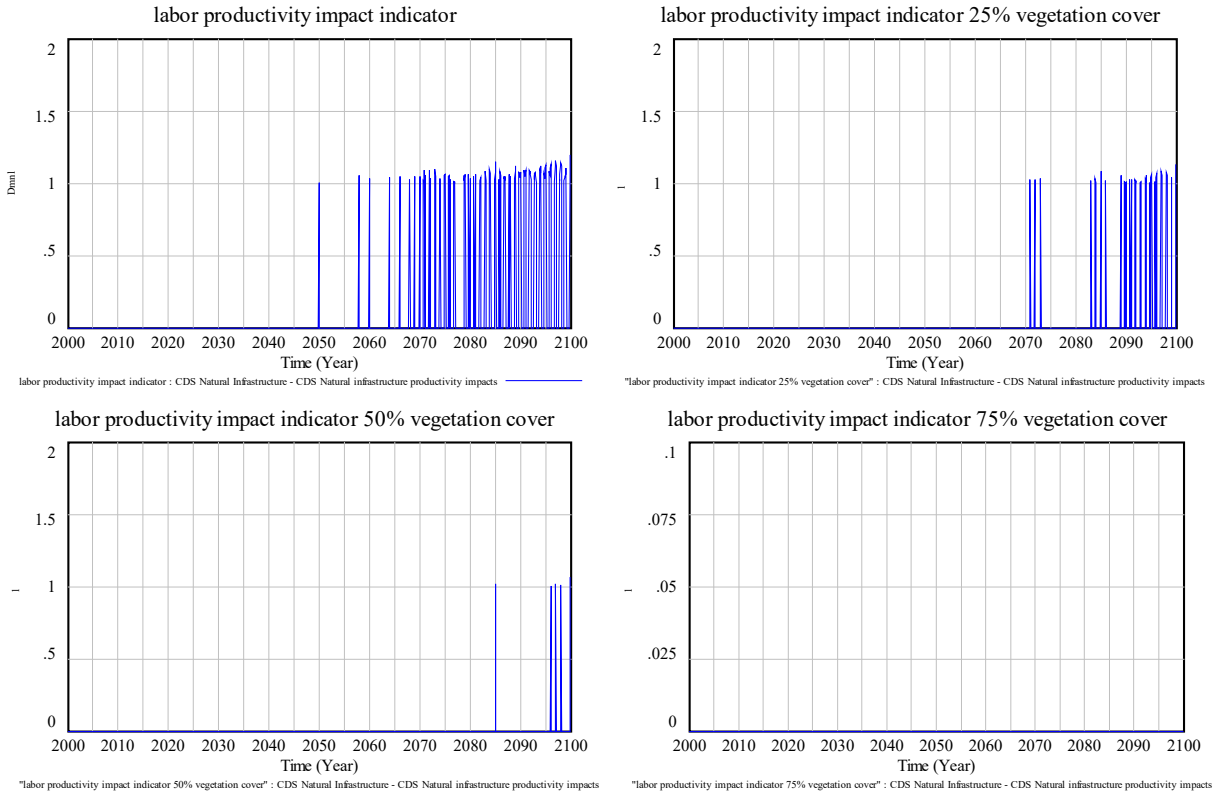

Figure 25. Labour productivity impact indicator and the impacts of vegetation cover

The results illustrate that increasing vegetation cover in the form of trees and green roofs could postpone the onset of temperature-related impacts on labour productivity or even mitigate it entirely (75% vegetation cover).

8 Reference List

Acclimatise. (2009). *Building business resilience to inevitable climate change. Carbon Disclosure Project report: Global Electric Utilities.* https://www.longfinance.net/media/documents/Acclimatise_CDP_Global_Electricity_Adaptation_Report_HR.pdf

Adeh, E. H., Good, E., & Calaf, S & Higgins, C. W. (2019). Solar PV power potential is greatest over croplands. *Scientific Reports, 9, art. 11442*. https://www.nature.com/articles/s41598-019-47803-3

Ahsan, S., Rahman, M. A., Kaneco, S., Katsumata, H., Suzuki, T., & Ohta, K. (2005). Effect of temperature on wastewater treatment with natural and waste materials. *Clean Technologies and Environmental Policy, 7*(3), 198–202. http://10.1007/s10098-005-0271-5

Akbari, H. (2005). *Energy saving potentials and air quality benefits of urban heat island mitigation.* https://www.osti.gov/biblio/860475/

Akbari, H., Davis, S., Dorsano, S., Huang, J., & Winnett, S. (1992). *Cooling our communities: A guidebook on tree planting and light-colored surfacing.* Environmental Protection Agency.

Alam, T., Mahmoud, A., Jones, K. D., Bezares-Cruz, J. C., & Guerrero, J. (2019). A comparison of three types of permeable pavements for urban runoff mitigation in the semi-arid South Texas, USA. *Water, 11*(10). http://www.doi.org/10.3390/w11101992

Allen, R. G., Pereira, L. S., Raes, D., & Smith, M. (2006). *Crop evapotranspiration* (FAO Irrigation and Drainage Paper No. 56). Food and Agriculture Organization of the United Nations. http://www.fao.org/tempref/SD/Reserved/Agromet/PET/FAO_Irrigation_Drainage_Paper_56.pdf

American Society of Landscape Architects. (2003). *Chicago City Hall Green Roof*. http://www.asla.org/meetings/awards/awds02/chicagocityhall.html

Asian Development Bank. (2012). *Adaptation to climate change: The case of a combined cycle power plant.* http://icem.com.au/wp-content/uploads/2013/07/OMon_summaary-paper.pdf

Attia, S. I. (2015). The influence of condenser cooling water temperature on the thermal efficiency of a nuclear power plant. *Annals of Nuclear Energy*, 371–378. http://www.doi.org/10.1016/j.anucene.2015.02.023

Bartos, M., Chester, M., Johnson, N., Gorman, B., Eisenberg, D., Linkov, I., & Bates, M. (2016). Impacts of rising air temperatures on electric transmission ampacity and peak electricity load in the United States. *Environmental Research Letters, 11*(11), 1. https://iopscience.iop.org/article/10.1088/1748-9326/11/11/114008/ampdf

Basha, M., Shaahid, S. M., & Al-Hadhrami, L. (2011). Impact of fuels on performance and efficiency of gas turbine power plants. 2nd International Conference on Advances in Energy Engineering, December 27–28, 2011, Bangkok, Thailand. *Energy Procedia, 14,* 558–565.

Bassi, A. M., Pallaske, G., Wuennenberg, L., Graces, L., & Silber, L. (2019, March). *Sustainable Asset Valuation Tool: Natural infrastructure.* https://www.iisd.org/sites/default/files/publications/sustainable-asset-valuation-tool-natural-infrastructure.pdf

Bengtson, H. (2020). *The rational method for estimation of design surface runoff rate for storm water control*. https://www.brighthubengineering.com/hydraulics-civil-engineering/60842-the-rational-method-for-calculation-of-peak-storm-water-runoff-rate/

Bergel-Hayat, R., Debbarh, M., Antoniou, C., & Yannis, G. (2013). Explaining the road accident risk: weather effects. *Accident Analysis & Prevention, 60*, 456–465. https://doi.org/10.1016/j.aap.2013.03.006

Berghage, R. D., Beattie, D., Jarrett, A. R., Thuring, C., Razaei, F., & O'Connor, T. P. (2009). *Green roofs for stormwater runoff control.* Environmental Protection Agency.

Bhatt, S., & Rajkumar, N. (2015). Effect of moisture in coal on station heat rate and fuel cost for Indian thermal power plants. *Power Research, 11*(4), 773-786. https://www.alcoxsteel.com/blog/effect-of-moisture-in-coal-on-station-heat-rate-and-fuel-cost-for-indian-thermal-power-plants/#:~:text=The%20effects%20of%20moisture%20in,the%20unit%20heat%20rate%20increases.

Bhattacharya, C., & Sengupta, B. (2016). Effect of ambient air temperature on the performance of regenerative air preheater of pulverised coal fired boilers. *International Journal of Energy Technology and Policy, 12*(2), 136–153. http://www.doi.org/10.1504/IJETP.2016.075672

Biswas, B. (2014). Construction and evaluation of rainwater harvesting system for domestic use in a remote and rural area of Khulna, Bangladesh. *International Scholarly Research Notices*. https://doi.org/10.1155/2014/751952

Brouwer, C., & Heibloem, M. (1986). *Irrigation water management and irrigation water needs. Training manual no. 3.* Food and Agriculture Organization of the United Nations. http://www.fao.org/tempref/agl/AGLW/fwm/Manual3.pdf

Brouwer, C., Prins, K., & Heibloem, M. (1989). *Irrigation water management: Irrigation scheduling.* Food and Agriculture Organization of the United Nations. http://www.fao.org/3/T7202E/t7202e00.htm#Contents

Büyükalaca, O., Bulut, H., & Yılmaz, T. (2001). Analysis of variable-base heating and cooling degree-days for Turkey. *Applied Energy, 69*(4), 269–283. https://doi.org/10.1016/S0306-2619(01)00017-4

Chinowsky, P. S., Price, J. C., & Neumann, J. E. (2013). Assessment of climate change adaptation costs for the U.S. road network. *Global Environmental Change, 23(4)*, 764-773. https://doi.org/10.1016/j.gloenvcha.2013.03.004

Chinowsky, P., Hayles, C., Schweikert, A., Strzepek, N., Strzepek, K., & Schlosser, A. (2011). Climate change: Comparative impact on developing and developed countries. *Engineering Project Organization Journal*, *1*(1), 67–80. https://doi.org/10.1080/21573727.2010.549608

Choi, T., Keith, L., Hocking, E., Friedman, K., & Matheu, E. (2011). *Dams and energy sectors interdependency study.* https://www.energy.gov/sites/prod/files/Dams-Energy%20Interdependency%20Study.pdf

City of Chicago. (2006). *Green roof test plot project: Annual project summary report.* https://www.chicago.gov/dam/city/depts/doe/general/GreenBldsRoofsHomes/2006_Annual_Project_Summary_Report.pdf

Colman, J. (2013, Avril 26). *The effect of ambient air and water temperature on power plant efficiency* [Master's thesis]. Duke University Libraries.

Crook, J. A., Jones, L. A., Forster, P. M., & Crook, R. (2011). Climate change impacts on future photovoltaic and concentrated solar power energy output. *Energy and Environmental Science, 4* (9), 3101–3109.

Cronshey, R., McCuen, R. H., Miller, N., Rawls, W., Robbins, S., & Woodward, D. (1986, June). *Urban hydrology for small watersheds.* United States Department of Agriculture https://www.nrcs.usda.gov/Internet/FSE_DOCUMENTS/stelprdb1044171.pdf

Das, T. K., Saharawat, Y. S., Bhattacharyya, R., Sudhishri, S., Bandyopadhyay, K. K., Sharma, A. R., & Jat, M. L. (2018). Conservation agriculture effects on crop and water productivity, profitability and soil organic carbon accumulation under a maize-wheat cropping system in the North-western Indo-Gangetic Plains. *Field Crops Research, 215*, 222–231.

Davies, Z. G., Edmondson, J. L., Heinemeyer, A., Leake, J. R., & Gaston, K. J. (2011). Mapping an urban ecosystem service: Quantifying above-ground carbon storage at a city-wide scale. *Journal of applied ecology, 48*(5), 1125–1134. https://doi.org/10.1111/j.1365-2664.2011.02021.x

Davy, R., Gnatiuk, N., Pettersson, L., & Bobylev, L. (2018). Climate change impacts on wind energy potential in the European domain with a focus on the Black Sea. *Renewable and Sustainable Energy Reviews, 81*(2), 1652–1659. https://doi.org/10.1016/j.rser.2017.05.253

De Oliveira, V., De Mello, C., Viola, M., & Srinivasan, R. (2017). Assessment of climate change impacts on the streamflow and hydropower potential in the headwater region of the Grande river basin, Southeastern Brazil. *International Journal of Climatology 37*(15), 5005–5023. https://doi.org/10.1002/joc.5138

De Rosa, M., Bianco, V., Scarpa, F., & Tagliafico, L. A. (2014). Heating and cooling building energy demand evaluation; a simplified model and a modified degree days approach. *Applied Energy, 128*, 217–229. https://doi.org/10.1016/j.apenergy.2014.04.067

De Sa, A., & Al Zubaidy, S. (2011). Gas turbine performance at varying ambient temperature. *Applied Thermal Engineering, 31*(14–15), 2735–2739. http://www.doi.org/10.1016/j.applthermaleng.2011.04.045

Demuzere, M., Orru, K., Heidrich, O., Olazabal, E., Geneletti, D., Orru, H., Bhave, A. G., Mittal, N., Feliu, E., Faehnle, M. (2014). Mitigating and adapting to climate change: Multi-functional and multi-scale assessment of green urban infrastructure. *Journal of Environmental Management, 146*, 107–115. https://doi.org/10.1016/j.jenvman.2014.07.025

Dhakal, S., & Hanaki, K. (2002). Improvement of urban thermal environment by managing heat discharge sources and surface modification in Tokyo. *Energy and Buildings, 34*(1), 13–23. https://doi.org/10.1016/S0378-7788(01)00084-6

Diaz, C. A., Osmond, P., & King, S. (2015). Precipitation and buildings: Estimation of the natural potential of locations to sustain indirect evaporative cooling strategies through hot seasons. *Living and Learning: Research for a Better Built Environment: 49th International Conference of the Architectural Science Association* (pp. 45-54). http://anzasca.net/wp-content/uploads/2015/12/005_Diaz-Sandoval_Osmond_King_ASA2015.pdf

Djaman, K., O'Neill, M., Owen, C. K., Smeal, D., Koudahe, K., West, M., & Irmak, S. (2018). Crop evapotranspiration, irrigation water requirement and water productivity of maize from meteorological data under semiarid climate. *Water, 10*(4), *405*. http://www.doi.org/10.3390/w10040405

Doorenbos, J., & Kassam, A. (1979). *Yield response to water irrigation and drainage* (Paper No. 33). Food and Agricultural Organization of the United Nations.

Drax. (2017, August 29). *What hot weather means for electricity*. https://www.drax.com/technology/hot-weather-means-electricity/

Du, L., Trinh, X., Chen, Q., Wang, C., Wang, H., Xia, X., Zhou, Q., Xu, D., & Wu, Z. (2018). Enhancement of microbial nitrogen removal pathway by vegetation in Integrated Vertical-Flow Constructed Wetlands (IVCWs) for treating reclaimed water. *Bioresource Technology, 249,* 644–651. https://doi.org/10.1016/j.biortech.2017.10.074

Dunn, A. D. (2007). *Green light for green infrastructure.* https://digitalcommons.pace.edu/lawfaculty/494

Durmayaz, A., & Sogut, O. S. (2006). Influence of cooling water temperature on the efficiency of a pressurized-water reactor nuclear-power plant. *International Journal of Energy Research, 30(10)*, 799–810. http://www.doi.org/10.1002/er.1186

Eliasson, J., & Ludvigsson, G. (2000, November 15–17). *Load factor of hydropower plants and its importance in planning and design.* Presented at the 11th International Seminar on Hydro Power Plants, Vienna, Austria. http://aldarafmaeli.hi.is/files/skjol/verkfraedi_og_natturuvisindasvid_deildir/umhv_og_byggv/vatnaverkfrstofa/Load_%2520facabstract.pdf

El-Refaie, G. (2010). Temperature impact on operation and performance of Lake Manzala Engineered Wetland, Egypt. *Ain Shams Engineering Journal, 1*(1), 1–9. https://www.sciencedirect.com/science/article/pii/S209044791000002X

El-Shobokshy, M. S., & Hussein, F. M. (1993). Degradation of photovoltaic cell performance due to dust deposition on to its surface. *Renewable Energy, 3*(6–7), 585–590. https://doi.org/10.1016/0960-1481(93)90064-N

Engineering ToolBox. (2009). *Pumping water: Energy cost calculator*. https://www.engineeringtoolbox.com/water-pumping-costs-d_1527.html

Engineering ToolBox. (n.d.). *Hydropower*. https://www.engineeringtoolbox.com/hydropower-d_1359.html

Environmental Protection Agency. (2014). *The economic benefits of green infrastructure: A case study of Lancaster, PA.* https://www.cnt.org/sites/default/files/publications/CNT_EPA_LancasterGICaseStudy.pdf

Eurostat. (2019). *Energy statistics: Cooling and heating degree days (nrg_chdd)*. https://ec.europa.eu/eurostat/cache/metadata/en/nrg_chdd_esms.htm

Evans, D. V., & Antonio, F. D. (Eds.). (1986). *Hydrodynamics of ocean wave-energy utilization: IUTAM Symposium Lisbon/Portugal 1985*. Springer Science & Business Media.

Farkas, Z. (2011). *Considering air density in wind power production.* Budapest.

Flowers, M. E., Smith, M. K., Parsekian, A. W., Boyuk, D. S., McGrath, J. K., & Yates, L. (2016). Climate impacts on the cost of solar energy. *Energy Policy, 94*, 264–273. https://doi.org/10.1016/j.enpol.2016.04.018

Gajbhiye, S., Mishra, S. K., & Pandey, A. (2013). Effects of seasonal/monthly variation on runoff curve number for selected watersheds of Narmada Basin. *International Journal of Environmental Sciences, Volume 3*(6), 2019–2030. http://www.doi.org/10.6088/ijes.2013030600021

Garfí, M., Pedescoll, A., Bécares, E., Hijosa-Valsero, M., Sidrach-Cardona, R., & García, J. (2012). Effect of climatic conditions, season and wastewater quality on contaminant removal efficiency of two experimental constructed wetlands in different regions of Spain. *Science of the Total Environment, 437*, 61–67. http://www.doi.org/10.1016/j.scitotenv.2012.07.087

Georgi, N. J., & Zafiriadis, K. (2006). The impact of park trees on microclimate in urban areas. *Urban Ecosystems, 9*(3), 195–209.

Gesellschaft für Internationale Zusammenarbeit (GIZ). (2016). *Solar Powered Irrigation Systems (SPIS) – Technology, economy, impacts.* https://energypedia.info/images/temp/2/23/20160630122544!phpeKHVUr.pdf

Ghamami, M., Fayazi Barjin, A., & Behbahani, S. (2016). Performance optimization of a gas turbine power plant based on energy and exergy analysis. *Mechanics, Materials Science & Engineering Journal, 29*.

Gomes, J., Diwan, L., Bernardo, R., & Karlsson, B. (2014). Minimizing the impact of shading at oblique solar angles in a fully enclosed asymmetric concentrating PVT collector. *Energy Procedia, 57*, 2176–2185. https://doi.org/10.1016/j.egypro.2014.10.184

Green, A. (2020). *The intersection of energy and machine learning*. https://adgefficiency.com/energy-basics-ambient-temperature-impact-on-gas-turbine-performance/

Haerter, J., Hagemann, S., Moseley, C., & Piani, C. (2011). Climate model bias correction and the role of timescales. *Hydrology and Earth System Sciences, 15*(3), 1065–1073.

Handayani, K., Filatova, T., & Krozer, Y. (2019). The vulnerability of the power sector to climate variability and change: evidence from Indonesia. *Energies, 12*(19), 3640. http://www.doi.org/10.3390/en12193640

Harrison, G. P., & Whittington, H. W. (2002). Vulnerability of hydropower projects to climate change. *IEE proceedings-generation, transmission and distribution, 149*(3), 249–255. http://www.doi.org/0.1049/ip-gtd:20020173

Harrison, G., & Wallace, A. (2005). Climate sensitivity of marine energy. *Renewable Energy, 30*(12), 1801–1817. https://doi.org/10.1016/j.renene.2004.12.006

Hassanpour, E., Good, S. P., Calaf, M., & Higgins, C. W. (2019). Solar PV power potential is greatest over croplands. *Scientific Reports, 9*(1), 1-6. http://www.doi.org/10.1038/s41598-019-47803-3

Hassanpour, E., Higgins, C. W. & Selker, J. S. (2017). *Remarkable solar panels Influence on soil moisture, micrometeorology and water-use efficiency-database*. http://www.doi.org/10.7267/N9W37T8D

Hassanpour, E., Selker, J. S. & Higgins, C. W. (2018). Remarkable agrivoltaic influence on soil moisture, micrometeorology and water-use efficiency. *PloS One, 13,* e0203256. https://doi.org/10.1371/journal.pone.0203256

Henry, C. L., & Pratson, L. F. (2016). Effects of environmental temperature change on the efficiency of coal and natural gas-fired power plants. *Environmental Science & Technology, 50(17)*, 9764–9772. https://doi.org/10.1021/acs.est.6b01503

How it Works: Water for Coal. (2010). *Union of Concerned Scientists.* https://www.ucsusa.org/resources/water-coal

Hutyra, L. R., Yoon, B., & Alberti, M. (2011). Terrestrial carbon stocks across a gradient of urbanization: a study of the Seattle, WA region. *Global Change Biology, 17*(2), 783–797. https://doi.org/10.1111/j.1365-2486.2010.02238.x

Ibrahim, S., Ibrahim, M., & Attia, S. (2014). The impact of climate changes on the thermal performance of a proposed pressurized water reactor: Nuclear-power plant. *International Journal of Nuclear Energy*. https://www.hindawi.com/journals/ijne/2014/793908/

Jabboury, B. G., & Darwish, M. A. (1990). Performance of gas turbine co-generation power desalting plants under varying operating conditions in Kuwait. *Heat Recovery Systems and CHP, 10*(3), 243–253. https://doi.org/10.1016/0890-4332(90)90005-5

Jackson, N., & Puccinelli, J. (2006). *Long-Term Pavement Performance (LTPP) data analysis support: National pooled fund study TPF-5 (013)-effects of multiple freeze cycles and deep frost penetration on pavement performance and cost* (No. FHWA-HRT-06-121). U.S. Department of Transportation.

Janssen, H., Carmeliet, J., & Hens, H. (2004). The influence of soil moisture transfer on building heat loss via the ground. *Building and Environment, 39*(7), 825–836. https://www.academia.edu/17540389/The_influence_of_soil_moisture_transfer_on_building_heat_loss_via_the_ground

Jerez, S., Tobin, I., Vautard, R., Montávez, J. P., López-Romero, J. M., Thais, F., Bartol, B., Christensen, O. B., Colette, A., Déqué, M., Nikuylin, G., Kotlarski, S., van Mijgaardm E., Teichmann, C, & Wild, M. (2015). The impact of climate change on photovoltaic power generation in Europe. *Nature Communications, 6*(1), 1–8. https://doi.org/10.1038/ncomms10014

JICA. (March 2003). *Manual on flood control planning.* Department of Public Works and Highways.

Jim, C. Y., & Chen, W. Y. (2008). Assessing the ecosystem service of air pollutant removal by urban trees in Guangzhou (China). *Journal of Environmental Management, 88*(4), 665–676. https://doi.org/10.1016/j.jenvman.2007.03.035

Kadlec, R. H., & Reddy, K. R. (2001). Temperature effects in treatment wetlands. *Water Environment Research, 73*(5), 543–557. http://www.doi.org/10.2175/106143001x139614

Kakaras, E., Doukelis, A., Prelipceanu, A., & Karellas, S. (2006). Inlet air cooling methods for gas turbine based power plants. *Proceedings of the ASME Turbo Expo 2008 Power for Land, Sea, and Air.* https://doi.org/10.1115/GT2004-53765

Kaldellis, J., & Fragos, P. (2011). Ash deposition impact on the energy performance of photovoltaic generators. *Journal of Cleaner Production, 19*(4), 311–317. http://www.doi.org/10.1016/j.jclepro.2010.11.008

Kappos, L., Ntouros, I., & Palivos, I. (1996). Pollution effect on PV system efficiency. *Proceedings of the 5th National Conference on Soft Energy Forms.* Athens, Greece.

Kivi, R. (2017, Avril 24). *How does geothermal energy work?* https://sciencing.com/geothermal-energy-work-4564716.html

Kloss, C., & Calarusse, C. (2011). *Rooftops to rivers: Green strategies for controlling stormwater and combined sewer overflows.* https://www.nrdc.org/sites/default/files/rooftopstoriversII.pdf

Koc, C. B., Osmond, P., & Peters, A. (2018). Evaluating the cooling effects of green infrastructure: A systematic review of methods, indicators and data sources. *Solar Energy, 166*, 486–508. https://doi.org/10.1016/j.solener.2018.03.008

Kosa, P. (2011). The effect of temperature on actual evapotranspiration based on Landsat 5 TM Satellite Imagery. *Evapotranspiration, 56*(56), 209–228. https://www.intechopen.com/books/evapotranspiration/the-effect-of-temperature-on-actual-evapotranspiration-based-on-landsat-5-tm-satellite-imagery

Krishna, P., Kumar, K., & Bhandari, N. M. (2002). IS: 875 (Part3): *Wind loads on buildings and structures-proposed draft & commentary* (Document No.: IITK-GSDMA-Wind, 02-V5). Department of Civil Engineering, Indian Institute of Technology Roorkee.

Kumpulainen, L., Laaksonen, H., Komulainen, R., Martikainen, A., Lehtonen, M., Heine, P., .Antii, S., Imris, P., Partanen, J., Lassila, J., Kaipia, T., Viljainen, S., Verho, P., Järventausta, P., Kivikko, K., Kauhaniemi, K., Lagland, H., & Saaristo, H. (2007). *Distribution Network 2030: Vision of the future power system.* VTT Technical Research Centre of Finaland.

Land, M., Granéli, W., Grimvall, A., Hoffmann, C. C., Mitsch, W. J., Tonderski, K. S., & Verhoeven, J. T. (2016). How effective are created or restored freshwater wetlands for nitrogen and phosphorus removal? A systematic review. *Environmental Evidence, 5*.

Larsen, P., Goldsmith, S., Wilson, M., Strzepek, K., Chinowsky, P., & Saylor, B. (2008). Estimating future costs for Alaska public infrastructure at risk from climate. *Global Environmental Change*, 442–457. http://www.doi.org/10.1016/j.gloenvcha.2008.03.005

Lavin, P. (2003). *A practical guide to design, production, and maintenance for architects and engineers.* Spon Press.

Linnerud, K., Mideksa, T. K., & Eskeland, G. S. (2011). The impact of climate change on nuclear power supply. *The Energy Journal, 32*(1). https://www.jstor.org/stable/41323396

Lise, W., & van der Laan, J. (2015). Investment needs for climate change adaptation measures of electricity power plants in the EU. *Energy for Sustainable Development, 28*, 10–20.

Manoli, G., Fatichi, S., Schläpfer, M., Yu, K., Crowther, T. W., Meili, N., Burlando, P., Katul, G. G., & Bou-Zeid, E. (2019). Magnitude of urban heat islands largely explained by climate and population. *Magnitude of Urban Nature, 573*(7772), 55–60. http://www.doi.org/10.1038/s41586-019-1512-9

Manwell, J. F., McGowan, J. G., & Rogers, A. L. (2010). *Wind energy explained: Theory, design and application.* John Wiley & Sons.

Maulbetsch, J. S., & Di Filippo, M. N. (2006). *Cost and value of water use at combined-cycle power plants.* California Energy Commission – Public Interest Energy Research Program.

Maupoux, M. (2010). *Solar photovoltaic water pumping.* Practical Action – The Schumacher Centre for Technology and Development. https://sswm.info/sites/default/files/reference_attachments/MAUPOUX%202010%20Solar%20Water%20Pumping.pdf

Meral, M. E., & Dincer, F. (2011). A review of the factors affecting operation and efficiency of photovoltaic based electricity generation systems. *Renewable and Sustainable Energy Reviews, 15*(5), 2176-2184. http://www.doi.org/10.1016/j.rser.2011.01.010

Miradi, M. (2004). Artificial neural network (ANN) models for prediction and analysis of ravelling severity and material composition properties. *CIMCA*, 892–903.

Mirgol, B., Nazari, M., & Eteghadipour, M. (2020). Modelling climate change impact on irrigation water requirement and yield of winter wheat (*Triticum aestivum L.*), barley (*Hordeum vulgare L.),* and fodder maize (*Zea mays L.)* in the semi-arid Qazvin Plateau, Iran. *Agriculture, 10*(3), 60. http://www.doi.org/10.3390/agriculture10030060

Mourshed, M. (2012). Relationship between annual mean temperature and degree-days. *Energy and buildings, 54*, 418-425. https://doi.org/10.1016/j.enbuild.2012.07.024

National Snow & Ice Data Center. (n.d.). *Freezing degree-days*. https://nsidc.org/cryosphere/glossary/term/freezing-degree-days

Nazahiyah, R., Yusop, Z., & Abustan, I. (2007). Stormwater quality and pollution loading from an urban residential catchment in Johor, Malaysia. *Water Science and Technology, 56*(7), 1–9. http://www.doi.org/10.2166/wst.2007.692

N.D. Lea International. (1995). *Modelling road deterioration and maintenance.* Asian Development Bank.

Nemry, F., & Demirel, H. (2012). *Impacts of climate change on transport: A focus on road and rail transport infrastructures.* Publications Office of the European Union.

Nichol, J. E. (1996). High-resolution surface temperature patterns related to urban morphology in a tropical city: A satellite-based study. *Journal of Applied Meteorology, 35*(1), 135–146.

Nordhaus, W. (2017). Revisiting the social cost of carbon. *PNAS*, *11*(7), 1518–1523.

Nowak, D. J., Greenfield, E. J., Hoehn, R. E., & Lapoint, E. (2013). Carbon storage and sequestration by trees in urban and community areas of the United States. *Environmental Pollution, 178,* 229–236. https://doi.org/10.1016/j.envpol.2013.03.019

Ould-Amrouche, S., Rekioua, D., & Hamidat, A. (2010). Modelling photovoltaic water pumping systems and evaluation of their CO2 emissions mitigation potential. *Applied Energy, 87*, 3451–3459.

Panagea, I. S., Tsanis, I. K., Koutroulis, A. G., & Grillakis, M. G. (2014). Climate change impact on photovoltaic energy output: the case of Greece. *Advances in Meteorology, 4,* 1–11. http://www.doi.org/10.1155/2014/264506

Pande, P., & Telang, S. (2014). Calculation of rainwater harvesting potential by using mean annual rainfall, surface runoff and catchment area. *Global Advanced Research Journal of Agricultural Science, 3*(7), 200–204.

Parker, J. H. (1989, February). The impact of vegetation on air conditioning consumption. In *Proceedings of the Workshop on Saving Energy and Reducing Atmospheric Pollution by Controlling Summer Heat Islands* (pp. 45–52). University of California Berkeley.

Parliamentary Office of Science and Technology (POST). (2011). Carbon footprint of electricity generation. *POST Note Update, 383*. https://www.parliament.uk/documents/post/postpn_383-carbon-footprint-electricity-generation.pdf

Pérez, G., Coma, J., Martorell, I., & Cabeza, L. F. (2014). Vertical Greenery Systems (VGS) for energy saving in buildings: A review. *Renewable and Sustainable Energy Reviews, 39*, 139–165.

Petchers, N. (2003). *Combined heating, cooling & power handbook. Technologies & applications: An integrated approach to energy resource optimization.* Fairmont Press.

Photovoltaic Softwares. (2020). *How to calculate the annual solar energy output of a photovoltac system.* Photovoltaic Software. https://photovoltaic-software.com/principle-ressources/how-calculate-solar-energy-power-pv-systems

Pierson Jr, W., & Moskowitz, L. (1964). A proposed spectral form for fully developed wind seas based on the similarity theory of SA Kitaigorodskii. *Journal of Geophysical Research*, 5181–5190.

Plósz, B. G., Liltved, H., & Ratnaweera, H. (2009). Climate change impacts on activated sludge wastewater treatment: a case study from Norway. *Water Science and Technology, 60*(2), 533–541.

Poullain, J. (2012). *Estimating Storm Water Runoff* (PDHonline Course H119 [2 PDH]). https://pdhonline.com/courses/h119/stormwater%20runoff.pdf

Prado, R. T., & Ferreira, F. L. (2005). Measurement of albedo and analysis of its influence the surface temperature of building roof materials. *Energy and Buildings, 37*(4), 295–300. https://doi.org/10.1016/j.enbuild.2004.03.009

Rademaekers, K., van der Laan, J., Boeve, S., Lise, W. (2011). *Investment needs for future adaptation measures in EU nuclear power plants and other electricity generation technologies due to effects of climate change* (EUR 24769). European Commission. https://ec.europa.eu/energy/sites/ener/files/documents/2011_03_eur24769-en.pdf

Ramos-Scharron, C., & MacDonald, L. (2007). Runoff and suspended sediment yields from an unpaved road segment. *Hydrological Processes, 21*(1), 35–50.

Roorda, J., & van der Graaf, J. (2000). Understanding membrane fouling in ultrafiltration of WWTP-effluent. *Water Science and Technology 41*(10–11), 345–353.

Rousseau, Y. (2013). *Impact of climate change on thermal power plants: Case study of thermal power plants in France.* [Master's thesis]. University of Iceland.

Saito, I., Ishihara, O., & Katayama, T. (1990). Study of the effect of green areas on the thermal environment in an urban area. *Energy and Buildings, 15*(3–4), 493–498. https://doi.org/10.1016/0378-7788(90)90026-F

Santamouris, M. (2014). Cooling the cities: A review of reflective and green roof mitigation technologies to fight heat island and improve comfort in urban environments. *Solar Energy, 103*, 682–703. https://doi.org/10.1016/j.solener.2012.07.003

Schnetzer, J., & Pluschke, L. (2017). *Solar-powered irrigation systems: A clean-energy, low-emission option for irrigation development and modernization.* Food and Agriculutre Organization of the United Nations. http://www.fao.org/3/a-bt437e.pdf

Shukla, A. K., & Singh, O. (2014). Effect of compressor inlet temperature & relative humidity on gas turbine cycle performance. *International Journal of Scientific & Engineering Research, 5*(5), 664-670.

Singh, S., & Kumar, R. (2012). Ambient air temperature effect on power plant performance. *International Journal of Engineering Science and Technology, 4*(8), 3916–3923. https://pdfs.semanticscholar.org/ddcf/398f0b93a1f3021404ea24b089cd8a4dbfb6.pdf

Singh, S., & Tiwari, S. (2019). *Climate change, water and wastewater treatment: Interrelationship and consequences.* Springer.

Song, Z., Zheng, Z., Li, J., Sun, X., Han, X., Wang, W., & Xu, M. (2006). Seasonal and annual performance of a full-scale constructed wetland system for sewage treatment in China. *Ecological Engineering, 26*(3), 272–282. https://doi.org/10.1016/j.ecoleng.2005.10.008

Souch, C. A., & Souch, C. (1993). The effect of trees on summertime below canopy urban climates: A case study Bloomington. *Journal of Arboriculture, 19*(5), 303–312.

Taha, H. (1996). Modeling impacts of increased urban vegetation on ozone air quality in the South Coast Air Basin. *Atmospheric Environment, 30*(20), 3423–3430. https://doi.org/10.1016/1352-2310(96)00035-0

Taha, H. (1997). Urban climates and heat islands: Albedo, evapotranspiration, and anthropogenic heat. *Energy and buildings, 25*(2). https://doi.org/10.1016/S0378-7788(96)00999-1

Taha, H., Akbari, H., & Rosenfeld, A. (1988). Vegetation canopy micro-climate: A field-project in Davis, California. *Journal of Climate and Applied Meteorology*.

Taha, H., Akbari, H., & Rosenfeld, A. (1991). Heat island and oasis effects of vegetative canopies: micro-meteorological field-measurements. *Theoretical and Applied Climatology, 44*(2), 123–138.

Tallis, M., Taylor, G., Sinnett, D., & Freer-Smith, P. (2011). Estimating the removal of atmospheric particulate pollution by the urban tree canopy of London, under current and future environments. *Landscape and Urban Planning, 103*(2), 129–138.

Tang, H. (2012). *Research on temperature and salt migration law of sulphate salty soil subgrade in Xinjiang Region*. Beijing Jiaotong University.

Taylor, C. R., Hook, P. B., Stein, O. R., & Zabinski, C. A. (2011). Seasonal effects of 19 plant species on COD removal in subsurface treatment wetland microcosms. *Ecological Engineering, 37*(5), 703–710. https://doi.org/10.1016/j.ecoleng.2010.05.007

Tiwary, A., Sinnett, D., Peachey, C., Chalabi, Z., Vardoulakis, S., Fletcher, T., Leonardi, G. Grundy, C., Azapagic, A., & Hutchings, T. R. (2009). An integrated tool to assess the role of new planting in PM10 capture and the human health benefits: A case study in London. *Environmental Pollution, 157*(10), 2645–2653. https://doi.org/10.1016/j.envpol.2009.05.005

Tsihrintzis, V. A., & Hamid, R. (1998). Runoff quality prediction from small urban catchments using SWMM. *Hydrological Processes, 12*(2), 311–329.

U.S. Department of Energy. (2013). *U.S. Energy sector vulnerabilities to climate change and extreme weather* (DOE/PI-0013). https://www.energy.gov/sites/prod/files/2013/07/f2/20130710-Energy-Sector-Vulnerabilities-Report.pdf

U.S. Environmental Protection Agency. (2003, September). *Cooling summertime temperatures: Strategies to reduce heat islands.* https://www.epa.gov/sites/production/files/2014-06/documents/hiribrochure.pdf

U.S. Environmental Protection Agency. (2014). *The economic benefits of green infrastructure: A case study of Lancaster, PA.* https://www.cnt.org/sites/default/files/publications/CNT_EPA_LancasterGICaseStudy.pdf

Ullrich, A., & Volk, M. (2009). Application of the Soil and Water Assessment Tool (SWAT) to predict the impact of alternative management practices on water quality and quantity. *Agricultural Water Management, 96*(8), 1207–1217. https://doi.org/10.1016/j.agwat.2009.03.010

Valkama, P., Mäkinen, E., Ojala, A., Vahtera, H., Lahti, K., Rantakokko, K., Vasander, H., Nikinmaa, E., & Wahlroos, O. (2017). Seasonal variation in nutrient removal efficiency

of a boreal wetland detected by high-frequency on-line monitoring. *Ecological Engineering, 98*, 307–317. https://doi.org/10.1016/j.ecoleng.2016.10.071

Van Vliet, M. T., Yearsley, J. R., Ludwig, F., Vögele, S., Lettenmaier, D. P., & Kabat, P. (2012). Vulnerability of U.S and European electricity supply to climate change. *Nature Climate Change, 2*(9), 676–681.

Vought, T. D. (2019, June 30). *An economic case for facility lightning protection systems in 2017*. https://vfclp.com/articles/an-economic-case-for-facility-lightning-protection-systems-in-2017/

Watkins, R., Littlefair, P., Kolokotroni, M., & Palmer, J. (2002). The London heat island: Surface and air temperature measurements in a park and street gorges. *ASHRAE Transactions, 108*(1), 419–427.

Wilbanks, T., Bhatt, V., Bilello, D., Bull, S., Ekmann, J., Horak, W., & Huang, Y. J. (2008). *Effects of climate change on energy production and use in the United States.* U.S. Department of Energy Publications.

Xiao, Q., & McPherson, E. G. (2002). Rainfall interception by Santa Monica's municipal urban forest. *Urban ecosystems, 6*(4), 291–302.

Yamba, F., Walimwipi, H., Jain, S., Zhou, P., Cuamba, B., & Mzezewa, C. (2011). Climate change/variability implications on hydroelectricity generation in the Zambezi River Basin. *Mitigation and Adaptation Strategies for Global Change*, 617–628. http://www.doi.org/10.1007/s11027-011-9283-0

Young, I. R., & Holland, G. J. (1996). Atlas of the oceans: Wind and wave climate. *Oceanographic Literature Review, 7*(43), 742.

Yuan, H., Nie, J., Zhu, N., Miao, C., & Lu, N. (2013). Effect of temperature on the wastewater treatment of a novel anti-clogging soil infiltration system. *Ecological engineering, 57*, 375–379. https://doi.org/10.1016/j.ecoleng.2013.04.007

Zhang, C., Liao, H., & Mi, Z. (2019). Climate impacts: Temperature and electricity consumption. *Natural Hazards, 99*(3), 1259–1275

Zhao, C., Liu, B., Piao, S., Wang, X., Lobell, D., Huang, Y., Huang, M., Yao, Y., Bassu, S., Ciais, P., Durand, J.-L., Elliot, J., Ewert, F., Janssens, I. A., Li, T., Lin, E., Liu, Q., Martre, P., Müller, C., … Asseng, S. (2017). Temperature increase reduces global yields of major crops in four independent estimates. *Proceedings of the National Academy of Sciences, 114*(35). https://doi.org/10.1073/pnas.1701762114

Zhao, M., Kong, Z. H., Escobedo, F. J., & Gao, J. (2010). Impacts of urban forests on offsetting carbon emissions from industrial energy use in Hangzhou, China. *Journal of Environmental Management, 91*(4), 807–813. https://doi.org/10.1016/j.jenvman.2009.10.010

Zhao, X., Shen, A., & Ma, B. (2018). Temperature adaptability of asphalt pavement to high temperatures and significant temperature differences. *Advances in Materials Science and Engineering*, 1–16.

Zheng, S., Huang, G., Zhou, X., & Zhu, X. (2020). Climate-change impacts on electricity demands at a metropolitan scale: A case study of Guangzhou, China. *Applied Energy, 261,* 114295.

Zhou, Z. C., Shangguan, Z. P., & Zhao, D. (2006). Modeling vegetation coverage and soil erosion in the Loess Plateau Area of China. *Ecological modelling, 198*(1–2), 263–268. http://doi.org/10.1016/j.ecolmodel.2006.04.019

Zoppou, C. (2001). Review of urban storm water models. *Environmental Modelling & Software, 16*(3), 195–231. https://doi.org/10.1016/S1364-8152(00)00084-0

Zoulia, I., Santamouris, M., & Dimoudi, A. (2009). Monitoring the effect of urban green areas on the heat island in Athens. *Environmental Monitoring and Assessment, 156*(1–4).

Zsirai, T., Buzatu, P., Maffettone, R., & Judd, S. (2012, April). *Sludge viscosity – The thick of it*. https://www.thembrsite.com/features/sludge-viscosity-in-membrane-bioreactors-the-thick-of-it/

Annex I: Code for Establishing the CDS Toolbox-SAVi Link

Code related to offline processing of CDS Toolbox and CDS API data for the C3S_428h_IISD-EU project.

How does this code relate to the CDS API ?

This code builds on the powerful CDS API but focuses on local impact analysis specific for the C3S_428h_IISD-EU project. It makes it easier to retrieve a time series for a specific location or region, and save the result to a CSV file (a simpler format than netCDF for most climate adaptation practitioners). Additionally, the code combines variables across multiple datasets, aggregate them into asset classes (such as all energy-related variables) and perform actions such as bias correction (use of ERA5 and CMIP5).

Code available for download

The easy way is to download the zipped archive: - latest (development): https://github.com/perrette/iisd-cdstoolbox/archive/master.zip - or check stable releases with description of changes: https://github.com/perrette/iisd-cdstoolbox/releases (see assets at the bottom of each release to download a zip version)

The hacky way is to use git (only useful during development, for frequent updates, to avoid having to download and extract the archive every time):

- First time: `git clone https://github.com/perrette/iisd-cdstoolbox.git`

- Subsequent updates: `git pull` from inside the repository

Installation steps

- Download the code (see above) and inside the folder.
- Install Python 3, ideally Anaconda Python which comes with pre-installed packages
- Install the CDS API key: https://cds.climate.copernicus.eu/api-how-to
- Install the CDS API client: pip install cdsapi
- Install other dependencies: conda install --file requirements.txt or pip install -r requirements.txt
- *Optional* dependency for coastlines on plots: conda install -c conda-forge cartopy or see docs
- *Optional* dependency: CDO (might be needed later, experimental): conda install -c conda-forge python-cdo

Troubleshooting: - If install fails, you may need to go through the dependencies in requirements.txt one by one and try either pip install or conda install or other methods specific to that dependency. - In the examples that follow, if you have both python2 and python3 installed, you might need to replace python with python3.

CDS API

Download indicators associated with one asset class.

Examples of use:

```
python download.py --asset energy --location Welkenraedt
```

The corresponding csv time series will be stored in `indicators/welkenraedt/energy`. Note that raw downloaded data from the CDS API (regional tiles in netcdf format, and csv for the required lon/lat, without any correction) are stored under `download/` and can be re-used across multiple indicators.

The `indicators` folder is organized by location, asset class, simulation set and indicator name. The aim is to provide multiple sets for SAVi simulation. For instance, `era5` for past simulations, and various `cmip5` versions for future simulations, that may vary with model and experiment. For instance the above command creates the folder structure (here a subset of all variables is shown):

```
indicators/
 welkenraedt/
  energy/
   era5/
    2m_temperature.csv
    precipitation.csv
    ...
   cmip5-ipsl_cm5a_mr-rcp_8_5/
    2m_temperature.csv
    precipitation.csv
    ...
   ...
```

with two simulation sets `era5` and `cmip5-ipsl_cm5a_mr-rcp_8_5`. It is possible to specify other models and experiment via `--model` and `--experiment` parameters, to add further simulation sets and thus test how the choice of climate models and experiment affect the result of SAVi simulations.

Compared to raw CDS API, some variables are renamed and scaled so that units match and are the same across simulation sets. For instance, temperature was adjusted from Kelvin to degree Celsius, and precipitation was renamed and units-adjusted into mm per month from original (mean_total_precipitation_rate (mm/s) in ERA5, and mean_precipitation_flux (mm/s) in CMIP5). Additionally, CMIP5 data is corrected so that climatological mean matches with ERA5 data (climatology computed over 1979-2019 by default).

Additionally to the files shown in the example folder listing above, figures can also be created for rapid control of the data, either for interactive viewing (`--view-timeseries` and `--view-region`) or or saved as PNG files (`--png-timeseries` and `--png-region`), e.g.

```
python download.py --asset energy --location Welkenraedt --png-timeseries --
png-region
```

Single indicators can be downloaded via:

```
python download.py --indicator 2m_temperature --location Welkenraedt
```

The choices available for `--indicator` , `--asset` and `--location` area defined in the following configuration files, respectively:

- controls which indicators are available, how they are renamed and unit-adjusted: indicators.yml (see sub-section below)
- controls the indicator list in each asset class: assets.yml
- controls the list of locations available: locations.yml

Full documentation, including fine-grained controls, is provided in the command-line help:

```
python download.py --help
```

Visit the CDS Datasets download pages, for more information about available variables, models and scenarios:

- ERA5: https://cds.climate.copernicus.eu/cdsapp#!/dataset/reanalysis-era5-single-levels-monthly-means?tab=form

- CMIP5: https://cds.climate.copernicus.eu/cdsapp#!/dataset/projections-cmip5-monthly-single-levels?tab=form

In particular, clicking on “Show API request” provides information about spelling of the parameters, e.g. that “2m temperature” is spelled `2m_temperature` and “RCP 8.5” is spelled `rcp_8_5`.

Indicator definition

This section is intended for users who wish to extend the list of indicators currently defined in indicators.yml. It can be safely ignored for users who are only interested in using the existing indicators.

Let’s see how `10m_wind_speed` is defined:

```
- name: 10m_wind_speed
 units: m / s
 description: Wind speed magnitude at 10 m
```

The fields `name` and `units` define the indicator. Description is optional, just to provide some context. It is possible to provide `scale` and `offset` fields to correct the data as `(data + offset) * scale`. Here for `2m temperature`:

```
- name: 2m_temperature
 units: degrees Celsius
 description: 2-m air temperature
 offset: -273.15 # Kelvin to degrees C
```

# denotes a comment to provide some context. Some indicators have different names in ERA5 and CMIP5, and possibly different units. That can be dealt with by providing `era5` and `cmip5` fields, which have precedence over the top-level fields. Here the `evaporation` definition:

```
- name: evaporation
 units: mm per month
 era5:
  name: mean_evaporation_rate # different name in ERA5
  scale: -2592000 # change sign and convert from mm/s to mm / month
 cmip5:
  scale: 2592000 # mm/s to mm / month
```

In that case both scaling and name depend on the dataset. In CMIP5 which variable name is identical to our indicator name, the `name` field can be omitted. In ERA5, evaporation is negative (downwards fluxes are counted positively), whereas it is counted positively in ERA5.

Indicators composed of several CDS variables can be defined via `compose` and `expression` fields. Let's look at `100m_wind_speed`:

```
- name: 100m_wind_speed
 units: m / s
 description: Wind speed magnitude at 100 m
 era5:
  compose:
   - 100m_u_component_of_wind
   - 100m_v_component_of_wind
  expression: (_100m_u_component_of_wind**2 + _100m_v_component_of_wind**2)**
0.5
 cmip5:
  name: 10m_wind_speed
  scale: 1.6 # average scaling from 10m to 100m, based on one test location (
approximate!)
```

In ERA5, vector components of 100m wind speed are provided. Our indicator is therefore a composition of these two variables, defined by the `expression` field, which is evaluated as a python expression. Note that variables that start with a digit are not licit in python and must be prefixed with an underscore _ in the `expression` field (only there).

For complex expressions, it is possible to provide a `mapping` field to store intermediate variables, for readability. This is used for the `relative_humidity` indicator:

```
- name: relative_humidity
 units: '%'
 era5:
  compose:
```

```
    - 2m_temperature
    - 2m_dewpoint_temperature
   expression: 100*(exp((17.625*TD)/(243.04+TD))/exp((17.625*T)/(243.04+T)))
   mapping: {T: _2m_temperature - 273.15, TD: _2m_dewpoint_temperature - 273.1
5}
  cmip5:
   name: near_surface_relative_humidity
```

where `T` and `TD` are provided as intermediary variables, to be used in `expression`.

ERA5-hourly dataset can be retrieved via `frequency: hourly` field, and subsequently aggregated to monthly indicators thanks to pre-defined functions `daily_max`, `daily_min`, `daily_mean`, `monthly_mean`, `yearly_mean`. For instance:

```
- name: maximum_daily_temperature
  units: degrees Celsius
  offset: -273.15
  cmip5:
   name: maximum_2m_temperature_in_the_last_24_hours
  era5:
   name: 2m_temperature
   frequency: hourly
   transform:
    - daily_max
    - monthly_mean
```

This variable is available directly for CMIP5, but not in ERA5. It is calculated from `2m_temperature` from ERA5 `hourly` dataset, and subsequently aggregated. Note the ERA5-hourly dataset takes significantly longer to retrieve than ERA5 monthly. Consider using in combination with `--year 2000` to retrieve a single year of the ERA5 dataset.

Currently CMIP5 daily is not supported.

Netcdf to csv conversion

Convert netcdf time series files downloaded from the CDS Toolbox pages into csv files (note: this does not work for netcdf files downloaded via the cds api):

```
python netcdf_to_csv.py data/*nc
```

Help:
```
python netcdf_to_csv.py --help
```

Copernicus Climate Change Service